This Document Does Not Contain Continuum Dynamics, Inc. Proprietary Information

CDI Report No. 07-17NP

Stress Assessment of Hope Creek Unit 1 Steam Dryer Based on Revision 4 Loads Model

Revision 2

Prepared by

Continuum Dynamics, Inc.
34 Lexington Avenue
Ewing, NJ 08618

Prepared under Purchase Order No. 4500413356 for

Nuclear Business Unit, PSEG Nuclear LLC
Materials Center, Alloway Creek Neck Road
Hancocks Bridge, NJ 08038

Approved by

Alan J. Bilanin

Reviewed by

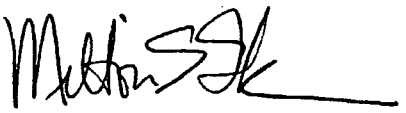

Milton E. Teske

August 2007

This report complies with Continuum Dynamics, Inc. Nuclear Quality Assurance Program currently in effect.

Executive Summary

A harmonic finite element stress analysis method is used to assess stresses on the Hope Creek Unit 1 (HC1) steam dryer resulting from acoustic and hydrodynamic loads. The harmonic stress analysis confers a number of useful computational advantages over a time-domain method including the ability to assess the effects of frequency scalings in the loads without the need for additional finite element calculations. [[

$^{3)}$]]

The analysis begins by developing a series of unit stress solutions corresponding to the application of a unit pressure at a MSL at specified frequency, f. Each unit solution is obtained by first calculating the associated acoustic pressure field using a separate analysis that solves the damped Helmholtz equation within the steam dryer [1]. This pressure field is then applied to a finite element structural model of the steam dryer and the stress response at frequency, f, calculated using the commercial ANSYS 10.0 finite element analysis software. This stress response constitutes the unit solution and is stored as a file for subsequent processing. Once all unit solutions have been computed, the stress response for any combination of MSL pressure spectrums (obtained by Fast Fourier Transform of the pressure histories in the MSLs) is determined by a simple matrix multiplication of these spectrums with the unit solutions.

This report provides details of the ANSYS 10.0 finite element structural model of the HC1 steam dryer and reviews pertinent modeling considerations. It also summarizes the framework underlying the development and application of unit solutions in the frequency domain and shows how these solutions are used to develop stress histories for general load conditions. Next, it reviews the assessment of these stresses for compliance with the ASME B&PV Code, Section III, subsection NG, for the load combination corresponding to normal operation (the Level A Service Condition). [[

$^{(3)}$]]

Results obtained from application of the methodology to the HC1 steam dryer using the Rev. 4 acoustic/hydrodynamic loads [2] show that at nominal CLTP operation the minimum stress ratio (SR) anywhere on the steam dryer is SR=1.58 and corresponds to a maximum stress intensity at a weld (where the skirt joins to the upper support ring). The smallest alternating stress intensity in the nominal case is negligible with SR>4. These results account for all the end-to-end biases and uncertainties in the loads model [2]. In order to account for uncertainties in the finite element model, the stresses are also computed for loads that are shifted in the frequency domain by ±2.5%, ±5%, ±7.5% and ±10%. The minimum stress ratio encountered at any frequency shift is still SR=1.58 occurring at the same location and at 0% frequency shift. The smallest alternating stress ratio however reduces to SR-a=1.86 occurring at the -7.5% shift. Inspection of the accumulative stress PSDs shows that the dominant stresses contributions occur in the 80.0 Hz – 80.2 Hz and, to a lesser extent, in the 40.5 Hz – 42.0 Hz range. A significant portion of the 80 Hz signal is non-physical. Upon filtering 90% of this signal, the smallest stress ratios increase to SR-P=1.66 (maximum stress intensity) and SR-a=3.58 (alternating stress intensity). Given that the biases and uncertainties in loads are already accounted for, this stress ratio is expected to qualify the dryer with considerable margin at EPU conditions.

Table of Contents

1. Introduction and Purpose

Plans to qualify the Hope Creek nuclear plant for operation at Extended Power Uprate (EPU) operating condition require an assessment of the steam dryer stresses experienced under the increased loads. The steam dryer loads due to pressure fluctuations in the main steam lines (MSLs) are potentially damaging and the cyclic stresses from these loads can produce fatigue cracking if loads are sufficiently high. The industry has addressed this problem with physical modifications to the dryers, as well as a program to define steam dryer loads and their resulting stresses.

The purpose of the stress analysis discussed here is to calculate the maximum and alternating stresses generated during Current Licensed Thermal Power (CLTP) and determine the margins that exist when compared to stresses that comply with the ASME Code (ASME B&PV Code, Section III, subsection NG). This step establishes whether the modifications done prior to commercial operations are adequate for sustaining structural integrity and preventing future weld cracking under planned EPU operating conditions. The load combination considered here corresponds to normal operation (the Level A Service Condition) and includes fluctuating pressure loads developed from Hope Creek Unit 1 (HC1) main steam line data, and steam dryer weight. The fluctuating pressure loads, induced by the flowing steam, are predicted using a separate acoustic circuit analysis of the steam dome and main steam lines [3]. Level B service conditions, which include seismic loads, are not included in this evaluation since no physical modifications were made to the HC1 steam dryer for EPU operation.

[[

[3]]] This approach also affords a number of additional computational advantages over transient simulations including: [[

[3]]] This last advantage is realized through the use of "unit" solutions representing the stress distribution resulting from the application of a unit fluctuating pressure at one of the MSLs at a particular frequency. [[

[3]]]

This report describes the overall methodology used to obtain the unit solutions in the frequency domain and how to assemble them into a stress response for a given combination of

pressure signals in the MSLs. This is followed by details of the HC1 steam dryer finite element model including the elements used and overall resolution, treatment of connections between elements, the hydrodynamic model, the implementation of structural damping and key idealizations/assumptions inherent to the model. Post-processing procedures are also reviewed including the computation of maximum and alternating stress intensities, identification of high stress locations, adjustments to stress intensities at welds, and evaluation of stress ratios used to establish compliance with the ASME Code.

The results for Rev. 4 acoustic/hydrodynamic loads [2] in terms of stress intensity distributions and stress ratios are presented next, together with accumulative PSDs of the dominant stress components. The latter show that the load and structural response are dominated by a strong 80 Hz component and a significant 41 Hz signal.

2. Methodology

2.1 Overview

Based on previous analysis undertaken at Quad Cities Units 1 and 2, the steam dryer can experience strong acoustic loads due to the fluctuating pressures in the MSLs connected to the steam dome containing the dryer. C.D.I. has developed an acoustic circuit model (ACM) that, given a collection of strain gauge measurements [4] of the fluctuating pressures in the MSLs, predicts the acoustic pressure field anywhere inside the steam dome and on the steam dryer [1-3]. The ACM is formulated in frequency space and contains two major components that are directly relevant to the ensuing stress analysis of concern here. [[

[3]]]

[[

[3]]]

[[

(3)]]

2.2 [[

(3)]]

[[

(3)]]

2.3 Computational Considerations

Focusing on the structural computational aspects of the overall approach, there are a number of numerical and computational considerations requiring attention. The first concerns the transfer of the acoustic forces onto the structure, particularly the spatial and frequency resolutions. The ANSYS finite element program inputs general distributed pressure differences using a table format. This consists of regular 3D rectangular (i.e., block) $n_X \times n_Y \times n_Z$ mesh where n_α is the number of mesh points in the α-th Cartesian direction and the pressure difference is provided at each mesh point (see Section 3.10). These tables are generated separately using a program that reads the loads provided from the ACM software, distributes these loads onto the finite element mesh using a combination of interpolation procedures on the surface and simple diffusion schemes off the surface (off-surface loads are required by ANSYS to ensure proper interpolation of forces), and written to ASCII files for input to ANSYS. A separate load file is written at each frequency for the real and imaginary component of the complex force.

The acoustic field is stored at 5 Hz intervals from 0 to 200 Hz. While a 5 Hz resolution is sufficient to capture frequency dependence of the acoustic field (i.e., the pressure at a point varies gradually with frequency), it is too coarse for representing the structural response especially at low frequencies. For 1% critical structural damping, one can show (as indicated in the design record file, DRF-CDI-174) that the frequency spacing needed to resolve a damped resonant peak at natural frequency, f_n, to within 5% accuracy is $\Delta f = 0.0064 \times f_n$ Thus for f_n=10 Hz where the lowest structural response modes occur, a frequency interval of 0.064 Hz or less is required. In our calculations we require that 5% maximum error be maintained over the range from f_n=5 Hz to 200 Hz resulting in a finest frequency interval of 0.0321 Hz at the low frequency end (this adequately resolves all structural modes up to 200 Hz). Since there are no structural modes between 0 to 5 Hz, a 0.5 Hz spacing is used over this range with minimal (less than 5%) error. The unit load, $\hat{\mathbf{f}}_n(\omega, \mathbf{R})$, at any frequency, ω_k, is obtained by linear interpolation of the acoustic solutions at the two nearest frequencies, ω_i and ω_{i+1}, spaced 5 Hz apart. Linear interpolation is sufficient since the pressure load varies slowly over each 5 Hz interval (linear interpolation of the structural response over these 5 Hz intervals would not be acceptable since it varies much more rapidly over these intervals).

Solution Management

[[

(3)]]

Upon completion of each frequency calculation, ANSYS is instructed to export the stresses which are stored in text files. There is one file per MSL per frequency per real/imaginary component, and each file contains the complete stress state over all nodes on the dryer. This format is convenient from a solution point of view. However, it makes it difficult to extract the stress response at a node since, in order to do so, thousands of files must be opened and searched through thousands of nodes until the node of interest is reached. [[

[3]]]

Structural Damping

In harmonic analysis one has a broader selection of damping models than in transient simulations. A damping factor, z, of 1% critical damping is used in the structural analysis. In transient simulations, this damping can only be enforced exactly at two frequencies (where the damping model is "pinned"). Between these two frequencies the damping factor can by considerably smaller, for example 0.5% or less depending on the pinning frequencies. Outside the pinning frequencies, damping is higher. With harmonic analysis it is straightforward to enforce very close to 1% damping over the entire frequency range. In this damping model, the damping matrix, **D**, is set to

$$\mathbf{D} = \frac{2z}{\omega}\mathbf{K} \tag{71}$$

where **K** is the stiffness matrix and ω the forcing frequency. One can show that with this model the damping factor varies between 0.995% and 1.005% which is a much smaller variation than using the pinned model required in transient simulation.

Load Frequency Rescaling

One way to evaluate the sensitivity of the stress results to approximations in the structural modeling and applied loads is to rescale the frequency content of the applied loads. In this procedure the nominal frequencies, ω_k, are shifted to $(1+\lambda)\omega_k$, where the frequency shift, λ, ranges between $\pm 10\%$, and the response recomputed for the shifted loads. The objective of the frequency shifting can be explained by way of example. Suppose that in the actual dryer a strong structural-acoustic coupling exists at a particular frequency, ω^*. This means that the following conditions hold simultaneously: (i) the acoustic signal contains a significant signal at ω^*; (ii) the structural model contains a resonant mode of natural frequency, ω_n, that is near ω^*; and (iii) the associated structural mode shape is strongly coupled to the acoustic load (i.e., integrating the product of the mode shape and the surface pressure over the steam dryer surface produces a significant modal force). Suppose now that because of discretization errors and modeling idealizations that the predicted resonance frequency differs from ω^* by a small amount (e.g., 1.5%). Then condition (ii) will be violated and the response amplitude therefore significantly diminished. By shifting the load frequencies one re-establishes condition (ii) when $(1+\lambda)\omega^*$ is near ω_n. The other two requirements also hold and a strong structural acoustic interaction is restored.

[[

(3)]]

Evaluation of Maximum and Alternating Stress Intensities

Once the unit solutions have been obtained, the most intensive computational steps in the generation of stress intensities are: (i) the FFTs to evaluate stress time histories from (5); and (ii) the calculation of alternating stress intensities. [[

(3)]]

The high computational penalty incurred in calculating the alternating stress intensities is due to the fact that this calculation involves comparing the stress tensors at every pair of points in the stress history. This comparison is necessary since in general the principal stress directions can vary during the response, thus for N samples in the stress history, there will be (N-1)N/2 such pairs or, for N=64K (the number required to accurately resolve the spectrum up to 200 Hz in 0.01 Hz intervals), 2.1×10^9 calculations per node each requiring the determination of the roots to a cubic polynomial. [[

(3)]]

3. Finite Element Model Description

A description of the ANSYS model of the Hope Creek Unit 1 steam dryer follows. This model is virtually identical to one developed for previous investigations using time domain-based analysis methods [7].

3.1 Steam Dryer Geometry

A geometric representation of the Hope Creek steam dryer was developed from available drawings (provided by PSE&G and included in the design record files, DRF-PSEG-258 and DRF-175C) within the Workbench module of ANSYS. Field measurements taken by C.D.I. on an identical spare dryer for the cancelled Hope Creek Unit 2 were also used to develop this model (also contained in DRF-175C). The completed model is shown in Figure 1. This model includes modifications made to the HC1 steam dryer on-site, prior to commercial operation. These are:

- Tie bars, outer hoods, and center end plates were replaced on the original dryer (FDI-041-79450).
- Reinforcement bars were added to the middle and inner hoods (HCI-KTI-415-7)
- Back-welding of the middle and inner hoods weld joint to their end plates (HCI-KTI-415-3 and -5)

The modified areas are shown in Figure 2.

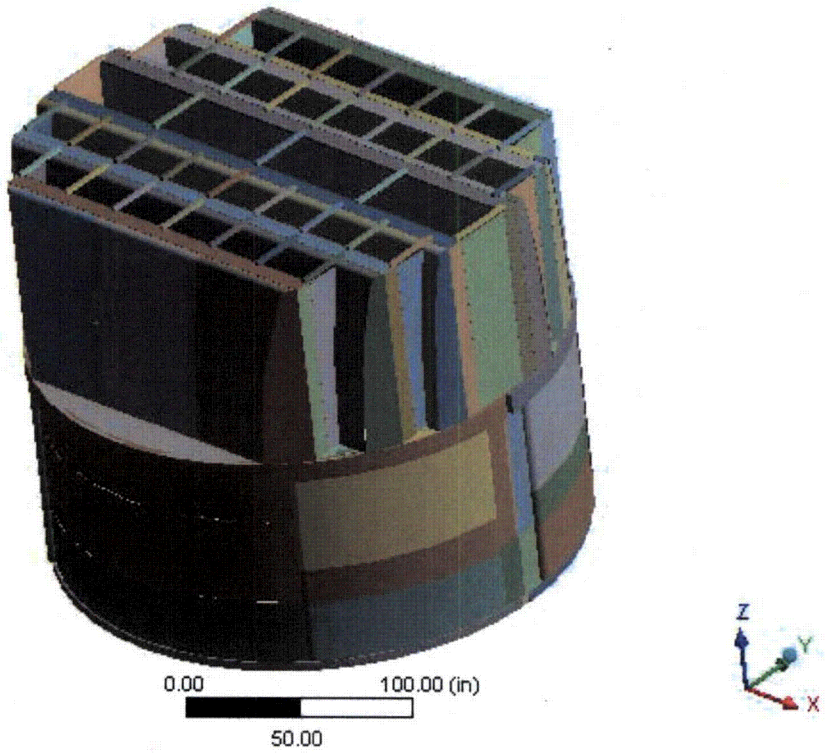

Figure 1. Overall geometry of the HC1 steam dryer model.

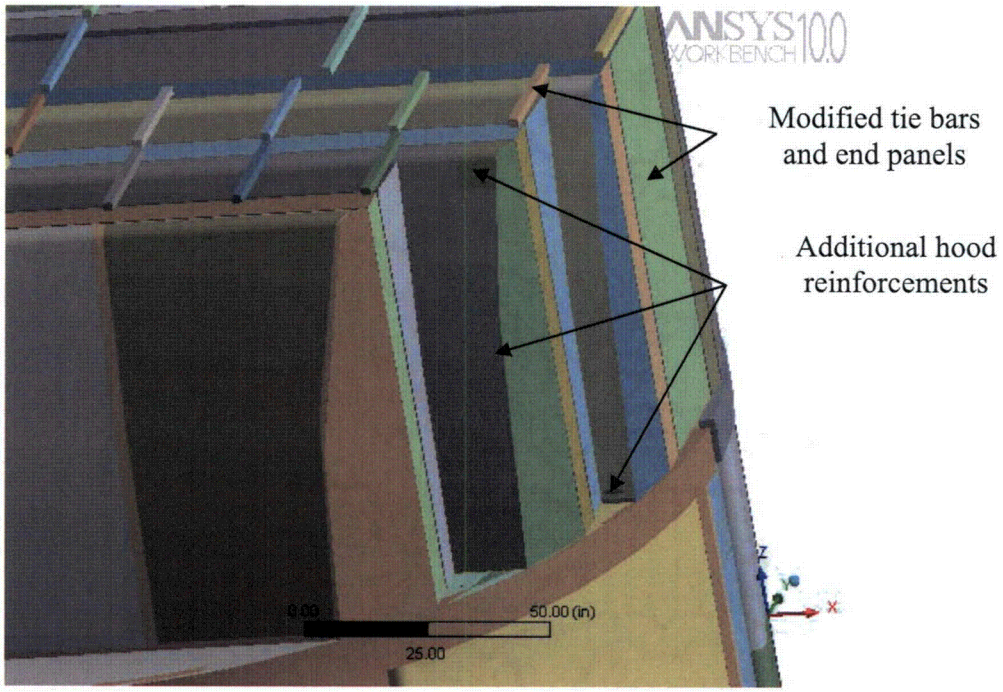

Figure 2. On-site modifications accounted for in the model and associated geometrical details.

3.2 Material Properties

The steam dryer is constructed from Type 304 stainless steel and has an operating temperature of 550°F. Properties used in the analysis are summarized below in Table 1.

Table 1. Material properties.

	Young's Modulus (10^6 psi)	Density (lbm/in^3)	Poisson's Ratio
structural steel	25.55	0.284	0.3
structural steel for perforated plates	15.33	0.227	0.3
structural steel with added water inertia	25.55	1.183	0.3

The structural steel modulus is taken from Appendix A of the ASME Code for Type 304 Stainless Steel at an operating temperature 550°F. The effective properties of perforated plates and submerged parts are discussed in Sections 3.4 and 3.6. Note that the increased effective density for submerged components is only used in the harmonic analysis. When calculating the stress distribution due to the static dead weight load, the unmodified density of steel (0.284 lbm/in^3) is used throughout.

3.3 Model Simplifications

The following simplifications were made to achieve reasonable model size while maintaining good modeling fidelity for key structural properties:

- Perforated plates were approximated as continuous plates using modified elastic properties designed to match the static and modal behaviors of the perforated plates. The perforated plate structural modeling is summarized in Section 3.4 and Appendix C.

- The drying vanes were replaced by point masses attached to the corresponding trough bottom plates and vane bank top covers. The bounding perforated plates, vane bank end plates, and vane bank top covers were explicitly modeled (see Section 3.5).

- The added mass properties of the lower part of the skirt below the reactor water level were obtained using a separate hydrodynamic analysis (see Section 3.6).

- Fixed constraints were imposed at the underside of the steam dryer upper support ring where it makes contact with the four steam dryer support brackets that are located on the reactor vessel and spaced at 90° intervals (Figure 3). No credit was taken for the constraints from the reactor vessel lift lugs.

- Most welds were replaced by node-to-node connections; interconnected parts share common nodes along the welds. In other locations the constraint equations between nodal degrees of freedom were introduced as described in Section 3.9.

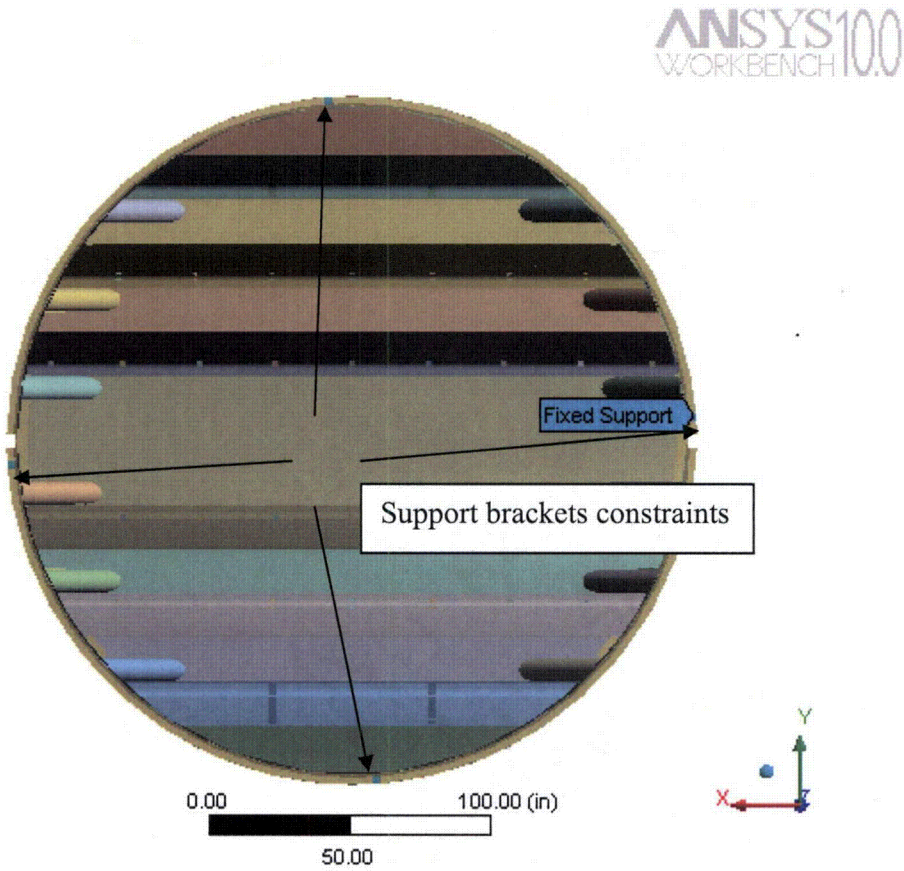

Figure 3. Fixed support constraints.

3.4 Perforated Plate Model

The perforated plates were modeled as solid plates with adjusted elastic and dynamic properties. Properties of the perforated plates were assigned according to the type and size of perforation. Based on [8], for an equilateral triangular pattern with given hole size and spacing, the effective moduli of elasticity were found. The hole pattern and thickness of the perforated plates was based on conservative estimates and field measurements of accessible plates. Subsequent more recent detailed measurements have confirmed that the actual plates are at least 50% thicker. Therefore, since maximum and alternating stresses scale as $1/(\text{thickness})^2$, the current analysis is conservative.

Tests were carried out to verify that this representation of perforated plates by continuous ones with modified elastic properties preserves the modal properties of the structure. These tests are summarized in Appendix C and compare the predicted first modal frequency for a cantilevered perforated plate against an experimentally measured value. The prediction was obtained using the analytical formula for a cantilevered plate and the modified Young's modulus and Poisson's ratio given by O'Donnell [8]. The measured and predicted frequencies are in close agreement, differing by less than 2%.

3.5 Vane Bank Model

The vane bank assemblies consist of many vertical angled plates that are computationally expensive to model explicitly, since a prohibitive number of elements would be required. These parts have significant weight which is transmitted through the surrounding structure, so it is important to capture their gross inertial properties. Here the vane banks are modeled as a collection of point masses located at the center of mass for each vane bank section (see Figure 4). The following masses were used for the vane bank sections, based on data found on provided drawings:

inner banks:	6,545 lbm
middle banks:	5,970 lbm; and
outer banks:	4,685 lbm.

These masses were applied to the base plates and vane top covers using the standard ANSYS point mass modeling option, element MASS21. ANSYS automatically distributes the point mass inertial loads to the nodes of the selected structure. The distribution algorithm minimizes the sum of the squares of the nodal inertial forces, while ensuring that the net forces and moments are conserved. Vane banks are not exposed to main steam lines directly, but rather shielded by the hoods.

The collective stiffness of the vane banks is expected to be small compared to the surrounding support structure and is neglected in the model. In the static case it is reasonable to expect that this constitutes a conservative approach, since neglecting the stiffness of the vane banks implies that the entire weight is transmitted through the adjacent vane bank walls and supports. In the dynamic case the vane banks exhibit only a weak response since (i) they have large inertia so that the characteristic acoustically-induced forces divided by the vane masses and inertias yield small amplitude motions, velocities and accelerations; and (ii) they are shielded from acoustic loads by the hoods, which transfer dynamic loads to the rest of the structure. Thus, compared to the hoods, less motion is anticipated on the vane banks so that approximating their inertial properties with equivalent point masses is justified. Nevertheless, the bounding parts, such as perforated plates, side panels, and top covers, are retained in the model since they can individually exhibit a strong modal response. Errors associated with the point mass representation of the vane banks are compensated for by frequency shifting of the applied loads.

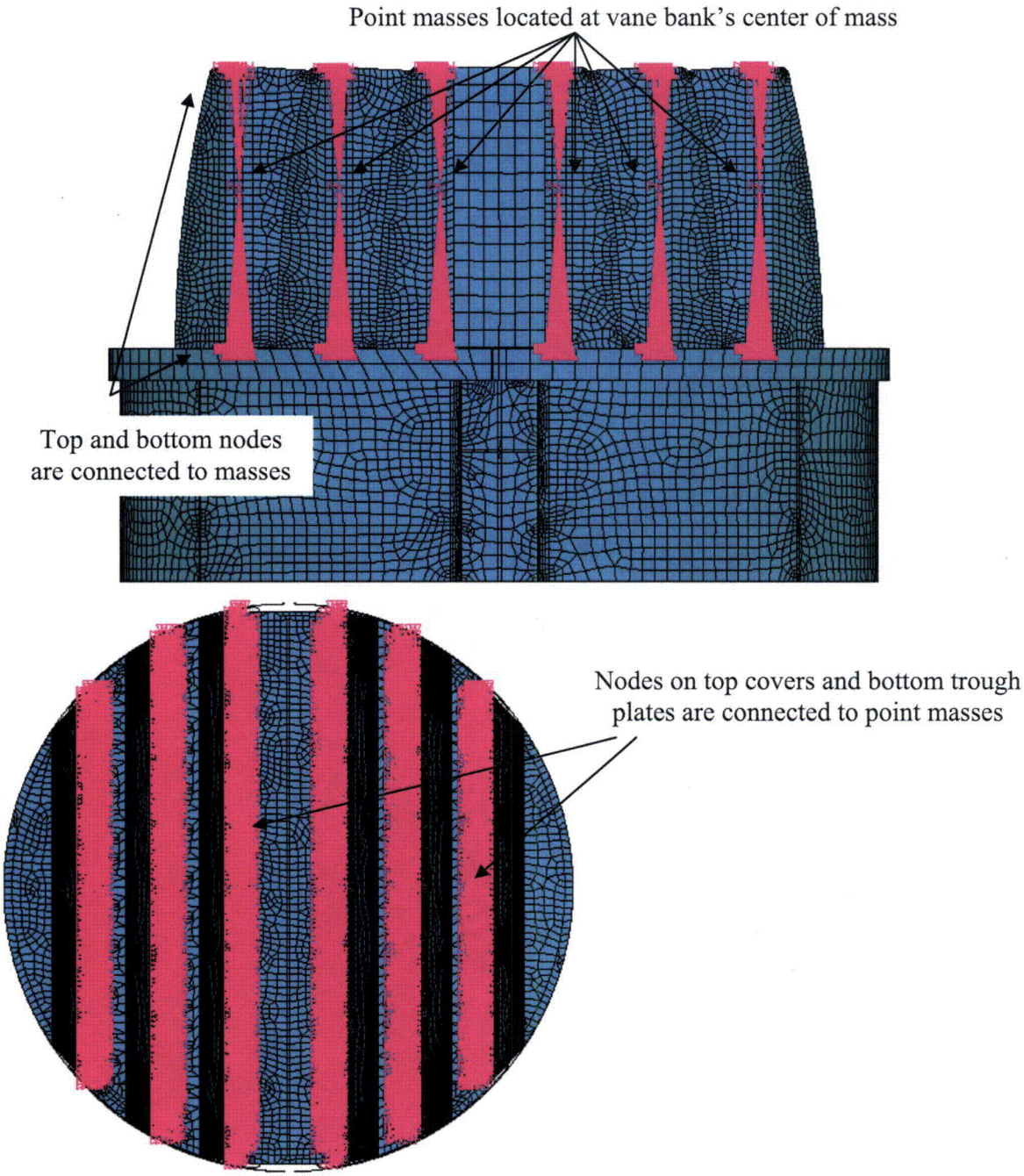

Figure 4. Point masses representing the vanes. The pink shading represents where constraint equations between nodes are applied in the point mass implementation.

3.6 Water Inertia Effect on Submerged Panels

Water inertia was modeled by an increase in density of the submerged structure to account for the added hydrodynamic mass. This added mass was found by a separate hydrodynamic analysis (included in DRF-175C supporting this report) to be 0.225 lbm/in^2 on the submerged

skirt area. This is modeled by effectively increasing the material density for the submerged portions of the skirt. Since the skirt is 0.25 inches thick, the added mass is equivalent to a density increase of 1.183 lbm/in^3. This added water mass was included in the ANSYS model by appropriately modifying the density of the submerged structural elements when computing harmonic response. For the static stresses, the unmodified density of steel is used throughout.

3.7 Structural Damping

Structural damping was defined as 1% of critical damping for all frequencies. This damping is consistent with guidance given on pg. 10 of NRC RG-1.20 [9]. Note that no credit is taken for other significant non-structural dissipation mechanisms such as the hydrodynamic losses in perforated plates. Hence additional conservatism is reflected in the results.

3.8 Mesh Details and Element Types

Shell elements were employed to model the skirt, hoods, perforated plates, side and end plates, trough bottom plates, reinforcements, base plates and cover plates. Specifically, the four-node, Shell Element SHELL63, was selected to model these structural components. This element models bending and membrane stresses, but omits transverse shear. The use of shell elements is appropriate for most of the structure where the characteristic thickness is small compared to the other plate dimensions. For thicker structures, such as the upper and lower support rings, solid brick elements were used to provide the full 3D stress. The elements SURF154 are used to assure proper application of pressure loading to the structure. Mesh details and element types are shown in Table 2 and Table 3.

Table 2. FE Model Summary.

Description	Quantity
Total Nodes	93,951
Total Elements	126,322
Element Types	5
Materials	3

Table 3. Listing of Element Types.

Generic Element Type Name	Element Name	ANSYS Name
20-Node Quadratic Hexahedron	SOLID186	20-Node Hexahedral Structural Solid
4-Node Elastic Shell	SHELL63	4-Node Elastic Shell
4-Node Linear Quadrilateral Shell	SHELL181	4-Node Finite Strain Shell
Mass Element	MASS21	Structural Mass
Pressure Surface Definition	SURF154	3D Structural Surface Effect

The mesh is generated automatically by ANSYS with adaptive refinement near edges. The maximum allowable mesh spacing is specified by the user. Here a 3 inch maximum allowable spacing is specified everywhere except in the following areas: drain pipes (2 inch maximum spacing); base plates (2.75 inches); perforated plates (2 inches); top tie rods (0.75 inches); and

the curved portions of the drain channels (1.5 inches). Details of the finite element mesh are shown in Figure 5. Numerical experiments carried out using the ANSYS code applied to simple analytically tractable plate structures with dimensions and mesh spacings similar to the ones used for the steam dryer, confirm that the natural frequencies are accurately recovered (less than 1% errors for the first modes). These errors are compensated for by the use of frequency shifting.

3.9 Connections Between Structural Components

Most connections between parts are modeled as node-to-node connections. This is the correct manner (i.e., within the finite element framework) of joining elements away from discontinuities. At joints between shells, this approach omits the additional stiffness provided by the extra weld material. Also, locally 3D effects are more pronounced. The latter effect is accounted for using weld factors. The deviation in stiffness due to weld material is negligible, since weld dimensions are on the order of the shell thickness. The consequences upon modal frequencies and amplitude are, to first order, proportional to t/L where t is the thickness and L a characteristic shell length. The errors committed by ignoring additional weld stiffness are thus small and readily compensated for by performing frequency shifts.

When joining shell and solid elements, however, the problem arises of properly constraining the rotations, since shell element nodes contain both displacement and rotational degrees of freedom at every node whereas solid elements model only the translations. A node-to-node connection would effectively appear to the shell element as a simply supported, rather than (the correct) cantilevered restraint and significantly alter the dynamic response of the shell structure.

To address this problem, constraint equations are used to properly connect adjacent shell- and solid-element modeled structures. Basically, all such constraints express the deflection (and rotation for shell elements) of a node, $\mathbf{R}_1$, on one structural component in terms of the deflections/rotations of the corresponding point, $\mathbf{P}_2$, on the other connected component. Specifically, the element containing $\mathbf{P}_2$ is identified and the deformations at $\mathbf{P}_2$ determined by interpolation between the element nodes. The following types of shell-solid element connections are used in the steam dryer model including the following:

1. Shell edge to shell edge connections with dissimilar meshes.
2. Connections of shell faces to solid faces (Figure 6a). While only displacement degrees of freedom are explicitly constrained, this approach also implicitly constrains the rotational degrees of freedom when multiple shell nodes on a sufficiently dense grid are connected to the same solid face.
3. Connections of shell edges to solids (e.g., connection of the bottom of closure plates with the upper ring). Since solid elements do not have rotational degrees of freedom, the coupling approach consists of having the shell penetrate into the solid by one shell thickness and then constraining both the embedded shell element nodes (inside the solid) and the ones located on the surface of the solid structure (see Figure 6b). Numerical tests involving simple structures show that this approach and penetration depth reproduce both the deflections and stresses of the same structure modeled using only solid elements or ANSYS' bonded contact technology. Continuity of rotations and displacements is achieved.

4. Connections of solid elements to shells, e.g., connections of the tie bars to the vane covers.

The use of constraint conditions rather than the bonded contacts advocated by ANSYS for connecting independently meshed structural components confers better accuracy and useful numerical advantages to the structural analysis of the steam dryer including better conditioned and smaller matrices. The smaller size results from the fact that equations and degrees of freedom are eliminated rather than augmented (in Lagrange multiplier-based methods) by additional degrees of freedom. Also, the implementation of contact elements relies on the use of very high stiffness elements (in penalty function-based implementations) or results in indefinite matrices (Lagrange multiplier implementations) with poorer convergence behavior compared to positive definite matrices.

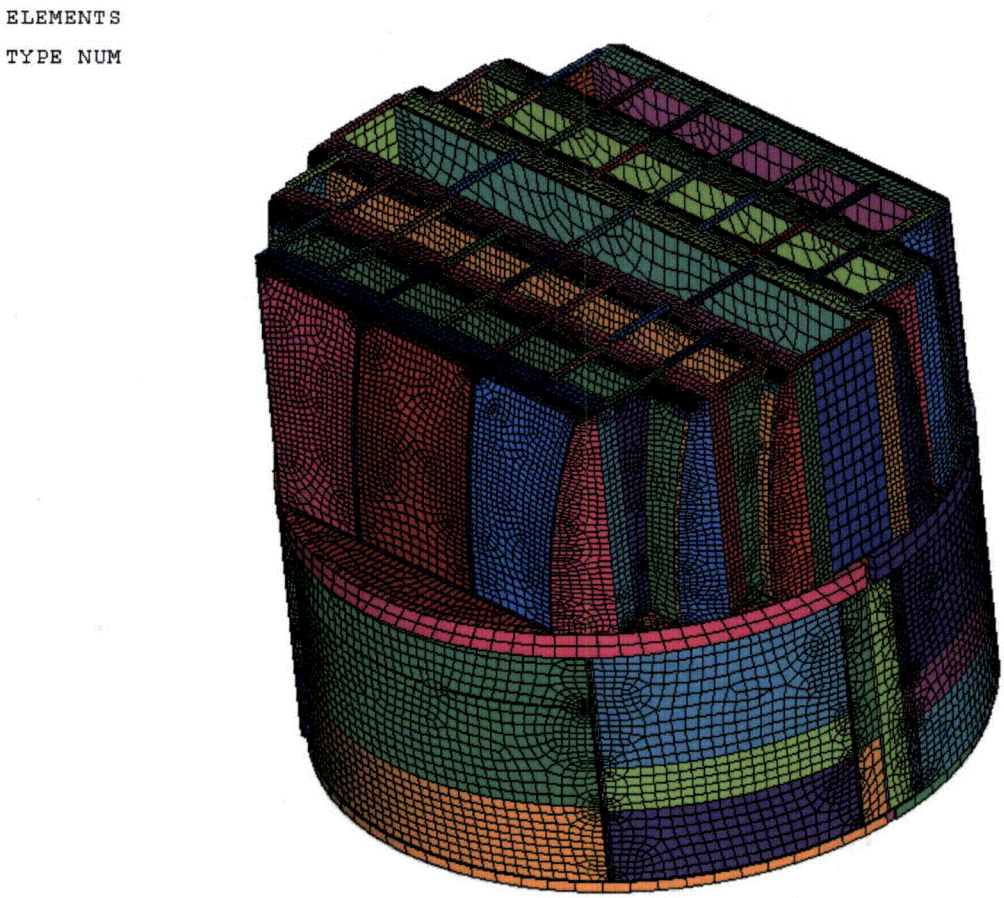

Figure 5a. Mesh overview. The colors emphasize element type.

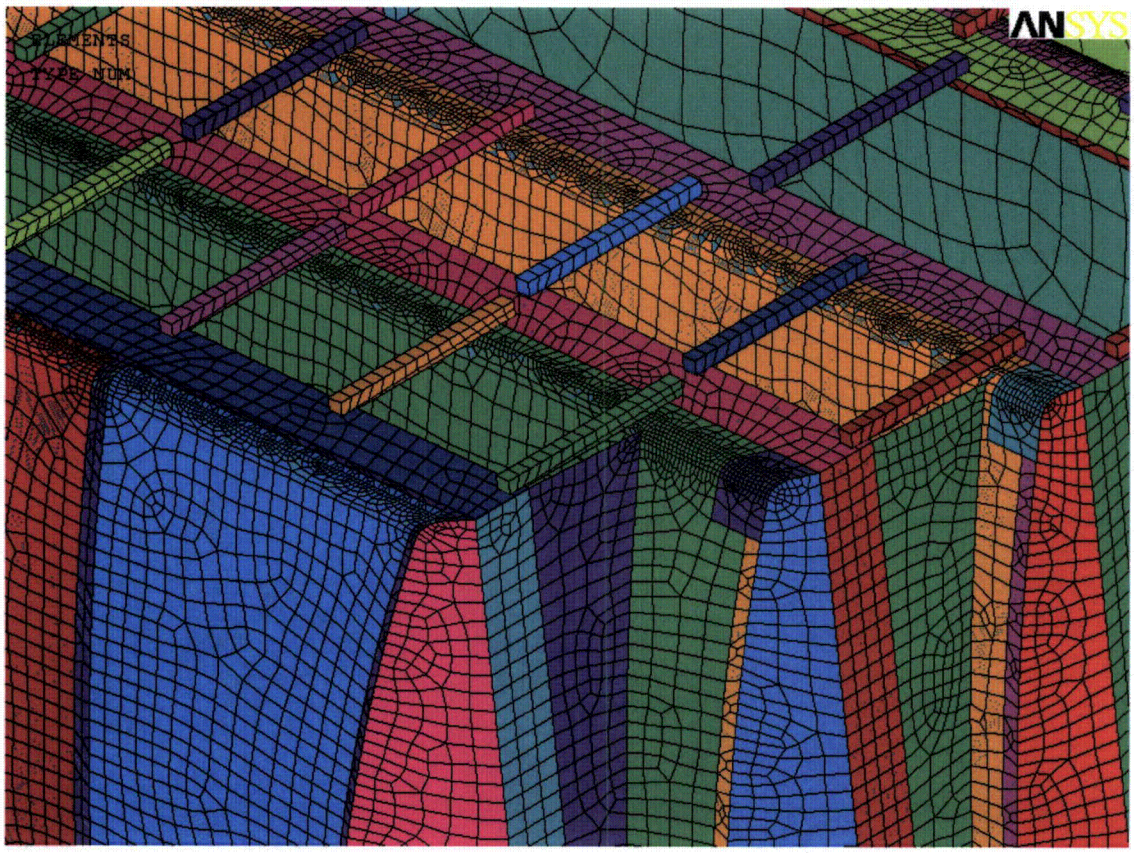

Figure 5b. Close up of mesh showing hoods, reinforcement panels and tie bars. The colors emphasize element type.

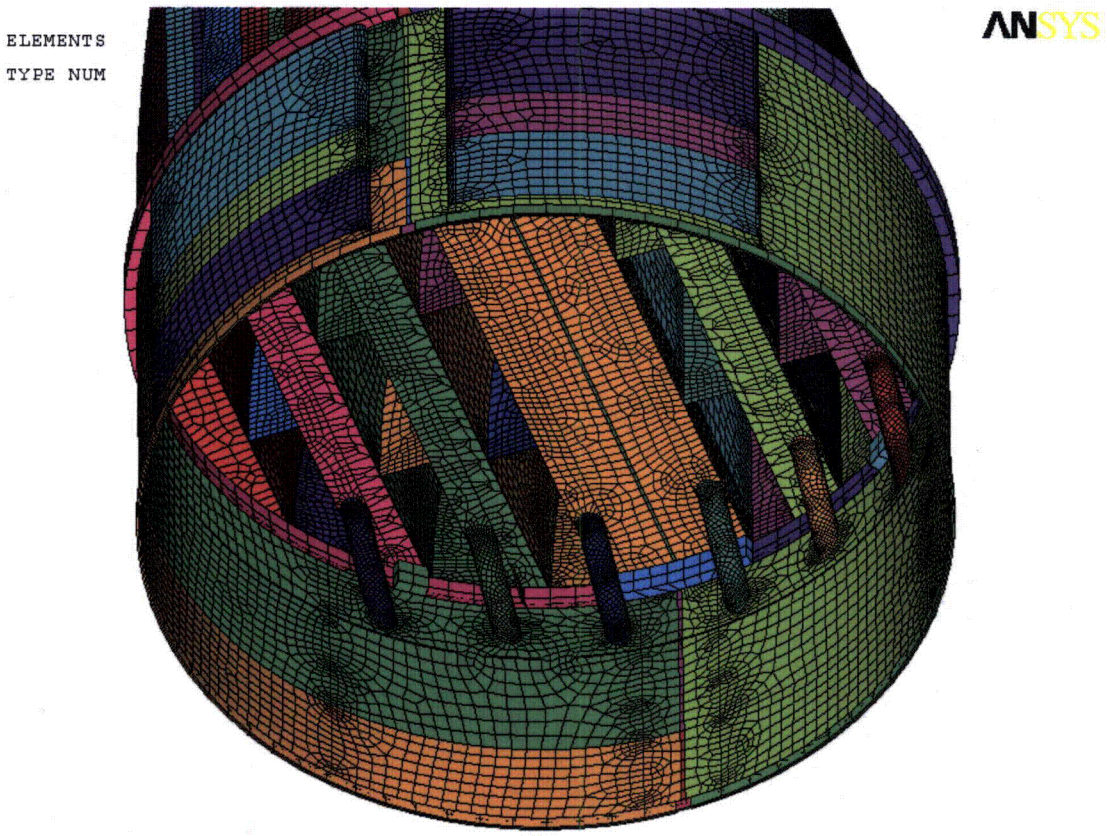

Figure 5c. Close up of mesh showing drain pipes and hood supports. The colors emphasize element type.

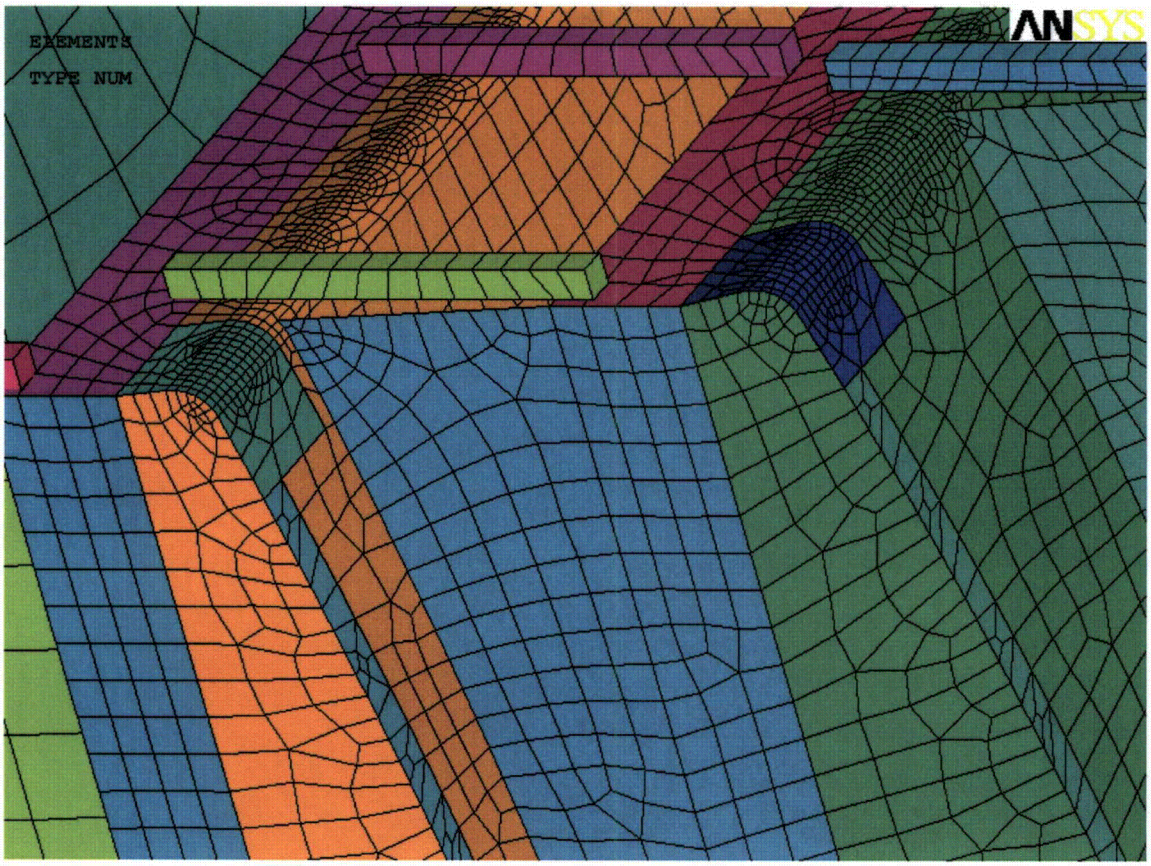

Figure 5d. Close up of mesh showing node-to-node connections between closure panels, end plates, and hoods. The colors emphasize element types.

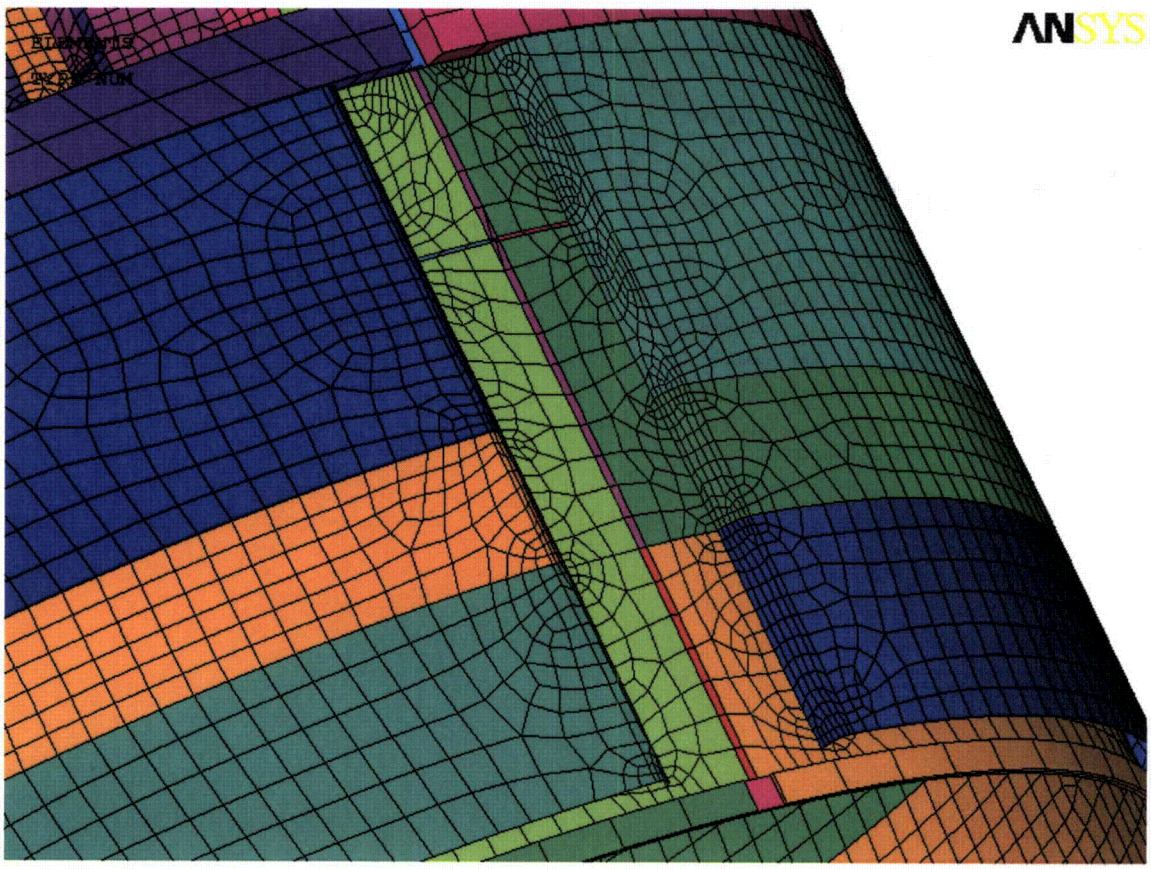

Figure 5e. Close up of mesh showing node-to-node connections between the skirt and drain channels. The colors emphasize element type.

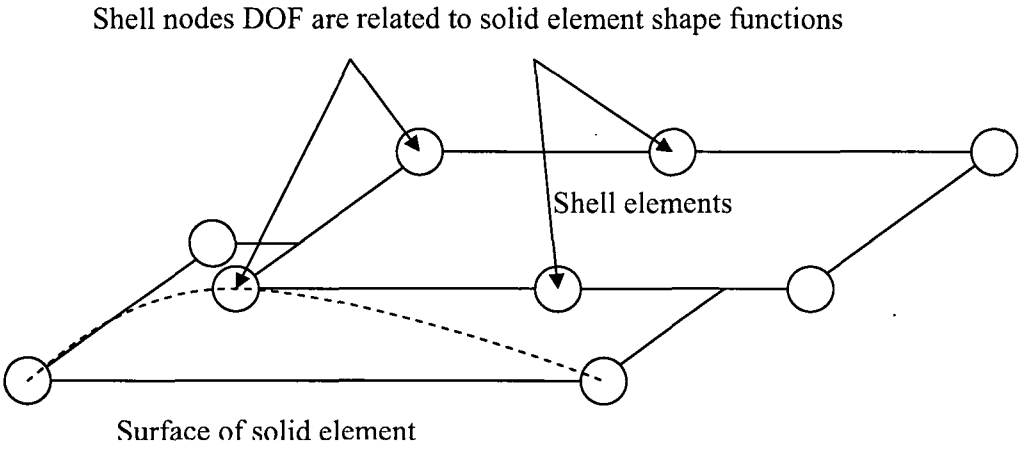

Figure 6a. Face-to-face shell to solid connection.

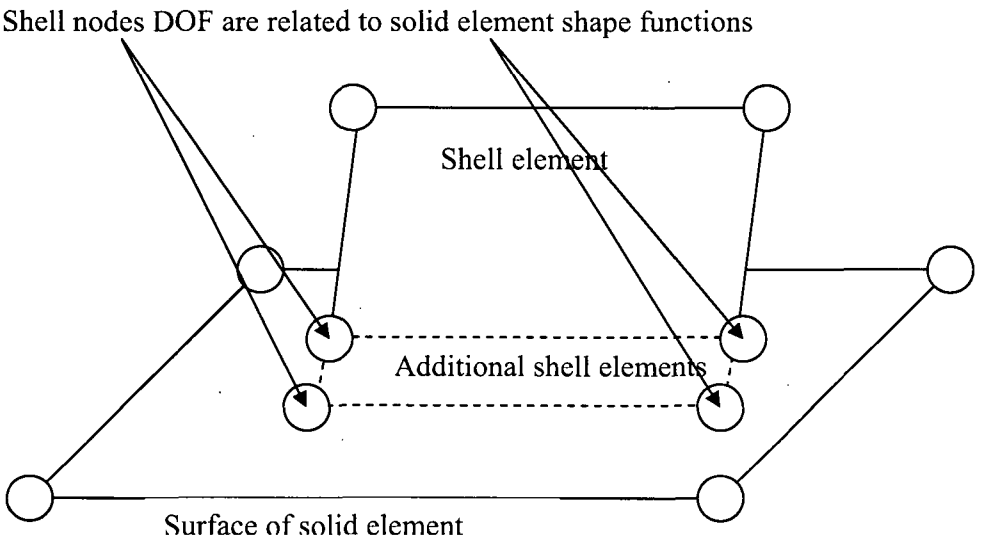

Figure 6b. Shell edge-to-solid face connection.

3.10 Pressure Loading

The harmonic loads are produced by the pressures acting on the exposed surfaces of the steam dryer. At every frequency and for each MSL, the pressure distribution corresponding to a unit pressure at the MSL inlet is represented on a three-inch grid lattice grid (i.e., a mesh whose lines are aligned with the x-, y- and z-directions) that is superimposed over the steam dryer surface. This grid is compatible with the "Table" format used by ANSYS to "paint" general pressure distributions upon structural surfaces. The pressures are obtained from the Helmholtz solver routine in the acoustic analysis [1].

In general, the lattice nodes do not lie on the surface, so that to obtain the pressure differences at the surface, it is necessary to interpolate the pressure differences stored at the lattice nodes. This is done using simple linear interpolation between the eight forming nodes of the lattice cell containing the surface point of interest. Inspection of the resulting pressures at selected nodes shows that these pressures vary in a well-behaved manner between the nodes with prescribed pressures. Graphical depictions of the resulting pressures and comparisons between the peak pressures in the original nodal histories and those in the final surface load distributions produced in ANSYS, all confirm that the load data are interpolated accurately and transferred correctly to ANSYS.

The harmonic pressure loads are only applied to surfaces above the water level, as indicated in Figure 7. In addition to the pressure load, the static loading induced by the weight of the steam dryer is analyzed separately. The resulting static and harmonic stresses are linearly combined to obtain total values which are then processed to calculate maximum and alternating stress intensities for assessment in Section 5.

[[

[3]]] This is useful since revisions in the loads model do not necessitate recalculation of the unit stresses.

The results produced here utilize the Rev. 4 acoustic/hydrodynamic loads model described in [2] to calculate the MSL pressure signals $P_n(\omega)$ and associated biases and uncertainties.

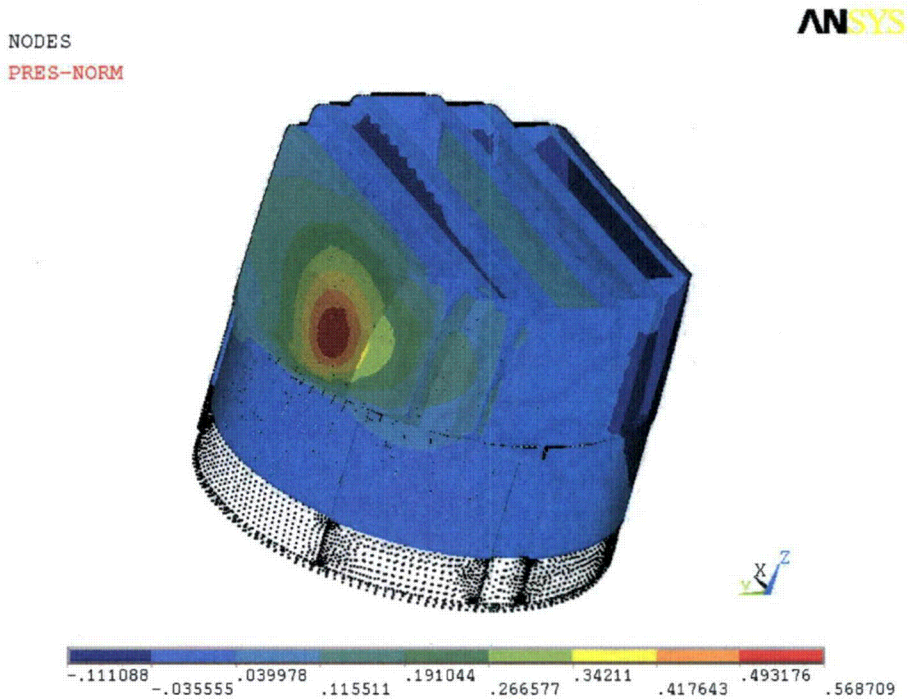

Frequency no. 372: 50.2 Hz

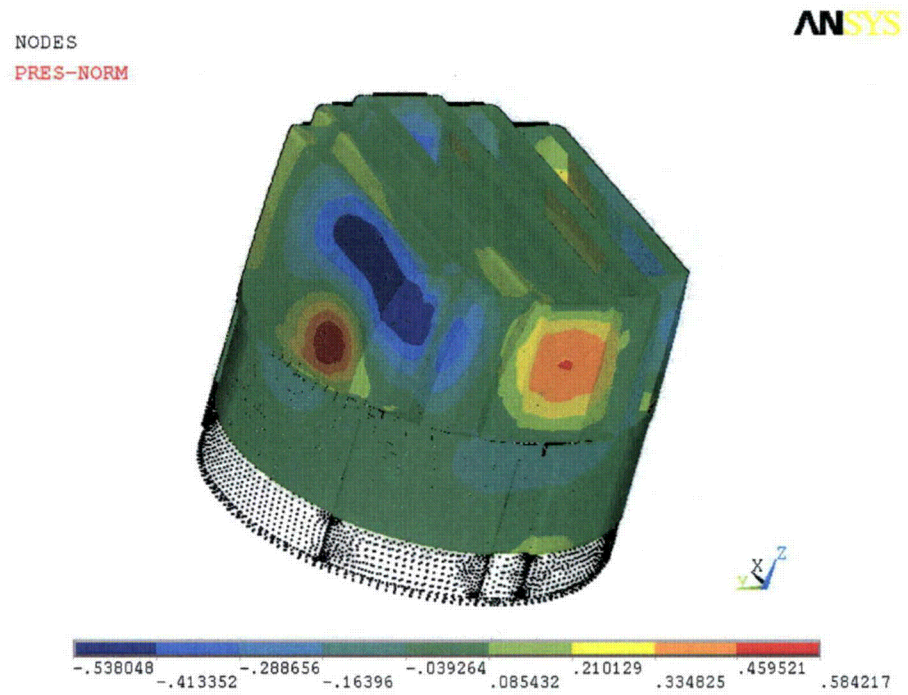

Frequency no. 544: 150.7 Hz

Figure 7. Real part of unit pressure loading MSL C (in psid) on the steam dryer at different frequencies. No loading is applied to submerged parts (nodes at the bottom).

4. Structural Analysis

The solution is decomposed into static and harmonic parts, where the static solution produces the stress field induced by the supported structure subjected to its own weight and the harmonic solution accounts for the harmonic stress field due to the unit pressure of given frequency in one of the main steam lines. All solutions are linearly combined, with amplitudes provided by signal measurements in each steam line, to obtain the final displacement and stress time histories. This decomposition facilitates the prescription of the added mass model accounting for hydrodynamic interaction and allows one to compare the stress contributions arising from static and harmonic loads separately. Proper evaluation of the maximum membrane and membrane+bending stresses requires that the static loads due to weight be accounted for. Hence both static and harmonic analyses are carried out.

4.1 Static Analysis

The results of the static analysis are shown in Figure 8. Only a few locations exhibited high stress intensity levels. These locations include the skirt/upper support ring connection with stress intensity 8,775 psi, the trough thin section/vane bank end plate/thick closure plate junction with stress intensity 5,416 psi and the thin closure plate/inner hood junction with stress intensity 8,133 psi. All locations are near the steam dryer support brackets. Close up views of these locations are shown in Figure 9. Note that these locations have high stress intensity also when static and transient runs are combined, primarily due to static loading.

4.2 Harmonic Analysis

The harmonic pressure loads were applied to the structural model at all surface nodes described in Section 3.10. Typical stress intensity distributions over the structure are shown in Figure 10. Stresses were calculated for each frequency, and results from static and harmonic calculations were combined.

To evaluate maximum stresses, the stress harmonics including the static component are transformed into a time history using FFT, and the maximum and alternating stress intensities for the response, evaluated. According to ASME B&PV Code, Section III, Subsection NG-3216.2 the following procedure was established to calculate alternating stresses. For every node, the stress difference tensors, $\boldsymbol{\sigma}'_{nm} = \boldsymbol{\sigma}_n - \boldsymbol{\sigma}_m$, are considered for all possible pairs of the stresses $\boldsymbol{\sigma}_n$ and $\boldsymbol{\sigma}_m$ at different time levels, t_n and t_m. Note that all possible pairs require consideration, since there are no "obvious" extrema in the stress responses. However, in order to contain computational cost, extensive screening of the pairs takes place (see Section 2.3), so that pairs known to produce alternating stress intensities less than 1,500 psi are rejected. For each remaining stress difference tensor, the principal stresses S_1, S_2, S_3 are computed and the maximum absolute value among principal stress differences, $S_{nm} = \max\{|S_1 - S_2|, |S_1 - S_3|, |S_2 - S_3|\}$, obtained. The alternating stress at the node is then one-half the maximum value of S_{nm} taken over all combinations (n,m), i.e., $S_{alt} = \frac{1}{2}\max_{n,m}\{S_{nm}\}$. This alternating stress is compared against allowable values, depending on the node location with respect to welds.

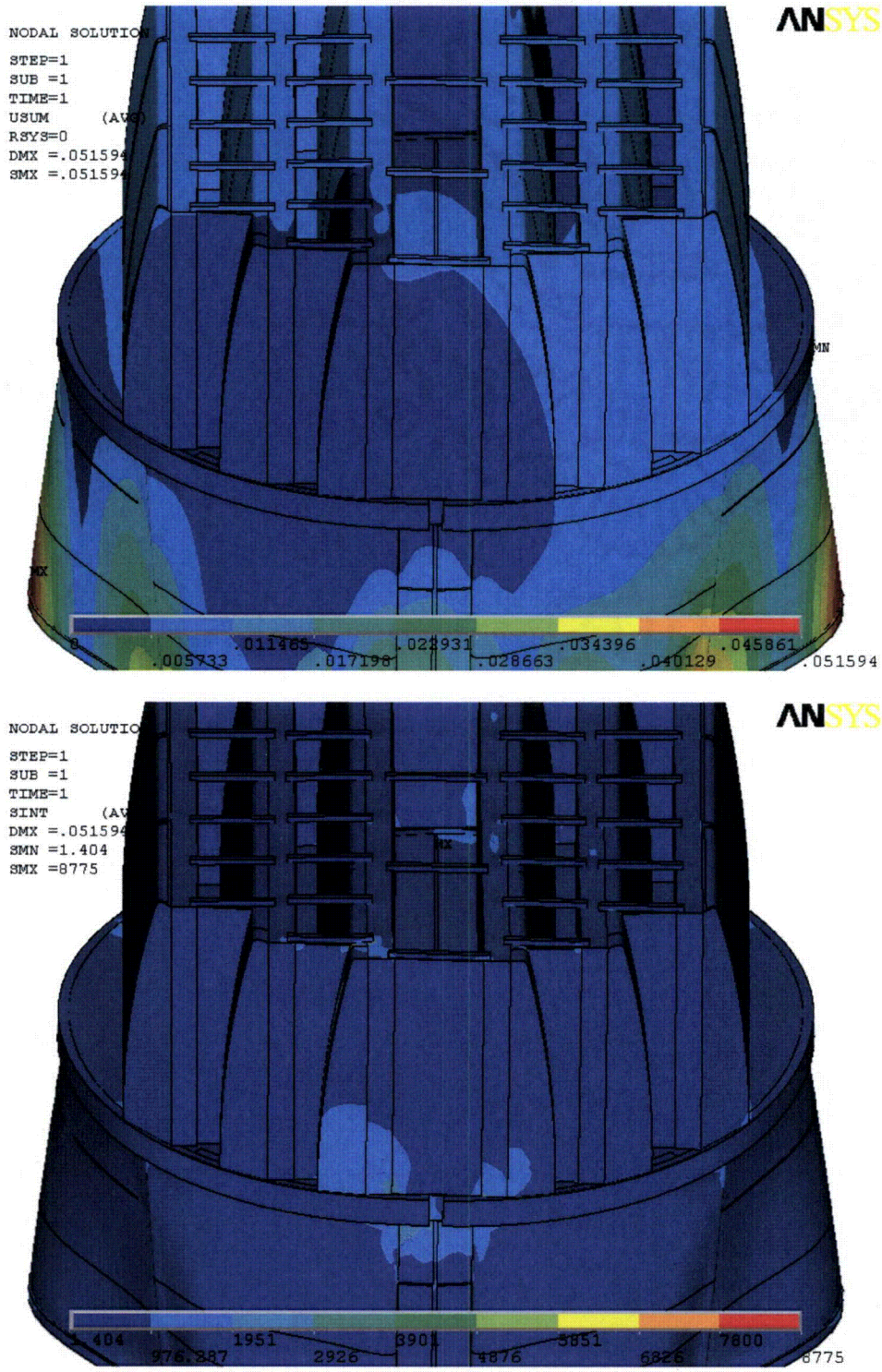

Figure 8. Overview of static calculations showing displacements (top, in inches) and stress intensities (bottom, in psi). Maximum displacement (DMX) is 0.052"; maximum stress intensity (SMX) is 8,775 psi. Note that displacements are amplified for visualization.

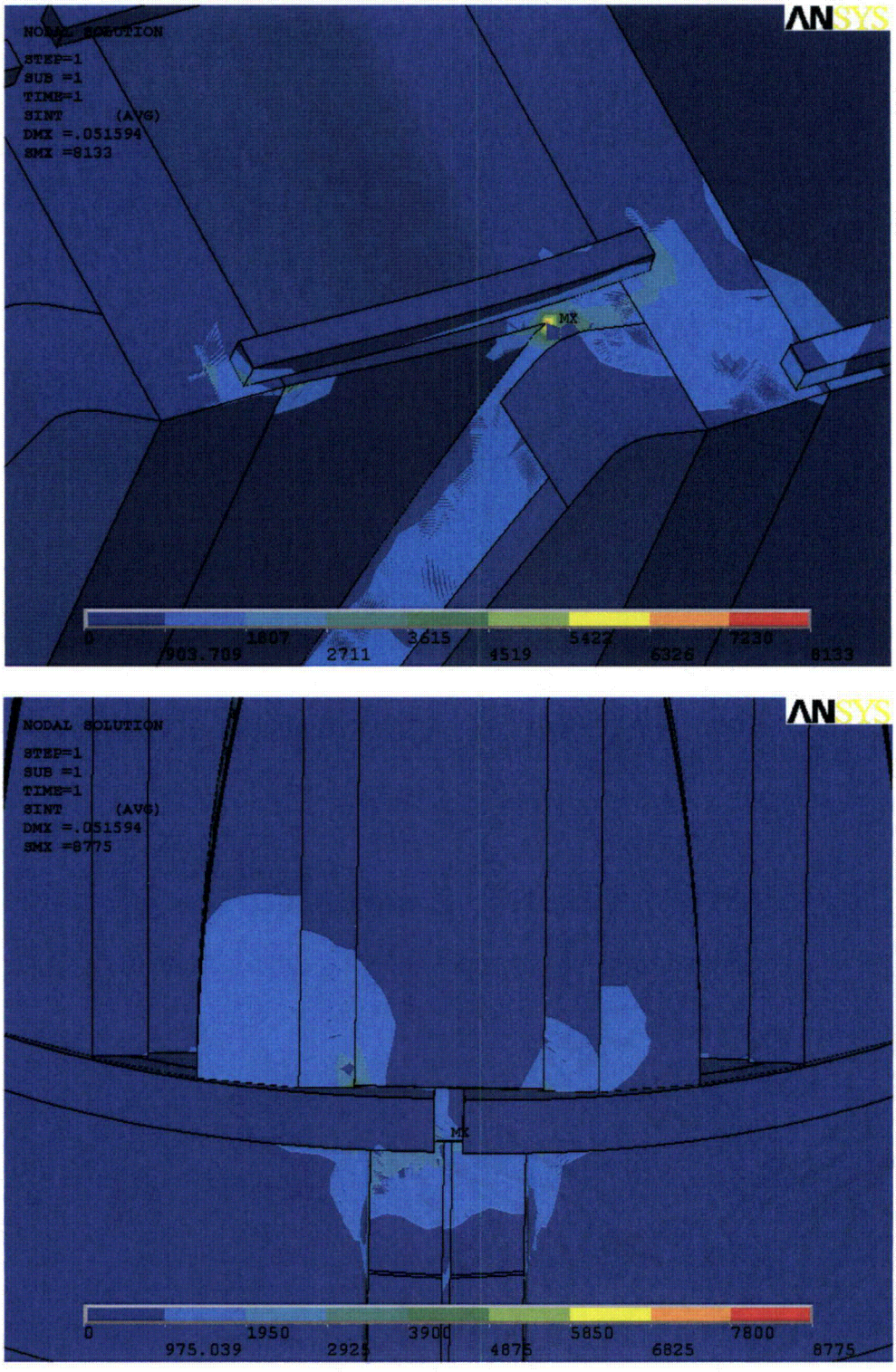

Figure 9. Close up of high static stress intensity (in psi) locations at closure plates and near support brackets.

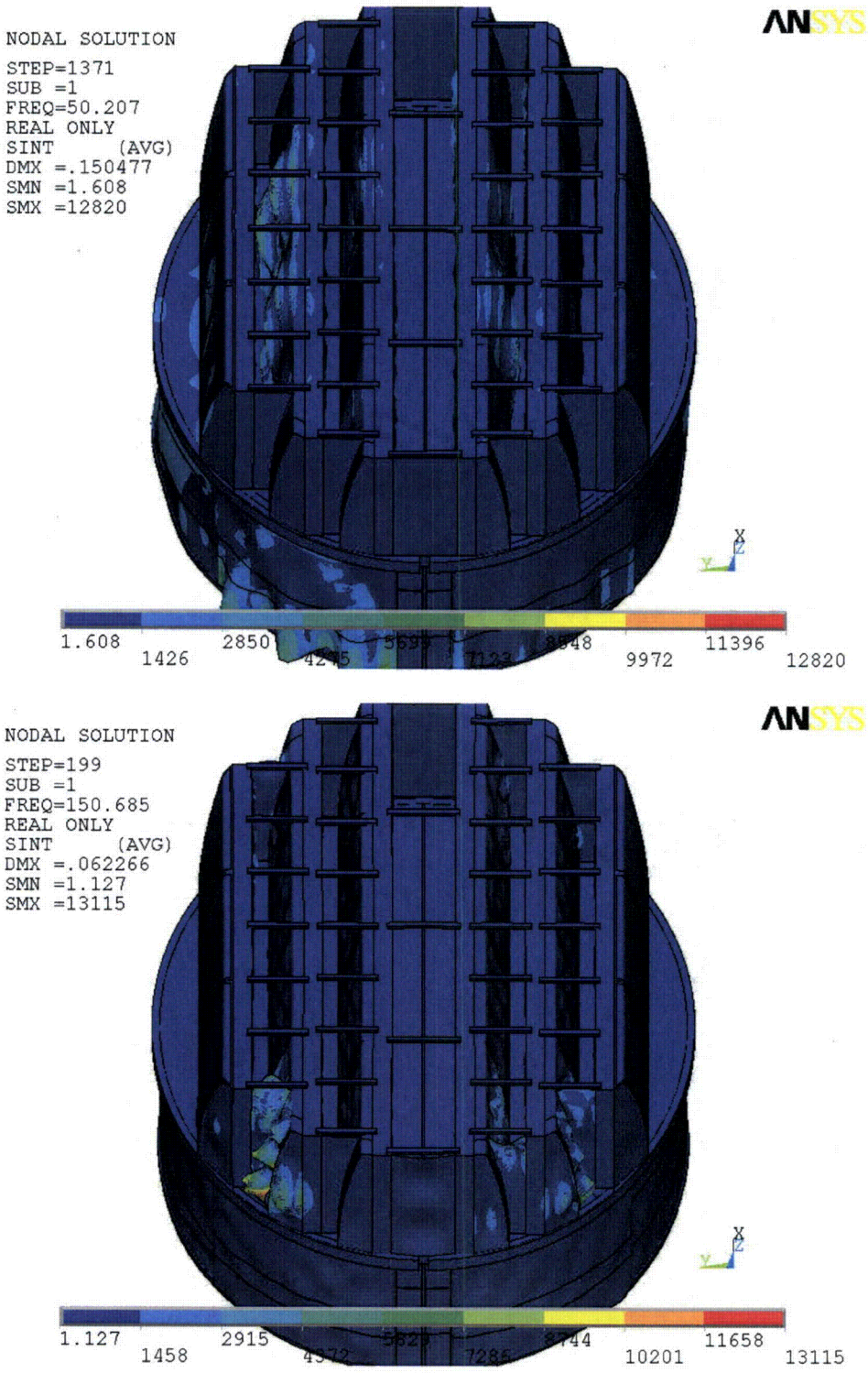

Figure 10. Overview of harmonic calculations showing real part of stress intensities (in psi) along with displacements. Unit loading MSL C for frequencies 50.2 Hz (top) and 150.7 Hz (bottom).

4.3 Post-Processing

The static and unsteady stresses computed at every node with ANSYS were exported into files for subsequent post-processing. These files were then read into separate customized software to compute the maximum and alternating stresses at every node. The maximum stress was defined for each node as the largest stress intensity occurring during the time history. Alternating stresses were calculated according to the ASME standard described above. For shell elements the maximum stresses were calculated separately at the mid-plane, where only membrane stress is present, and at top/bottom of the shell, where bending stresses are also present.

For nodes that are shared between several structural components or lie on junctions, the maximum and alternating stress intensities are calculated as follows. First, the nodal stress tensor is computed separately for each individual component by averaging over all finite elements meeting at the node and belonging to the same structural component. The time histories of these stress tensors are then processed to deduce the maximum and alternating stress intensities for each structural component. Finally, for nodes shared across multiple components, the highest of the component-wise maximum and alternating stresses is recorded as the "nodal" stress. This approach prevents averaging of stresses across components and thus yields conservative estimates for nodal stresses at the weld locations where several components are joined together.

The maximum stresses are compared against allowable values which depend upon the stress type (membrane, membrane+bending, alternating – Pm, Pm+Pb, S_{alt}) and location (at a weld or away from welds). These allowables are specified in the following section. For solid elements the most conservative allowable for membrane stress, Pm, is used, although bending stresses are nearly always present also. The structure is then assessed in terms of stress ratios formed by dividing allowables by the computed stresses at every node. Stress ratios less than unity imply that the associated maximum and/or alternating stress intensities exceed the allowable levels. Post-processing tools calculate the stress ratios, identifying the nodes with low stress ratios and generating files formatted for input to the 3D graphics program, TecPlot, which provides more general and sophisticated plotting options than currently available in ANSYS.

4.4 Computation of Stress Ratios for Structural Assessment

The ASME B&PV Code, Section III, subsection NG provides different allowable stresses for different load combinations and plant conditions. The stress levels of interest in this analysis are for the normal operating condition, which is the Level A service condition. The load combination for this condition is:

Normal Operating Load Combination = Weight + Pressure + Thermal

The weight and fluctuating pressure contributions have been calculated in this analysis and are included in the stress results. The static pressure differences and thermal expansion stresses are small, since the entire steam dryer is suspended inside the reactor vessel and all surfaces are exposed to the same conditions. Seismic loads only occur in Level B and C cases, and are not

considered in this analysis. No physical modifications were made to the HC1 steam dryer since commercial operation; therefore, seismic loading would not change.

Allowable Stress Intensities

The ASME B&PV Code, Section III, subsection NG shows the following (Table 4) for the maximum allowable stress intensity (Sm) and alternating stress intensity (Sa) for the Level A service condition. The allowable stress intensity values for type 304 stainless steel at operating temperature 550°F are taken from Table I-1.2 and Fig. I-9.2.2 of Appendix I of Section III, in the ASME B&PV Code. The calculation for different stress categories is performed in accordance with Fig. NG-3221-1 of Division I, Section III, subsection NG.

Table 4. Maximum allowable stress intensity and alternating stress intensity for all areas other than welds. The notation Pm represents membrane stress; Pb represents stress due to bending; Q represents secondary stresses (from thermal effects and gross structural discontinuities, for example); and F represents additional stress increments (due to local structural discontinuities, for example).

Type	Notation	Service Limit	Allowable Value (psi)
Maximum Stress Allowables:			
General Membrane	Pm	Sm	18,300
Membrane + Bending	Pm + Pb	1.5 Sm	27,450
Primary + Secondary	Pm + Pb + Q	3.0 Sm	54,900
Alternating Stress Allowable:			
Peak = Primary + Secondary + F	S_{alt}	Sa	13,600

When evaluating welds, either the calculated or allowable stress was adjusted, to account for stress concentration factor and weld quality. Specifically:

- For maximum allowable stress intensity, the allowable value is decreased by multiplying its value in Table 4 by 0.55.

- For alternating stress intensity, the calculated weld stress intensity is multiplied by a weld stress intensity (fatigue) factor of 1.8, before comparison to the Sa value given above.

The weld factors of 0.55 and 1.8 were selected based on the observable quality of the shop welds and liquid penetrant NDE testing of all welds (excluding tack and intermittent welds, which were subject to 5X visual inspection) during fabrication. These factors are consistent with fatigue strength reduction factors recommended by the Welding Research Council, [10], and stress concentration factors at welds, provided in [11] and [12]. GE Purchase Specification for the HCGS Steam Dryer (21A9355 Section 9.2) called for liquid penetrant testing of all welds (excluding tack and intermittent welds) along the entire length or circumference, using the guidance of ASME Boiler and Pressure Code, Paragraph N-6127.3. In addition, critical welds are subject to periodical visual inspections in accordance with the requirements of GE SIL 644 SIL and BWR VIP-139 [13]. Therefore, for weld stress intensities, the allowable values are shown in Table 5.

These factors (0.55 and 1.8) also conservatively presume that the structure is joined using fillet welds unless specified otherwise. Since fillet welds correspond to larger stress concentration factors than other types of welds, this assumption is a conservative one.

Table 5. Weld Stress Intensities.

Type	Notation	Service Limit	Allowable Value (psi)
Maximum Stress Allowables:			
General Membrane	Pm	0.55 Sm	10,065
Membrane + Bending	Pm + Pb	0.825 Sm	15,098
Primary + Secondary	Pm + Pb + Q	1.65 Sm	30,195
Alternating Stress Allowables:			
Peak = Primary + Secondary + F	S_{alt}	Sa	13,600

Comparison of Calculated and Allowable Stress Intensities

The classification of stresses into general membrane or membrane + bending types was made according to the exact location, where the stress intensity was calculated; namely, general membrane, Pm, for middle surface of shell element, and membrane + bending, Pm + Pb, for other locations. For solid elements the most conservative, general membrane, Pm, allowable is used.

The structural assessment is carried out by computing stress ratios between the computed maximum and alternating stress intensities, and the allowable levels. Locations where any of the stresses exceed allowable levels will have stress ratios less than unity. Since computation of stress ratios and related quantities within ANSYS is time-consuming and awkward, a separate FORTRAN code was developed to compute the necessary maximum and alternating stress intensities, Pm, Pm+Pb, and S_{alt}, and then compare it to allowables. Specifically, the following quantities were computed at every node:

1. The maximum membrane stress intensity, Pm (evaluated at the mid-thickness location for shells),
2. The maximum membrane+bending stress intensity, Pm+Pb, (taken as the largest of the maximum stress intensity values at the bottom, top, and mid thickness locations, for shells),
3. The alternating stress, S_{alt}, (the maximum value over the three thickness locations is taken).
4. The stress ratio due to a maximum stress intensity assuming the node lies at a non-weld location (note that this is the minimum ratio obtained considering both membrane stresses and membrane+bending stresses):
   SR-P(nw) = min{ Sm/Pm, 1.5 * Sm/(Pm+Pb) }.
5. The alternating stress ratio assuming the node lies at a non-weld location,
   SR-a(nw) = Sa / (1.1 * S_{alt}),
6. The same as 4, but assuming the node lies on a weld,
   SR-P(w)=SR-P(nw) * f_{sw} * 0.55

7. The same as 5, but assuming the node lies on a weld,
   SR-a(w)=SR-a(nw) * f_{sw} / 1.8.

where f_{sw}=1 at all welds (when justified, f_{sw} can be adjusted to reflect different weld types). Note that in steps 4 and 6, the minimum of the stress ratios based on Pm and Pm+Pb, is taken. The allowables listed in Table 4, Sm=18,300 psi and Sa=13,600 psi. The factors, 0.55 and 1.8, are the weld factors discussed above. The factor of 1.1 accounts for the differences in Young's moduli for the steel used in the steam dryer and the values assumed in alternating stress allowable. According to NG-3222.4 in subsection NG of Section III of the ASME Code, the effect of elastic modulus upon alternating stresses is taken into account by multiplying alternating stress S_{alt} at all locations by the ratio, E/E_{model}=1.1, where:

$E = 28.3\ 10^6$ psi, as shown on Fig. I-9.2.2. ASME BP&V Code
$E_{model} = 25.55\ 10^6$ psi (Table 1)

The nodes with stress ratios lower than 4 are plotted in TecPlot (a 3D graphics plotting program widely used in engineering communities [14]) to establish whether they lie on a weld or not. The appropriate maximum and alternating stress ratios, SR-P and SR-a, are thus determined and a final listing of nodes having the smallest stress ratios is generated. These nodes are tabulated and depicted in the following Results Section.

5. Results

The stress intensities and associated stress ratios resulting from the Rev. 4 acoustic/hydrodynamic loads [2] with associated biases and uncertainties factored in, are presented below. Section 5.1 tabulates the highest maximum and alternating stress intensities and presents contour plots of these stresses to indicate which points on the dryer experience significant stress concentration and/or modal response. Section 5.2 compares the stresses against allowable values, accounting for stress type (maximum and alternating) and location (on or away from a weld). The results are presented in terms of stress ratios and the locations with the lowest stress ratios are identified. Section 5.3 examines the spectral content of select nodes showing the presence of a strong 80 Hz signal in the stress response. The origins of this signal are briefly discussed in section 5.4 together with justifications for removing part of it. Since the results in sections 5.1 to 5.3 included the entire 80 Hz component, section 5.4 also tabulates the stress ratios resulting when 90% of this signal is removed.

In each section, results are presented both at nominal conditions (no frequency shift) and with frequency shift included. Frequency shifts are generally performed at 2.5% increments except in section 5.3 where they are performed at higher resolution (0.5%) for the nodes identified as having the lowest stress ratios.

Finally, the tabulated stresses and stress ratios are obtained using a 'blanking' procedure that is designed to prevent reporting a large number of high stress nodes from essentially the same location on the structure. In the case of stress intensities (section 5.1) this procedure is as follows. The relevant stress intensities are first computed at every node and then nodes sorted according to stress level. The highest stress node is noted and all neighboring nodes within 10 inches of the highest stress node and its symmetric images (i.e., reflections across the x=0 and y=0 planes) are "blanked" (i.e., excluded from the search for subsequent high stress locations). Of the remaining nodes, the next highest stress node is identified and its neighbors (closer than 10 inches) blanked. The third highest stress node is similarly located and the search continued in this fashion until all nodes are either blanked or have stresses less than half the highest value on the structure. In Section 5.2, a similar blanking procedure is applied to the stress ratios rather than stresses. Thus the lowest stress ratio of a particular type in a 10" neighborhood and its symmetric images is identified and all other nodes in these regions excluded from listing in the table. Of the remaining nodes, the one with the lowest stress ratio is reported and its neighboring points similarly excluded, and so on until all nodes are either blanked or have a stress ratio higher than 4.

5.1 General Stress Distribution and High Stress Locations

The maximum stress intensities obtained by post-processing the ANSYS stress histories for CLTP at nominal frequency and with frequency shift operating conditions are listed in Table 6. Contour plots of the stress intensities over the steam dryer structure are shown on Figure 11 (nominal frequency), Figure 12 (maximum stress over all nine frequency shifts including nominal), and Figure 13 (-7.5% frequency shift where the alternating stress response is strongest). The figures are oriented to emphasize the high stress regions. Note that these stress intensities *do not* account for weld factors but do include end-to-end bias and uncertainty.

Further, it should be noted that since the allowable stresses vary with location, stress intensities do not necessarily correspond to regions of primary structural concern. Instead, structural evaluation is more accurately made in terms of the stress ratios which compare the computed stresses to allowable levels with due account made for stress type and weld factors. Comparisons on the basis of stress ratios are made in Section 5.2.

The maximum stress intensities in most areas are low (less than 500 psi, or 5% of the most conservative critical stress). For the membrane stresses (Pm) the high stress regions tend to occur at: (i) the outermost portion of the inner hood near the connection to the closure plate; (ii) the weld joining the skirt and the upper support ring near the supports; and (iii) the central base plate/vane bank junction. In all cases the stress is dominated by static stresses as evidenced by the small alternating stresses (less than 1500 psi) in the rightmost columns in the table. The closure plates and regions in the vicinity of where they connect to adjacent hoods or vane banks, experience high stresses since they restrain any deflection of the adjacent vane banks.

The membrane + bending stress (Pm+Pb) distributions evidence a more pronounced modal response in all cases. However, the highest stress locations are still dominated by the static component as is confirmed by the low alternating stress values in the right hand column of Table 6. Modal excitations are most pronounced on the hoods, perforated plates and skirt structure. Comparison of the nominal (0% frequency shift) and -7.5% frequency shift results shows that different modes are excited in each case. For example, in the nominal case the central plate in the outer hood shows the strongest response on this hood whereas at the -7.5% shift the outer two portions exhibit the dominant response. Stress concentrations are visible near the hood supports, at the bottoms of the hoods, near the tops of the closure plates and along the skirt/drain channel welds.

The alternating stresses are generally small at nominal operation with the highest reported value (1,821 psi) occurring on a non-weld location on the perforated plates and the highest value on a weld being only 1,625 psi at the bottom of a perforated plate. This is very close to the 1,500 psi cutoff value used in the alternating stress calculation so that alternating stresses can be safely summarized as being essentially marginal or negligible (i.e., having an associated stress ratio > 4) at zero frequency shift. These stresses are, however, sensitive to frequency shift and all five of the locations identified as having the highest alternating stresses over all frequency shifts assume their highest values at the -7.5% shift. The alternating stress intensity contour plots essentially record the modes excited by this signal, which here are seen to be confined to perforated plates and inner or middle hoods which, though not directly exposed to the main MSL pressure fluctuations (like the outer hoods are) are of thinner construction and therefore exhibit a significant response. The largest alternating stress is more than twice the nominal shift value further evidencing a strong frequency-dependence upon the load spectrum.

Table 6a. Locations with highest predicted stress intensities for CLTP conditions with no frequency shift. Alternating stresses are only computed at nodes where stresses can exceed 1500 psi.

Stress Category	Location		Location (in)				Stress Intensities (psi)		
		Weld	x	y	z	node	Pm	Pm+Pb	S_{alt}
Pm	outer portion of inner hood (top near closure plate)	No	109.0	-27.6	95.3	44886	5963	8481	<1500
"	central base plate/inner vane bank/side panel	Yes	-118.8	14.4	7.5	85994	4062	5595	<1500
"	skirt/upper support ring	Yes	118.7	-5.9	-2.0	91960	3967	5903	<1500
"	closure plate/top cover plate/vane side plate/ perforated plate	Yes	108.4	-45.9	95.9	91627	3719	4277	<1500
"	inner hood backing bar/closure plate	Yes	-108.4	38.4	8.1	87035	3673	3874	<1500
Pm+Pb	skirt/upper support ring	Yes	118.8	0.6	-2.0	88325	2330	9575	<1500
"	outer portion of inner hood (top near closure plate)	No	109.0	-27.6	95.3	44886	5963	8481	<1500
"	central base plate/inner vane bank/side panel	Yes	-118.8	14.4	7.5	85994	4062	5595	<1500
"	cover plate/outer hood	Yes	59.1	101.4	7.5	93493	1437	5455	<1500
"	drain pipe/skirt	Yes	88.2	79.6	-20.5	91083	1925	5418	<1500
S_{alt}	middle vane bank perforated entry plate	No	26.3	-54.4	48.5	71368	239	1867	1821
"	middle vane bank/perforated entry plate	Yes	38.9	-54.4	21.5	80204	286	1742	1625
"	inner hood	No	30.0	-35.8	51.7	43406	707	1614	1578
"	outer hood	No	0.3	94.9	74.9	33378	267	1576	1570
"	outer hood	No	-4.7	90.3	94.9	33995	267	1652	1567

Node numbers are retained for further reference.
Spatial coordinate are in the coordinate system, defined by the origin at the centerline of steam dryer 7.5" below bottom plates. The x-axis is parallel to the hoods, y-axis is normal to the hoods pointing from MSL AB to MSL CD, z-axis is vertical, positive up.

Table 6b. Locations with highest predicted stress intensities taken over all frequency shifts CLTP conditions. Alternating stresses are only computed at nodes where stresses can exceed 1500 psi.

Stress Category	Location	Weld	% Freq. Shift	Location (in)				Stress Intensities (psi)		
				x	y	z	node	Pm	Pm+Pb	S_{alt}
Pm	outer portion of inner hood (top near closure plate)	No	-10	109.0	-27.6	95.3	44886	6433	9178	<1500
"	central base plate/inner vane bank/side panel	Yes	-10	-118.8	14.4	7.5	85994	4122	5664	<1500
"	inner hood backing bar/closure plate	Yes	-7.5	-108.4	38.4	8.1	87035	4005	4184	<1500
"	skirt/upper support ring	Yes	0	118.7	-5.9	-2.0	91960	3967	5903	<1500
"	closure plate/middle side panel/top cover plate/ top perforated plate	Yes	-10	-108.4	45.9	95.9	85891	3852	4516	<1500
Pm+Pb	skirt/upper support ring	Yes	0	118.8	0.6	-2.0	88325	2330	9575	<1500
"	outer portion of inner hood (top near closure plate)	No	-10	109.0	-27.6	95.3	44886	6433	9178	<1500
"	cover plate/outer hood	Yes	-7.5	-59.1	-101.4	7.5	93288	1957	6607	2447
"	central base plate/inner vane bank/side panel	Yes	-10	-118.8	14.4	7.5	85994	4122	5664	<1500
"	drain pipe/skirt	Yes	+5	88.2	79.6	-20.5	91083	1973	5522	<1500
S_{alt}	outer vane bank/perforated entry plate	Yes	-7.5	1.9	85.9	21.5	82290	213	3773	3699
"	middle base plate/middle vane bank	Yes	-7.5	-83.4	54.4	7.5	86424	414	3823	3630
"	outer vane bank perforated entry plate	No	-7.5	3.8	85.9	34.9	61491	202	3610	3556
"	outer vane bank perforated entry plate	No	-7.5	2.2	85.9	63.0	61581	230	3517	3475
"	middle vane bank perforated entry plate	No	-7.5	95.6	54.4	80.6	69772	895	3440	3315

See Table 6a for coordinates description.

Table 6c. Locations with highest predicted stress intensities for CLTP conditions with -7.5% frequency shift. Alternating stresses are only computed at nodes where stresses can exceed 1500 psi.

Stress Category	Location		Location (in)				Stress Intensities (psi)		
		Weld	x	y	z	node	Pm	Pm+Pb	S_{alt}
Pm	outer portion of inner hood (top near closure plate)	No	109.0	-27.6	95.3	44886	6283	8951	<1500
"	central base plate/inner vane bank/side panel	Yes	-118.8	14.4	7.5	85994	4074	5604	<1500
"	inner hood backing bar/closure plate	Yes	-108.4	38.4	8.1	87035	4005	4184	<1500
"	skirt/upper support ring	Yes	118.7	-5.9	-2.0	91960	3929	5770	<1500
"	closure plate/middle side panel/top cover plate/ top perforated plate	Yes	-108.4	45.9	95.9	85891	3774	4459	<1500
Pm+Pb	skirt/upper support ring	Yes	118.8	0.6	-2.0	88325	2287	9359	<1500
"	outer portion of inner hood (top near closure plate)	No	109.0	-27.6	95.3	44886	6283	8951	<1500
"	cover plate/outer hood	Yes	-59.1	-101.4	7.5	93288	1957	6607	2447
"	central base plate/inner vane bank/side panel	Yes	-118.8	14.4	7.5	85994	4074	5604	<1500
"	drain pipe/skirt	Yes	88.2	79.6	-20.5	91083	1932	5444	<1500
S_{alt}	outer vane bank/perforated entry plate	Yes	1.9	85.9	21.5	82290	213	3773	3699
"	middle base plate/middle vane bank	Yes	-83.4	54.4	7.5	86424	414	3823	3630
"	outer vane bank perforated entry plate	No	3.8	85.9	34.9	61491	202	3610	3556
"	outer vane bank perforated entry plate	No	2.2	85.9	63.0	61581	230	3517	3475
"	middle vane bank perforated entry plate	No	95.6	54.4	80.6	69772	895	3440	3315

See Table 6a for coordinates description.

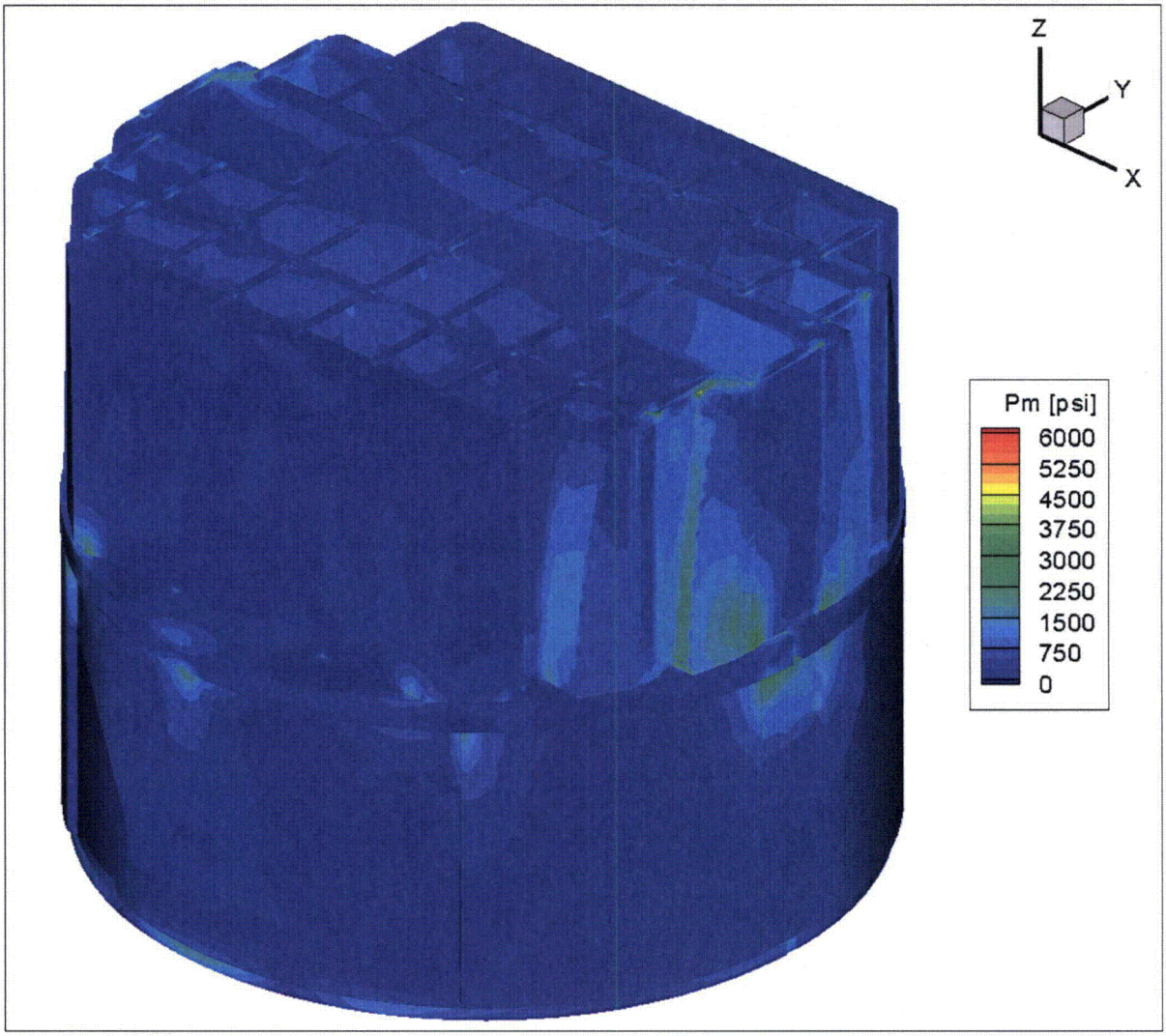

Figure 11a. Contour plot of maximum membrane stress intensity, Pm, for CLTP load. The maximum stress intensity is 5,963 psi.

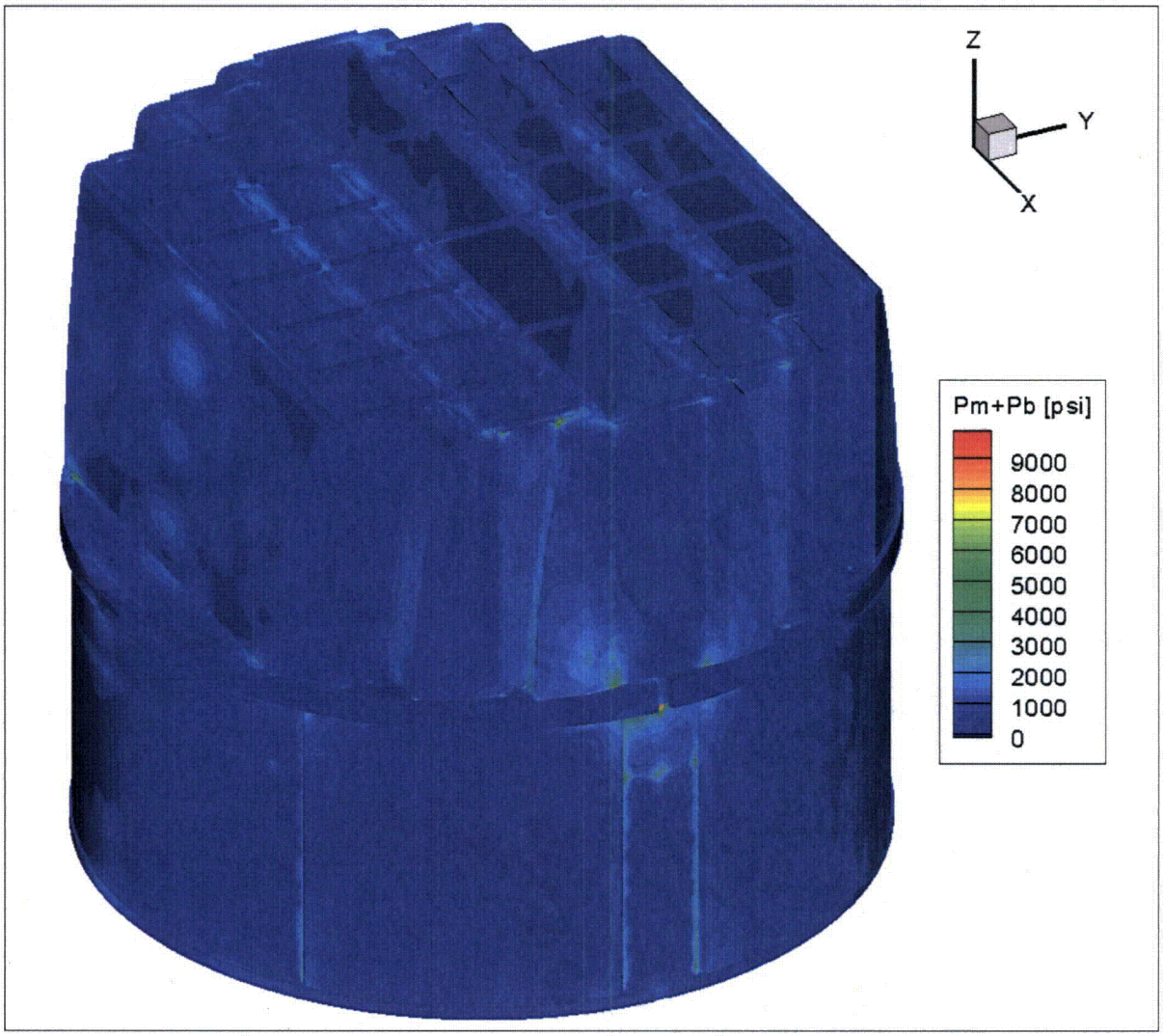

Figure 11b. Contour plot of maximum membrane+bending stress intensity, Pm+Pb, for CLTP load. The maximum stress intensity is 9,575 psi. First view.

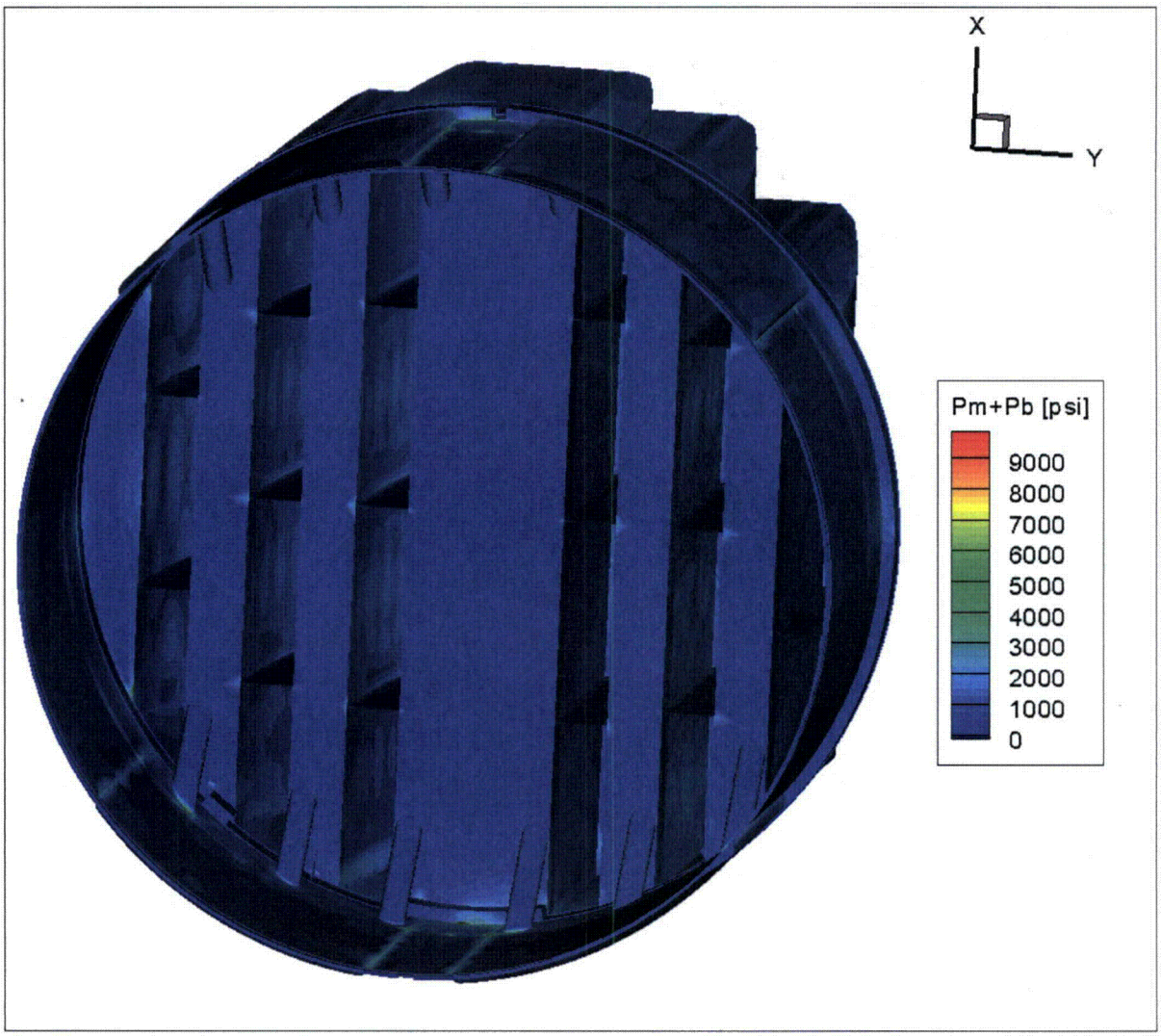

Figure 11c. Contour plot of maximum membrane+bending stress intensity, Pm+Pb, for CLTP load. Second view from below.

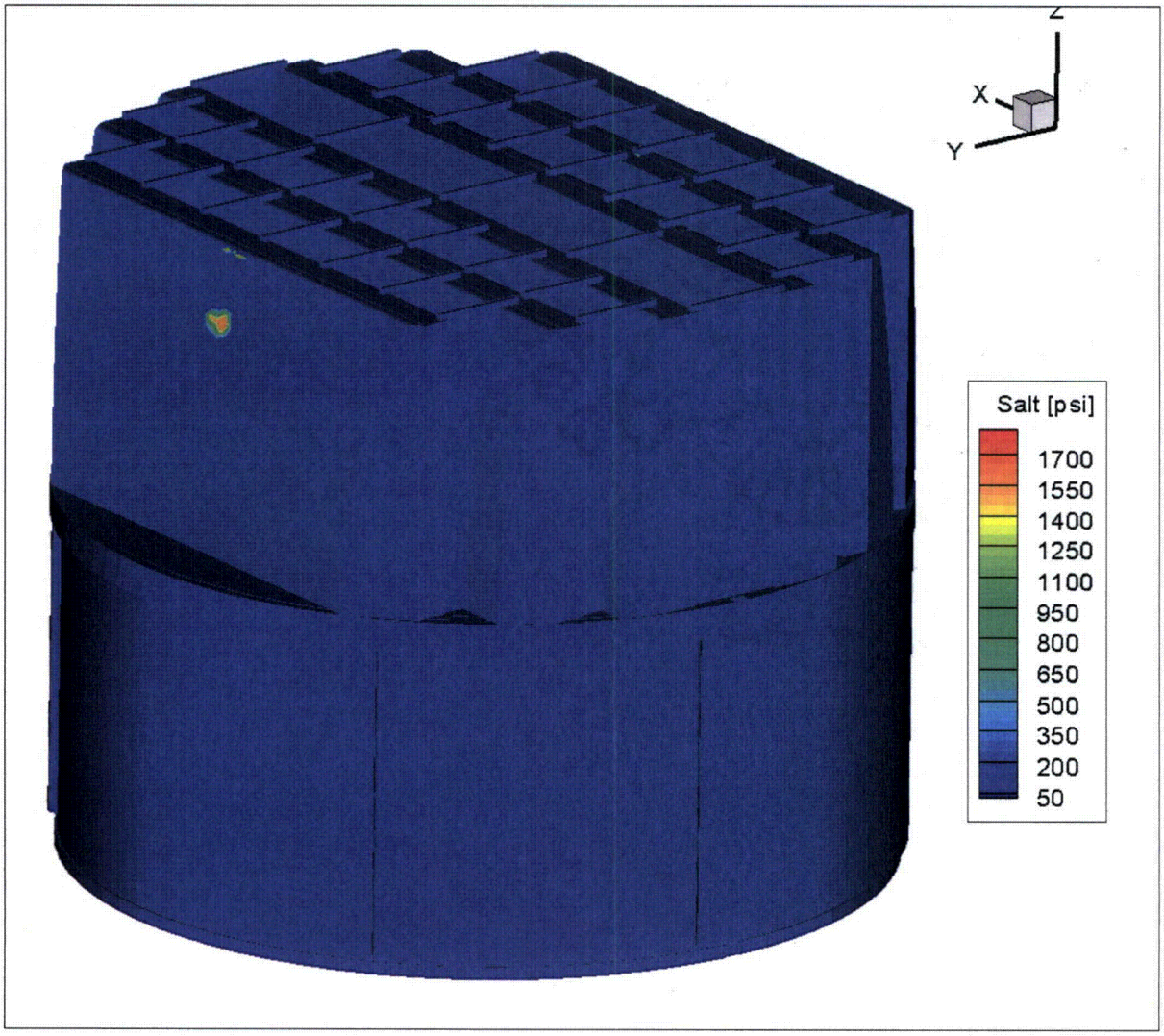

Figure 11d. Contour plot of alternating stress intensity, S_{alt}, for CLTP load. The highest alternating stress intensity is 1,821 psi. First view.

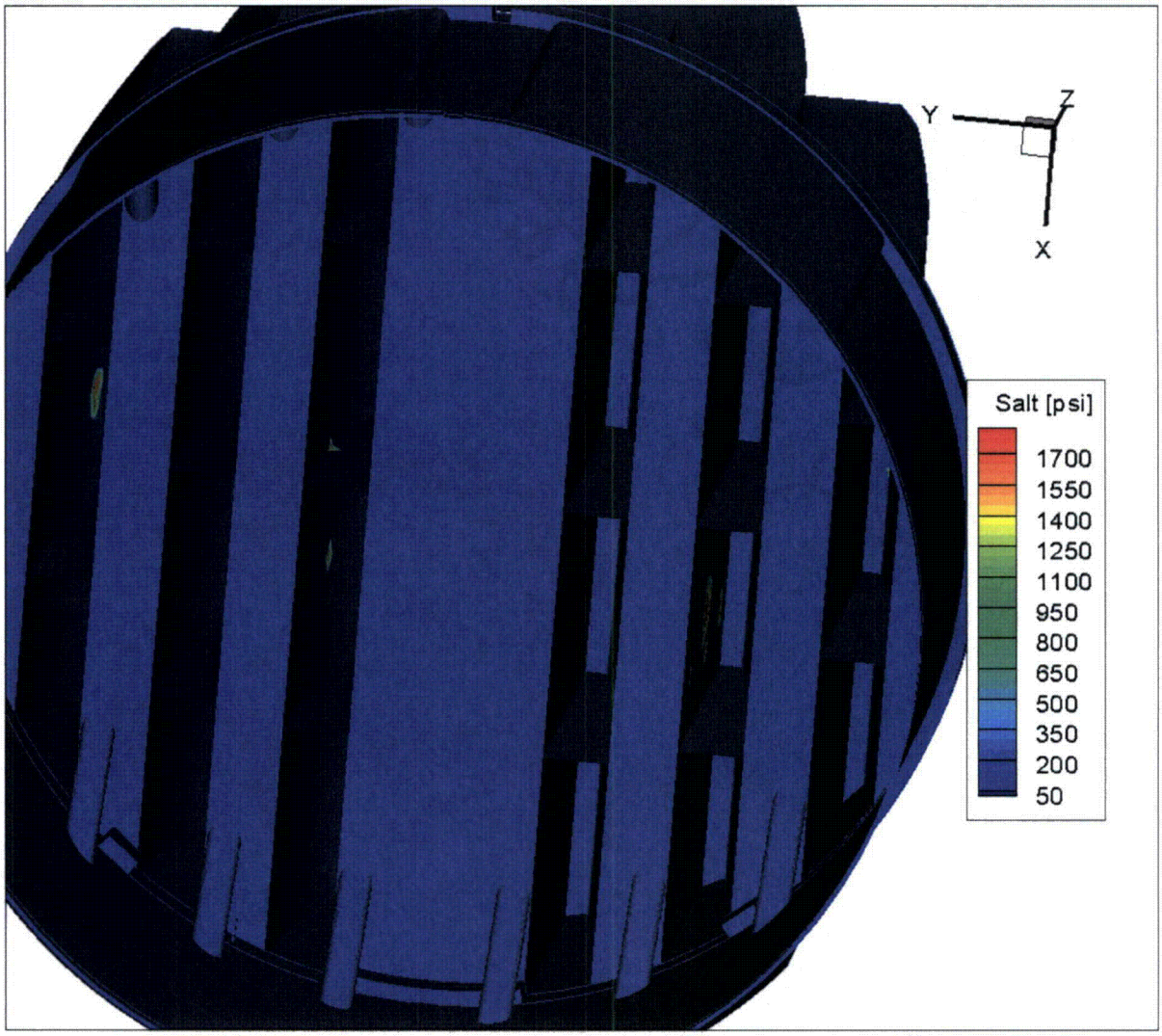

Figure 11e. Contour plot of alternating stress intensity, S_{alt}, for CLTP load. This second view from below shows the high alternating stress intensity near the hood supports and on perforated plates.

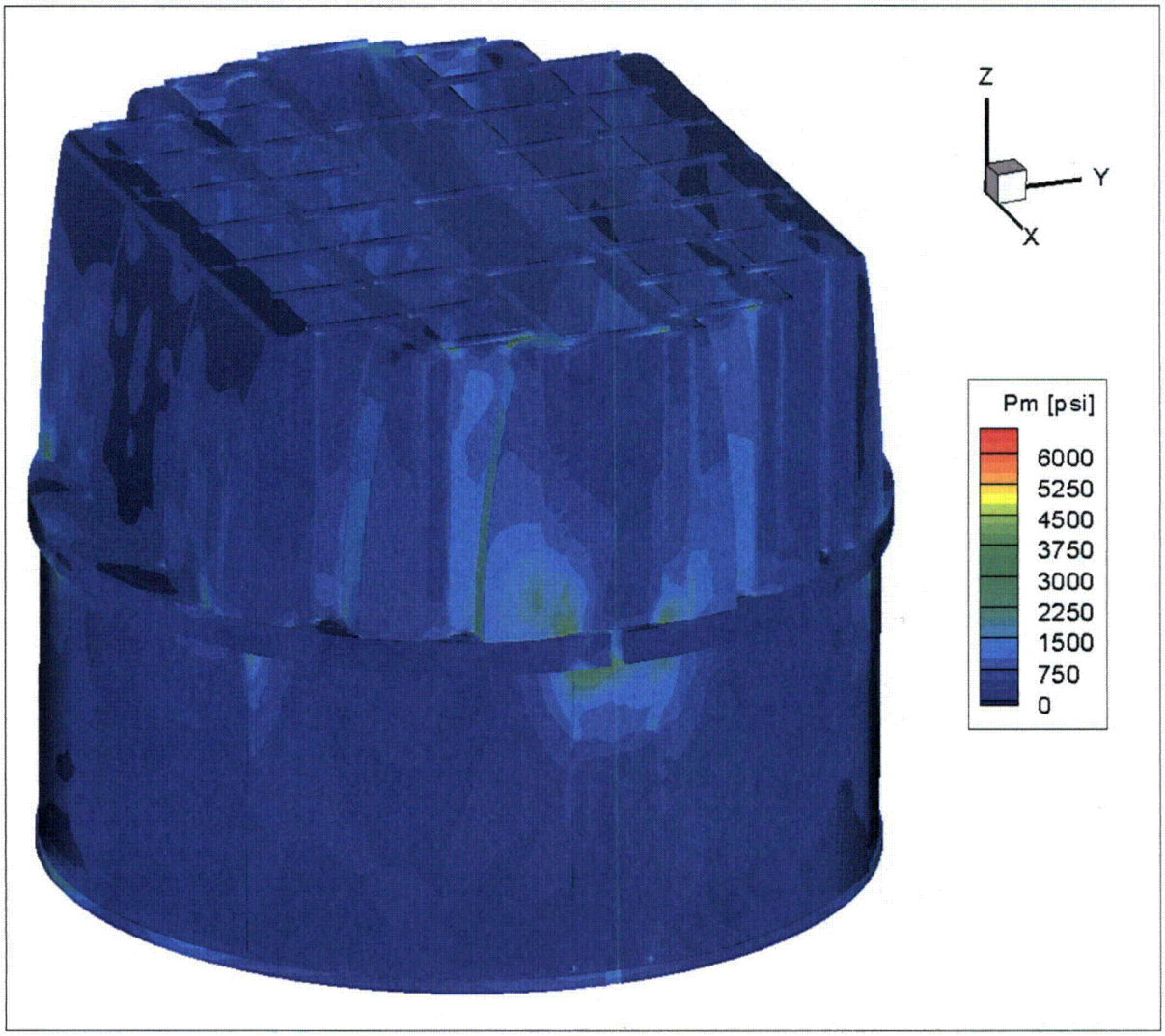

Figure 12a. Contour plot of maximum membrane stress intensity, Pm, for CLTP operation with frequency shifts. The recorded stress at a node is the maximum value taken over all frequency shifts. The maximum stress intensity is 6,433 psi.

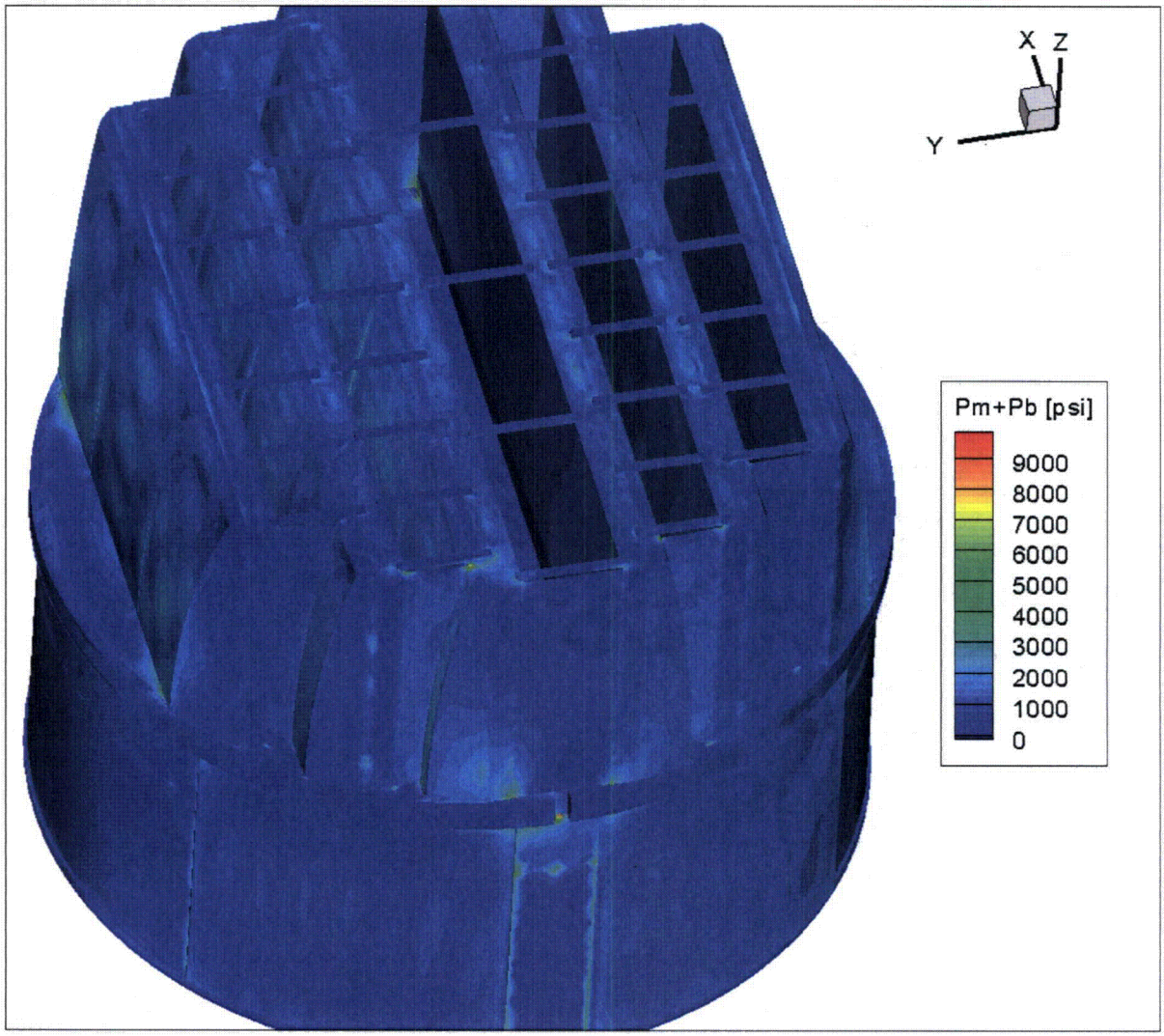

Figure 12b. Contour plot of maximum membrane+bending stress intensity, Pm+Pb, for CLTP operation with frequency shifts. The recorded stress at a node is the maximum value taken over all frequency shifts. The maximum stress intensity is 9,575 psi. First view.

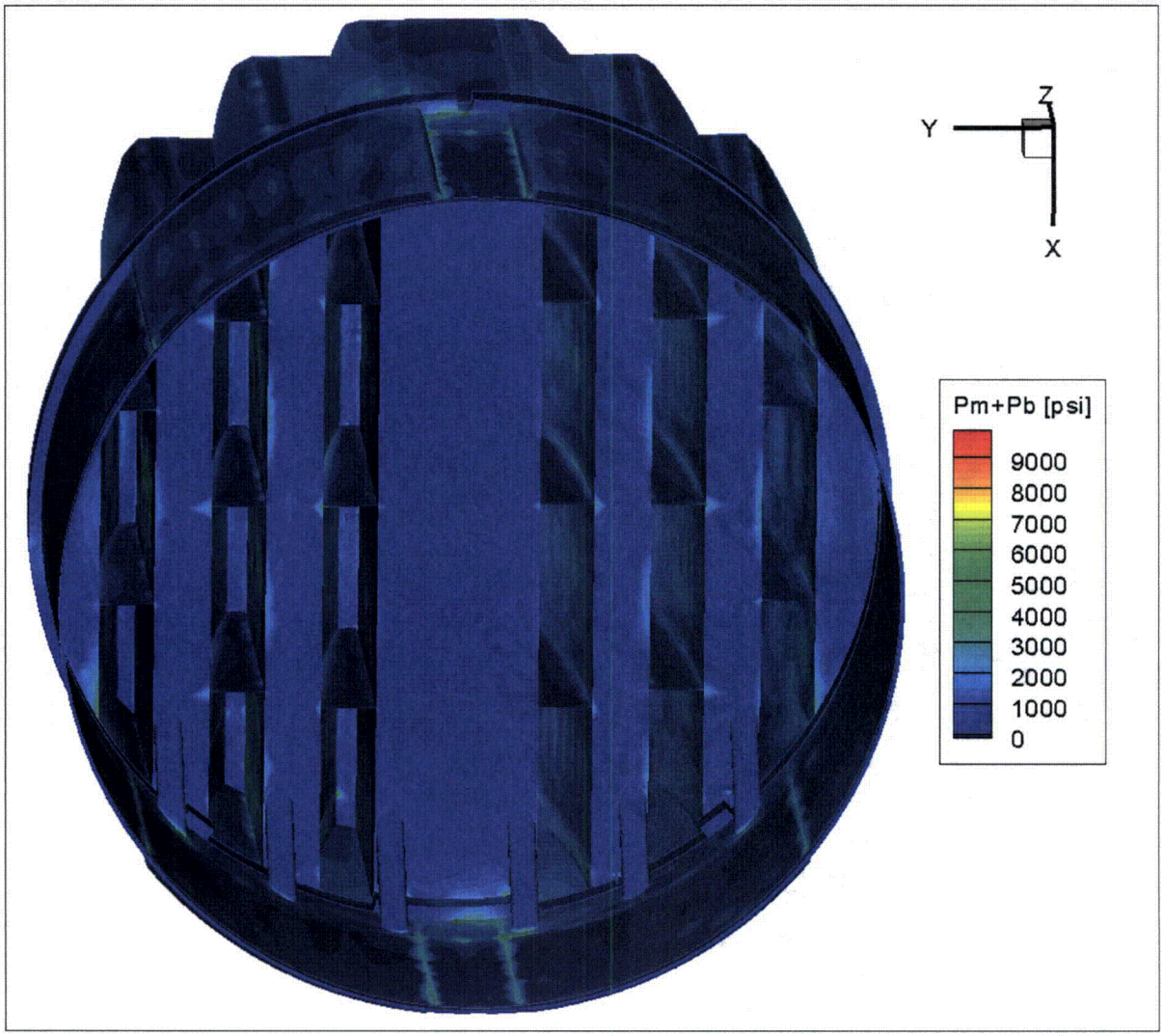

Figure 12c. Contour plot of maximum membrane+bending stress intensity, Pm+Pb, for CLTP operation with frequency shifts. This second view from beneath reveals high stress and modal response of the hoods, perforated plates and hood supports.

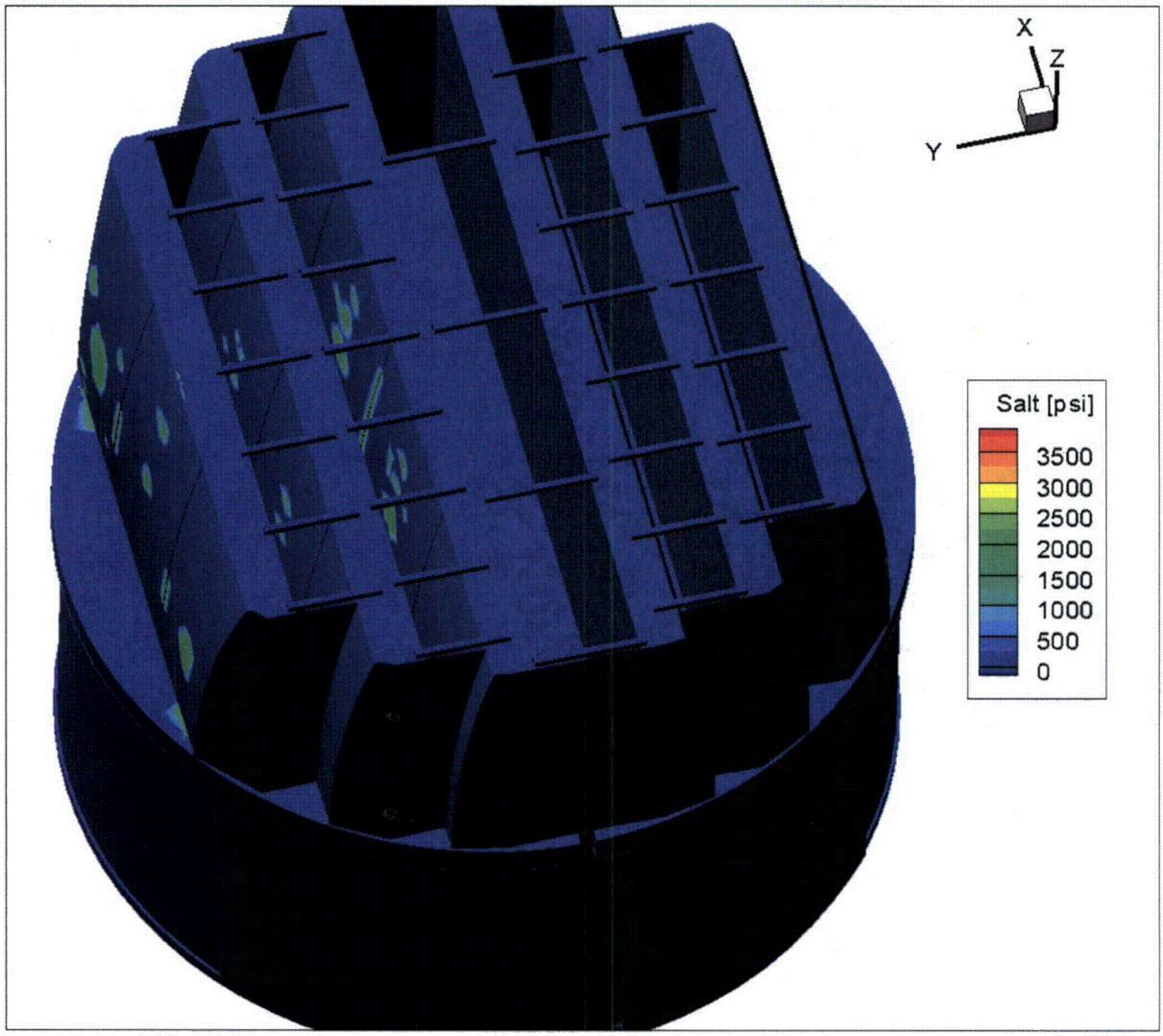

Figure 12d. Contour plot of alternating stress intensity, S_{alt}, for CLTP operation with frequency shifts. The recorded stress at a node is the maximum value taken over all frequency shifts. The maximum alternating stress intensity is 3,699 psi. First view.

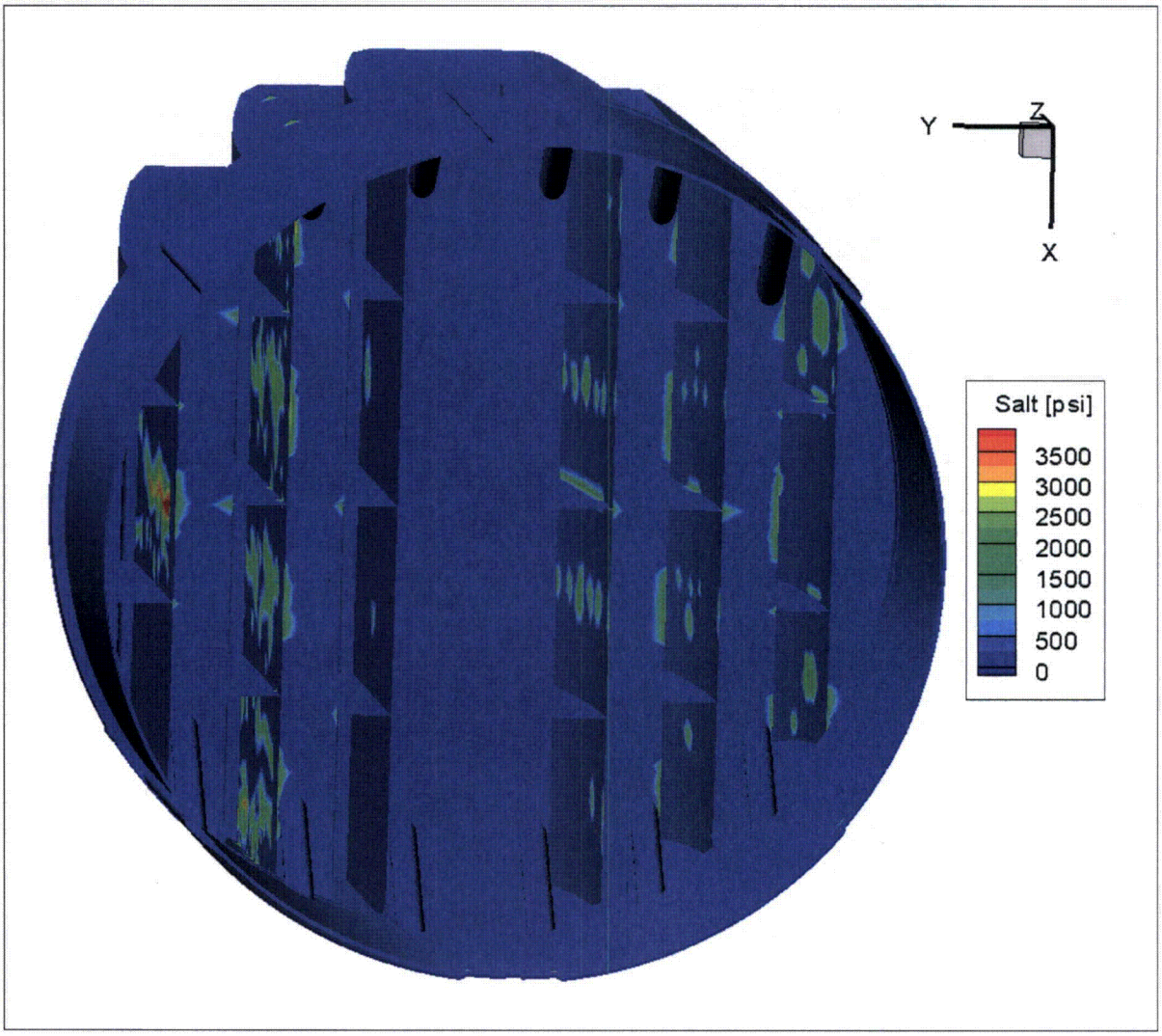

Figure 12e. Contour plot of alternating stress intensity, S_{alt}, for CLTP operation with frequency shifts. This second view from beneath reveals more of the high stress regions on the hoods and perforated plates.

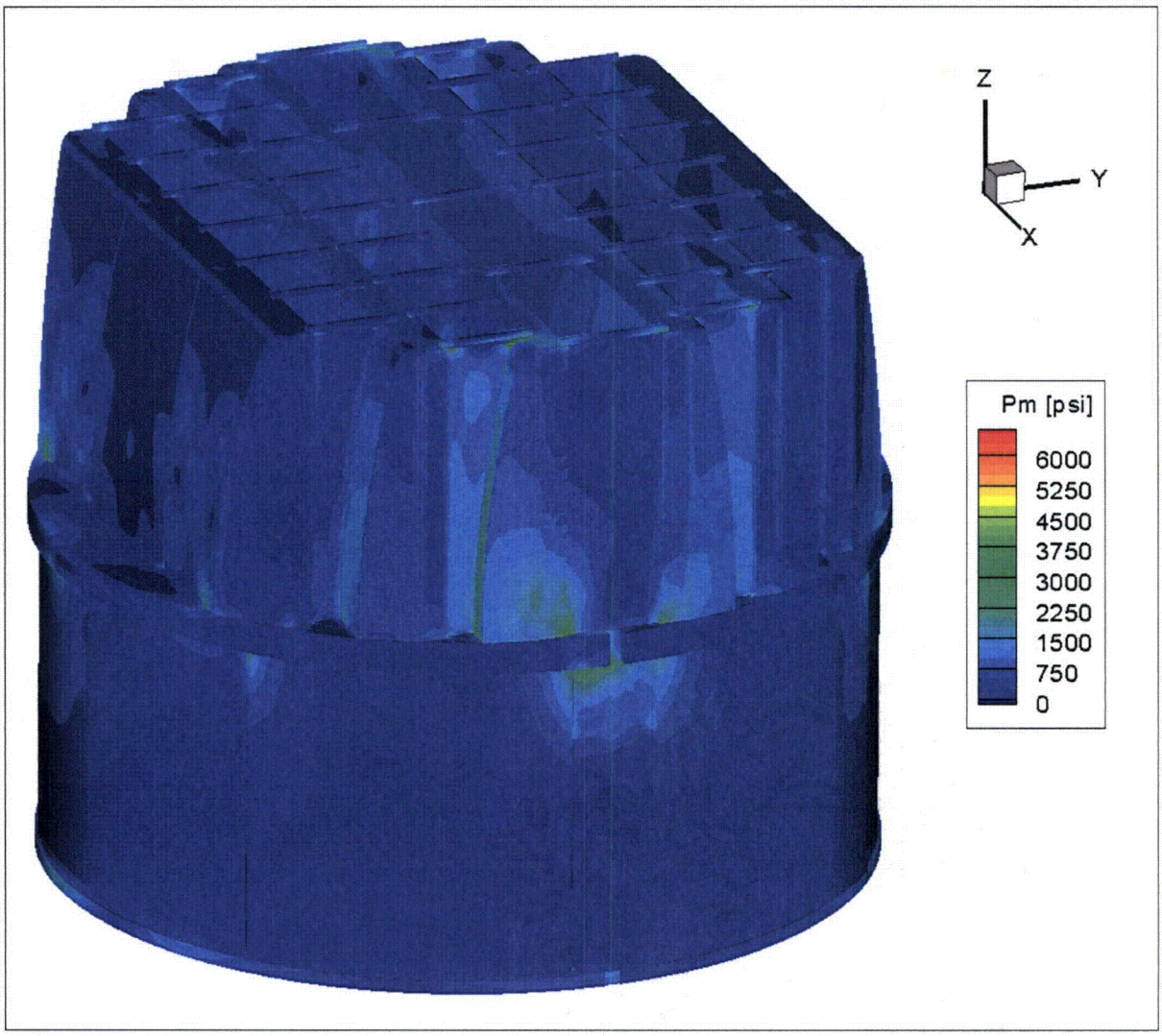

Figure 13a. Contour plot of maximum membrane stress intensity, Pm, for CLTP load with -7.5% frequency shift. The maximum stress intensity is 6,283 psi.

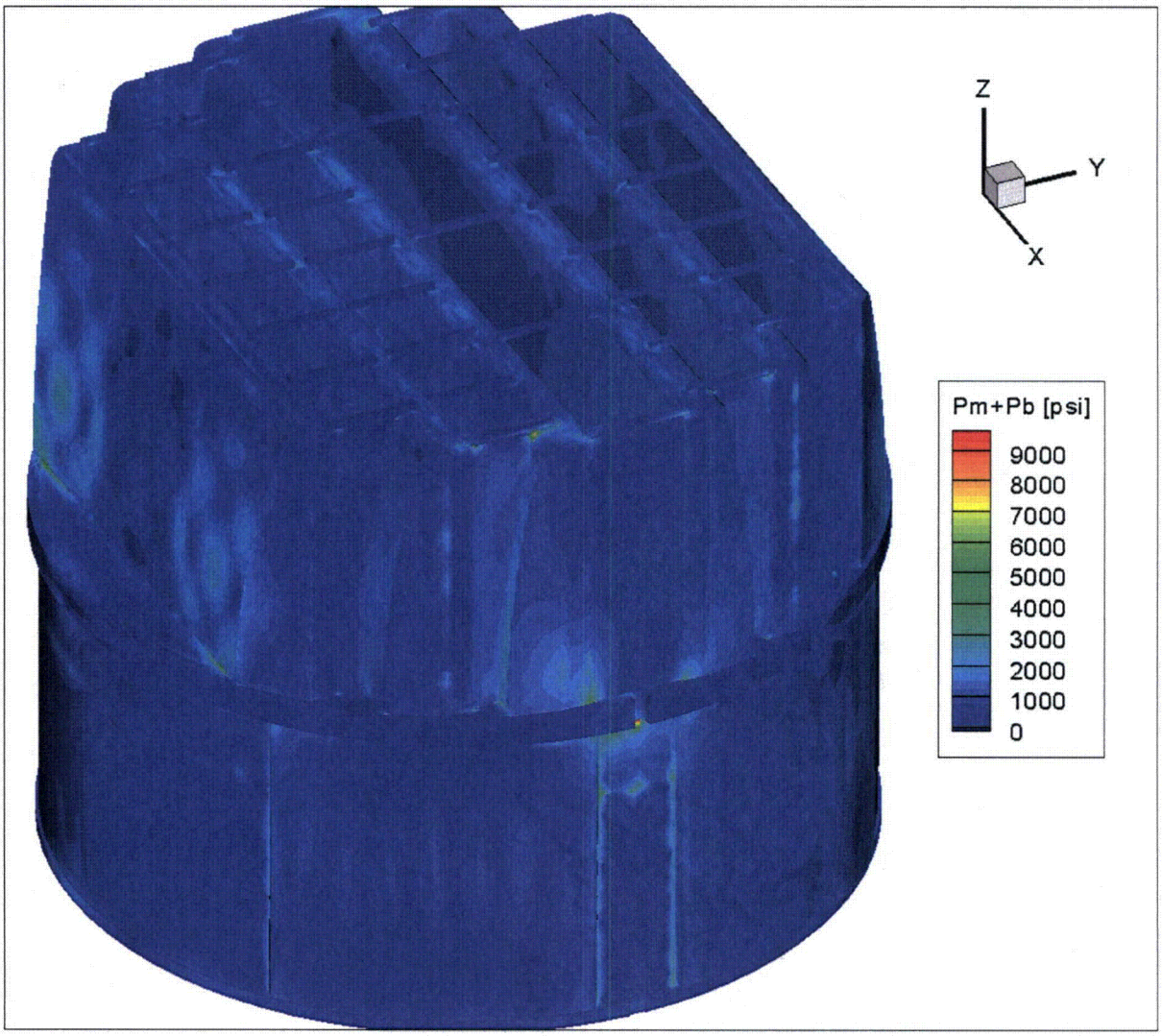

Figure 13b. Contour plot of maximum membrane+bending stress intensity, Pm+Pb, for CLTP load with -7.5% frequency shift. The maximum stress intensity is 9,359 psi.

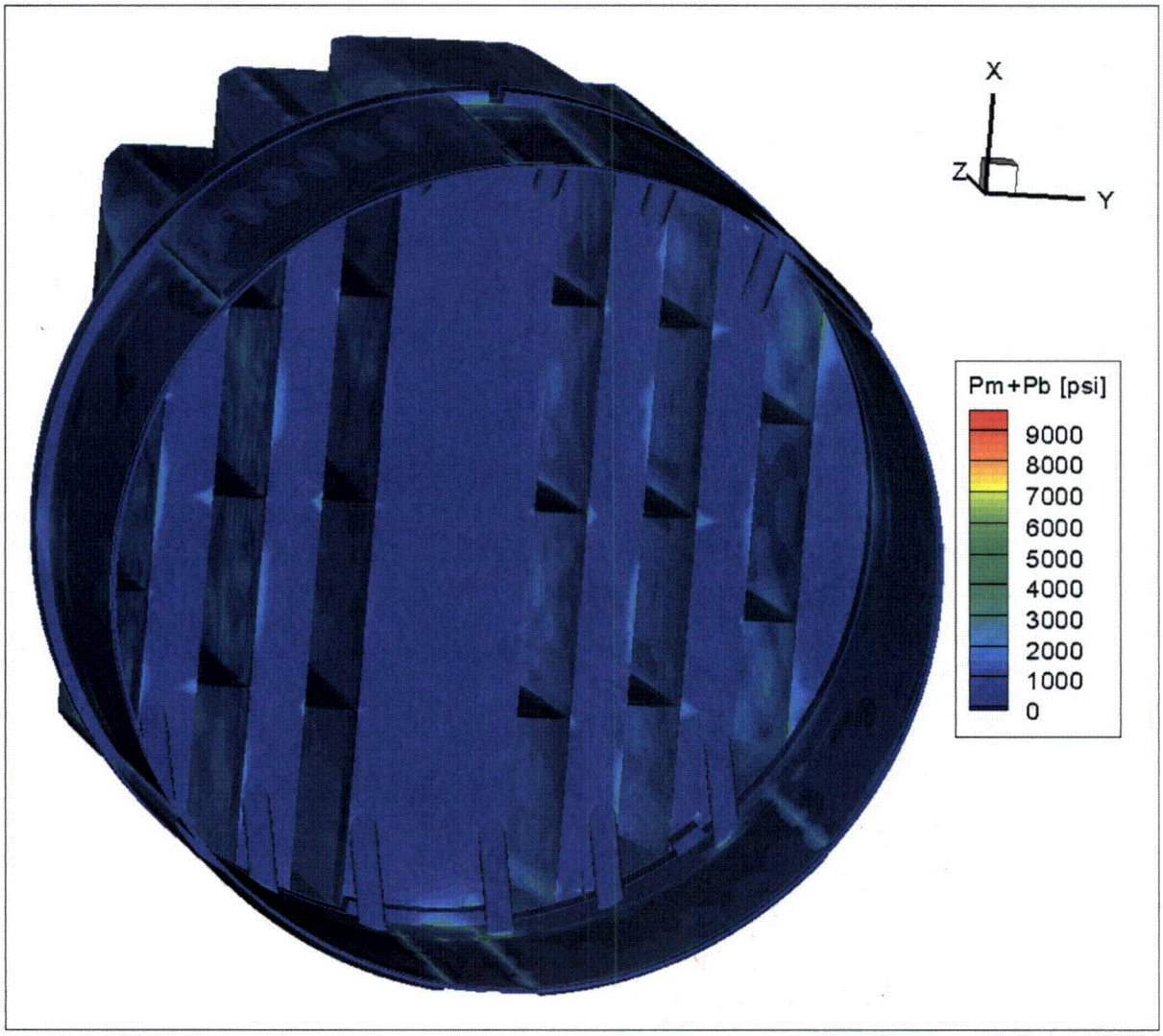

Figure 13c. Contour plot of maximum membrane+bending stress intensity, Pm+Pb, for CLTP load with -7.5% frequency shift. Second view from beneath.

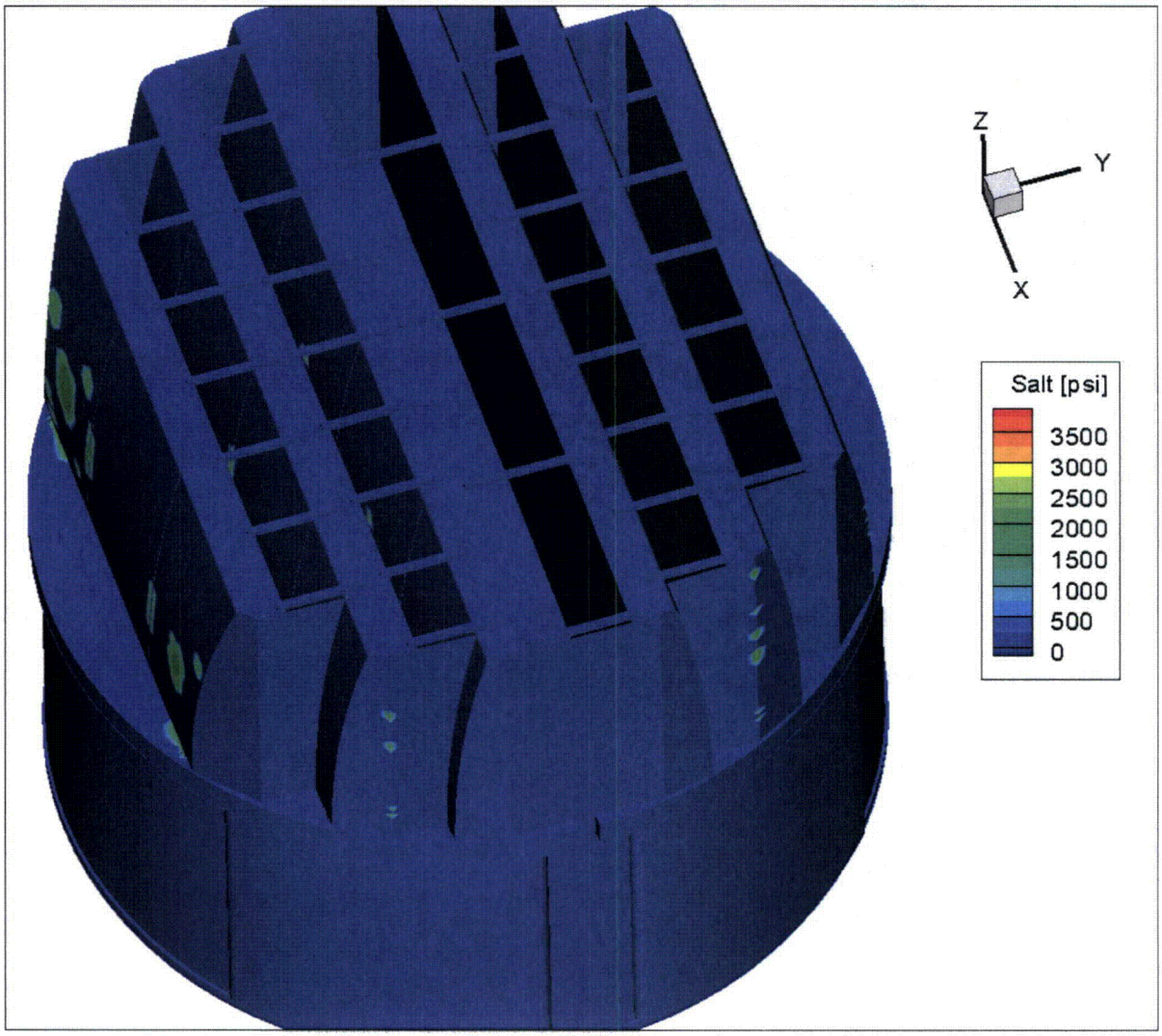

Figure 13d. Contour plot of alternating stress intensity, S_{alt}, for CLTP load with -7.5% frequency shift. The maximum alternating stress intensity is 3,699 psi. First view.

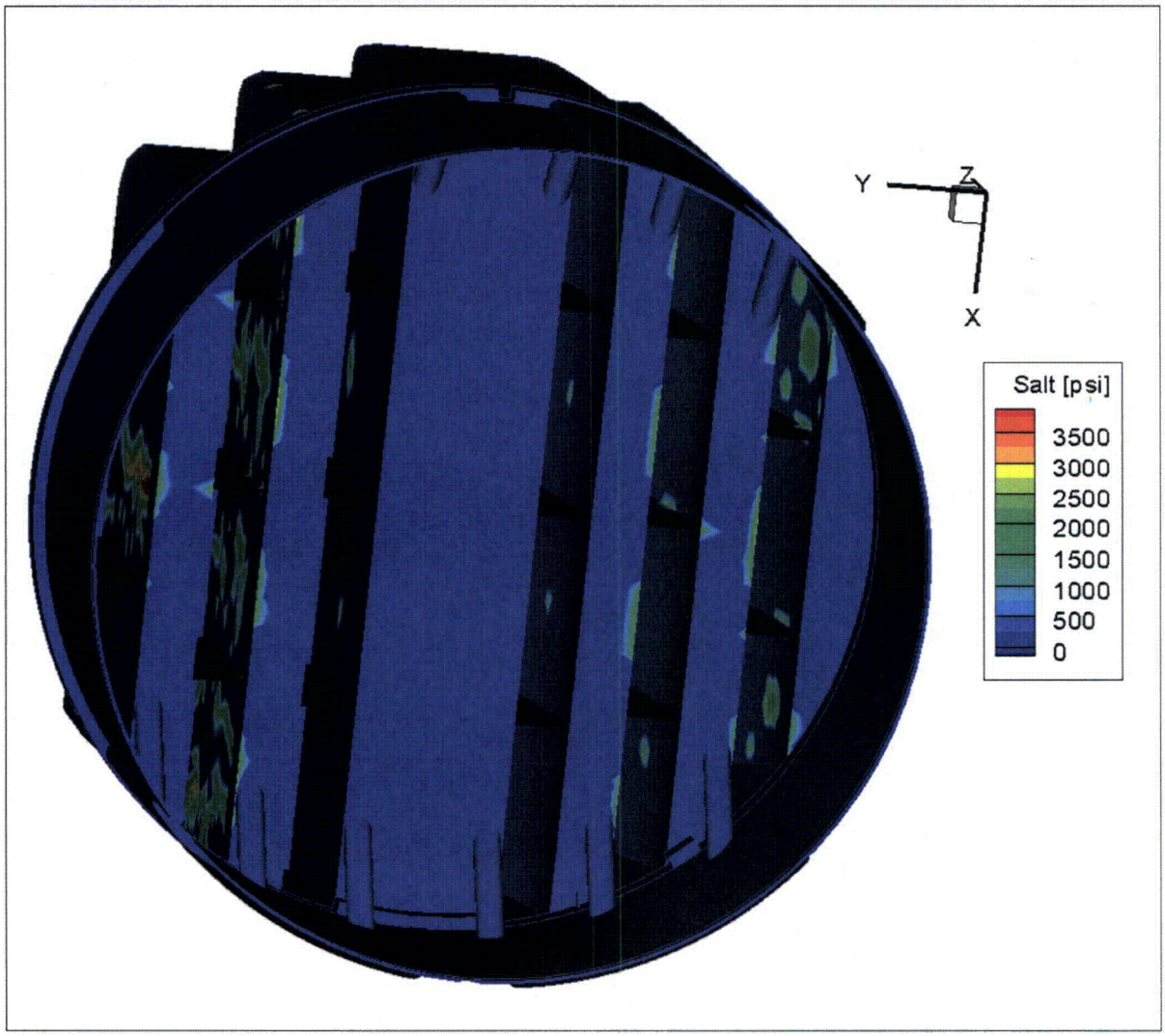

Figure 13e. Contour plot of alternating stress intensity, S_{alt}, for CLTP load with -7.5% frequency shift. Second cutaway view showing high stress locations on the hoods and perforated plates.

5.2 Load Combinations and Allowable Stress Intensities

The stress ratios computed for CLTP at nominal frequency and with frequency shifting are listed in Table 7. The stress ratios are grouped according to type (SR-P for maximum membrane and membrane+bending stress, SR-a for alternating stress) and location (away from welds or on a weld).

For CLTP operation at nominal frequency the minimum stress ratio is identified as a maximum stress, SR-P=1.58, and occurs at the junction of the skirt and upper support ring. At this condition, the dryer stress state is effectively governed by maximum stresses and, more specifically, by the weight-induced static stress field. This is clear from Table 7a where all entries in the right hand column show negligible alternating stress ratios, SR-a>4. In fact all nodes on the steam dryer have alternating stress ratios higher than 4.0 so that no entries for this stress type appear in Table 7a. All remaining locations for maximum stresses are listed in Table 7a and depicted in the accompanying Figure 14.

The effects of frequency shifts can be conservatively accounted for by identifying the minimum stress ratio at every node, where the minimum is taken over all the frequency shifts considered (including the nominal or 0% shift case). The resulting stress ratios are then processed as before to identify the smallest stress ratios anywhere on the structure, categorized by stress type (maximum or alternating) and location (on or away from a weld). The results are summarized in Table 7b and show that the minimum stress ratio, SR-P=1.58, is the same as before and is still identified with a maximum stress. This is the smallest stress ratio encountered anywhere on the structure for any frequency shift at the CLTP condition. Because the alternating stress ratio at this location exceeds 4.0, the minimum stress ratio does not change appreciably with frequency shift. For similar reasons, increasing the loads by $(115\%)^2$ (the approximate increase when proceeding to 115% CLTP operation) is unlikely to significantly alter the value of this minimum stress ratio.

The minimum alternating stress ratio at any frequency shift, SR-a=1.86, is less than one half the value at the zero shift case and occurs on the welded perimeter of the bottom perforated plate. This increase in stress intensity is due to the dynamic modal response resulting when the forcing frequencies are scaled by -7.5%. In fact, virtually all of the lowest alternating stress ratios occur at this shift. Since the structure contains tens of modes per 1 Hz interval, the strong modal response at this shift is indicative of close coupling between the acoustic pressure variation and structural mode shapes at the dominant response frequency which, here, is 74 Hz (80 Hz shifted by -7.5%, with the 80 Hz signal being the dominant component in the stress response as discussed in section 5.3).

Because the worst case stress ratios (i.e., the minimum stress ratio over all frequency shifts) are most important for conservative structural assessment, the locations of *all* nodes having maximum stress ratios SR-P<2.0 are plotted in Figure 15e, and all nodes having alternating stress ratios SR-a<2.0 are plotted in Figure 15h. Note that all plotted stress ratios occur on welds since all stress ratios at non-welds are 2.84 or higher. These plots differ from the preceding ones where the smallest stress ratio in a 10 inch region is identified and all other nodes in this region excluded from display and tabulation. In the current plots, this blanking is not performed so that

a more complete picture of where stress ratios are low, is conveyed. These plots show that all stress ratios, SR-P<2.0 occur at: (i) the steam dryer supports and (ii) the closure plate/inner hood junctions. All alternating stress ratios, SR-a<2.0 occur at: (i) the welded perimeters of perforated plates and (ii) the junction between the middle base plate and middle vane bank. The same conclusion is inferred from Table 7b.

Because it shows the highest alternating stress response, the results are also tabulated for the -7.5% frequency shift in Table 7c. However, all of the tabulated values already appear in Table 7b so that little new insight is gained. Also, depicting the nodes with the smallest stress ratios effectively duplicates the series of plots in Figure 15. Hence rather than repeating the series, the reader is referred to the preceding Table 7b and the corresponding figures to locate the important low stress ratio nodes.

In summary, the general picture that emerges is that at CLTP loads the frequency shifts significantly affect the minimum alternating stress ratios and reposition the high stress locations to different parts of the structure. However, these ratios are well above allowable levels and contain considerable margin for increase to EPU operation. The smallest stress ratio encountered anywhere on the structure at any frequency shift, SR-P=1.58, is identified with a maximum stress and shows negligible variation with frequency shift.

Table 7a. Locations with minimum stress ratios for CLTP conditions with no frequency shift. Stress ratios are grouped according to stress type (maximum – SR-P; or alternating – SR-a) and location (away from a weld or at a weld). Bold text indicates minimum stress ratio of any type on the structure. Locations are depicted in Figure 14. Alternating stress ratios are all greater than 4.0.

Stress Ratio	Weld	Location	Location (in.)				Stress Intensity (psi)			Stress Ratio	
			x	y	z	node	Pm	Pm+Pb	S_{alt}	SR-P	SR-a
SR-P	No	1. outer portion of inner hood (top near closure plate)	109.0	-27.6	95.3	44886	5963	8481	<1500	3.07	>4
SR-a	No	NONE (All SR-a > 4)									
SR-P	**Yes**	**1. skirt/upper support ring**	**118.8**	**0.6**	**-2.0**	**88325**	**2330**	**9575**	**<1500**	**1.58**	**>4**
"	"	2. closure plate/inner hood	108.4	27.9	94.9	85409	4943	7239	<1500	2.04	>4
"	"	3. central base plate/inner vane bank/side panel	-118.8	14.4	7.5	85994	4062	5595	<1500	2.48	>4
"	"	4. closure plate/middle side panel/top cover plate/ top perforated plate	108.4	-45.9	95.9	91627	3719	4277	<1500	2.71	>4
SR-a	Yes	NONE (All SR-a > 4)									

See Table 6a for coordinates description.

Table 7b. Locations with minimum stress ratios for CLTP conditions with frequency shifts. Stress ratios at every node are recorded as the lowest stress ratio identified during the frequency shifts. Stress ratios are grouped according to stress type (maximum – SR-P; or alternating – SR-a) and location (away from a weld or at a weld). Bold text indicates minimum stress ratio of any type on the structure. Locations are depicted in Figure 15.

Stress Ratio	Weld	Location	% Freq. Shift	Location (in.)				Stress Intensity (psi)			Stress Ratio	
				x	y	z	node	Pm	Pm+Pb	S_{alt}	SR-P	SR-a
SR-P	No	1. outer portion of inner hood (top near closure plate)	-10	109.0	-27.6	95.3	44886	6433	9178	<1500	2.84	>4
SR-a	No	1. outer vane bank perforated entry plate	-7.5	1.8	85.9	27.6	61564	211	3658	3603	7.50	3.43
"	"	2. outer vane bank perforated entry plate	-7.5	2.2	85.9	63.0	61581	230	3517	3475	7.81	3.56
SR-P	**Yes**	**1. skirt/upper support ring**	**0**	**118.8**	**0.6**	**-2.0**	**88325**	**2330**	**9575**	**<1500**	**1.58**	**>4**
"	"	2. closure plate/inner hood	-10	-108.4	-27.9	94.9	88252	5612	8317	1764	1.79	3.89
"	"	3. cover plate/outer hood	-7.5	-59.1	-101.4	7.5	93288	1957	6607	2447	2.29	2.81
"	"	4. central base plate/inner vane bank/side panel	-10	-118.8	14.4	7.5	85994	4122	5664	<1500	2.44	>4
"	"	5. inner hood backing bar/closure plate	-7.5	-108.4	38.4	8.1	87035	4005	4184	<1500	2.51	>4
SR-a	Yes	1. outer vane bank/perforated entry plate	-7.5	1.9	85.9	21.5	82290	213	3773	3699	4.00	1.86
"	"	2. middle base plate/middle vane bank	-7.5	-83.4	54.4	7.5	86424	414	3823	3630	3.95	1.89
"	"	3. perforated entry plate/vane bank top vertical plate	-7.5	99.4	54.4	94.4	82652	676	3450	3252	4.38	2.11
"	"	4. middle base plate/middle vane bank	-7.5	-26.2	54.4	7.5	93931	242	2936	2864	5.14	2.40
"	"	5. outer base plate/outer vane bank	-7.5	0.0	-85.9	7.5	86643	216	2924	2746	5.16	2.50

See Table 6a for coordinates description.

Table 7b (continued). Locations with minimum stress ratios for CLTP conditions with frequency shifts. Stress ratios at every node are recorded as the lowest stress ratio identified during the frequency shifts. Stress ratios are grouped according to stress type (maximum – SR-P; or alternating – SR-a) and location (away from a weld or at a weld).

Stress Ratio	Weld	Location	% Freq. Shift	Location (in.)				Stress Intensity (psi)			Stress Ratio	
				x	y	z	node	Pm	Pm+Pb	S_{alt}	SR-P	SR-a
SR-a	Yes	6. end plate/perforated entry plate/middle side panel	-7.5	108.4	54.4	87.1	79914	880	2792	2639	5.41	2.60
"	"	7. perforated entry plate/vane bank top vertical plate	-5	-12.1	-54.4	94.4	93858	485	2852	2632	5.29	2.61
"	"	8. hood support/middle vane bank	-7.5	-54.5	54.4	18.6	84068	401	2648	2604	5.70	2.64
"	"	9. end plate/perforated entry plate/middle side panel	-7.5	108.4	54.4	48.2	79942	764	2687	2483	5.62	2.77

See Table 6a for coordinates description.

Table 7c. Locations with minimum stress ratios at CLTP conditions with -7.5% frequency shift. Stress ratios are grouped according to stress type (maximum – SR-P; or alternating – SR-a) and location (away from a weld or at a weld). Bold text indicates minimum stress ratio of any type on the structure. Since all nodes in this table also appear in Table 7b, for depictions of the node locations refer to that table and the accompanying Figure 15.

Stress Ratio	Weld	Location	Location (in.)				Stress Intensity (psi)			Stress Ratio	
			x	y	z	node	Pm	Pm+Pb	S_{alt}	SR-P	SR-a
SR-P	No	1. outer portion of inner hood (top near closure plate)	109.0	-27.6	95.3	44886	6283	8951	<1500	2.91	>4
SR-a	No	1. outer vane bank perforated entry plate	1.8	85.9	27.6	61564	211	3658	3603	7.50	3.43
	"	2. outer vane bank perforated entry plate	2.2	85.9	63.0	61581	148	3517	3475	7.81	3.56
SR-P	**Yes**	**1. skirt/upper support ring**	**118.8**	**0.6**	**-2.0**	**88325**	**2287**	**9359**	**<1500**	**1.61**	**>4**
"	"	2. closure plate/inner hood	-108.4	-27.9	94.9	88252	5281	7821	<1500	1.91	>4
"	"	3. cover plate/outer hood	-59.1	-101.4	7.5	93288	1957	6607	2447	2.29	2.81
"	"	4. central base plate/inner vane bank/side panel	-118.8	14.4	7.5	85994	4074	5604	<1500	2.47	>4
"	"	5. inner hood backing bar/closure plate	-108.4	38.4	8.1	87035	4005	4184	<1500	2.51	>4
SR-a	Yes	1. outer vane bank/perforated entry plate	1.9	85.9	21.5	82290	213	3773	3699	4.00	1.86
"	"	2. middle base plate/middle vane bank	-83.4	54.4	7.5	86424	414	3823	3630	3.95	1.89
"	"	3. perforated entry plate/vane bank top vertical plate	99.4	54.4	94.4	82652	617	3450	3252	4.38	2.11
"	"	4. middle base plate/middle vane bank	-26.2	54.4	7.5	93931	242	2936	2864	5.14	2.40
"	"	5. outer base plate/outer vane bank	0.0	-85.9	7.5	86643	216	2924	2746	5.16	2.50
"	"	6. end plate/perforated entry plate/middle side panel	108.4	54.4	87.1	79914	813	2792	2639	5.41	2.60
"	"	7. hood support/middle vane bank	-54.5	54.4	18.6	84068	401	2648	2604	5.70	2.64
"	"	8. end plate/perforated entry plate/middle side panel	108.4	54.4	48.2	79942	749	2687	2483	5.62	2.77

See Table 6a for coordinates description.

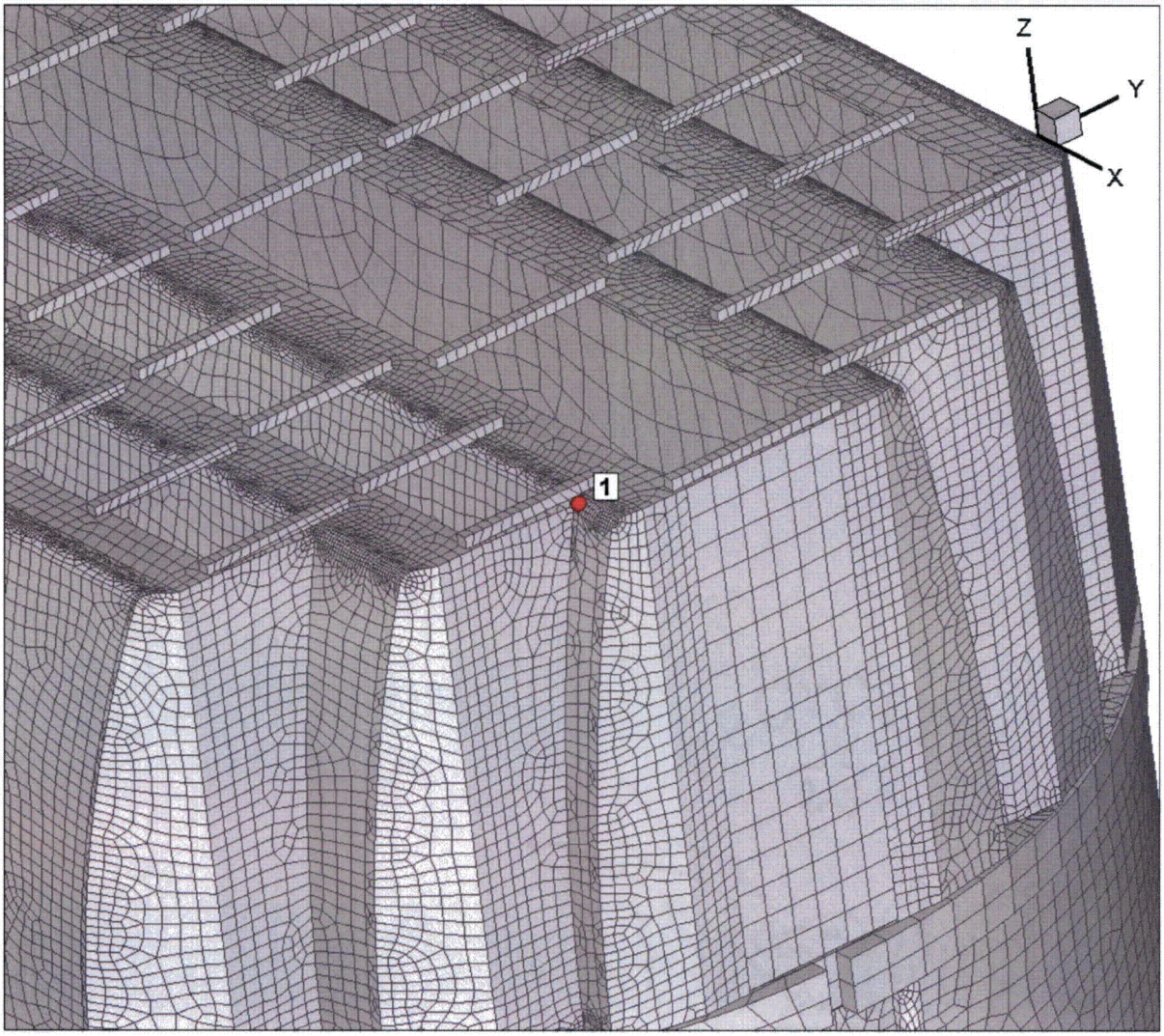

Figure 14a. Location of smallest maximum stress ratio, SR-P, at non-welds for nominal CLTP operation. Number refers to the enumerated locations for SR-P values at non-welds in Table 7a.

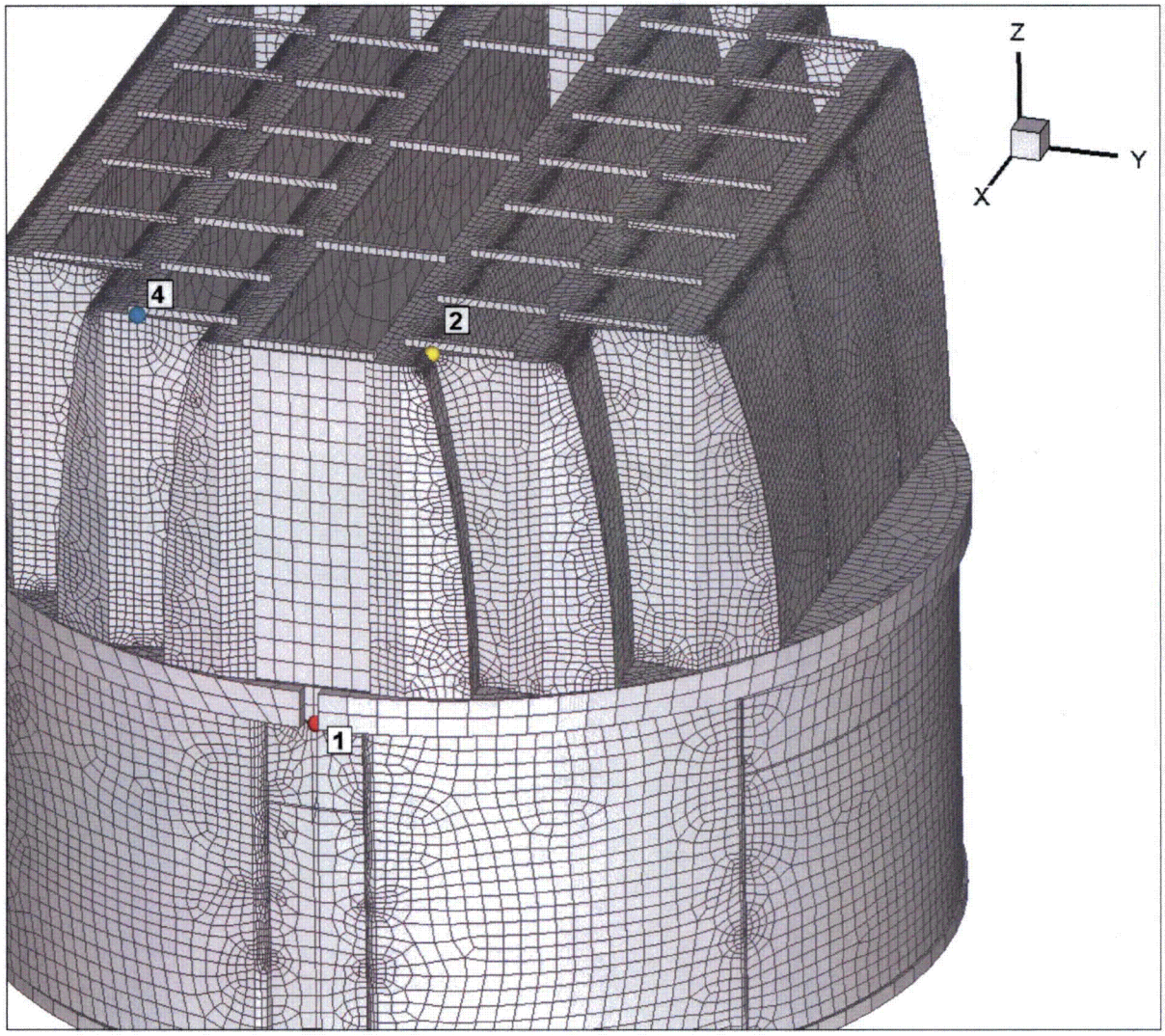

Figure 14b. Locations of smallest maximum stress ratios, SR-P, at welds for nominal CLTP operation. Numbers refer to the enumerated locations for SR-P values at welds in Table 7a. First view showing locations 1, 2 and 4.

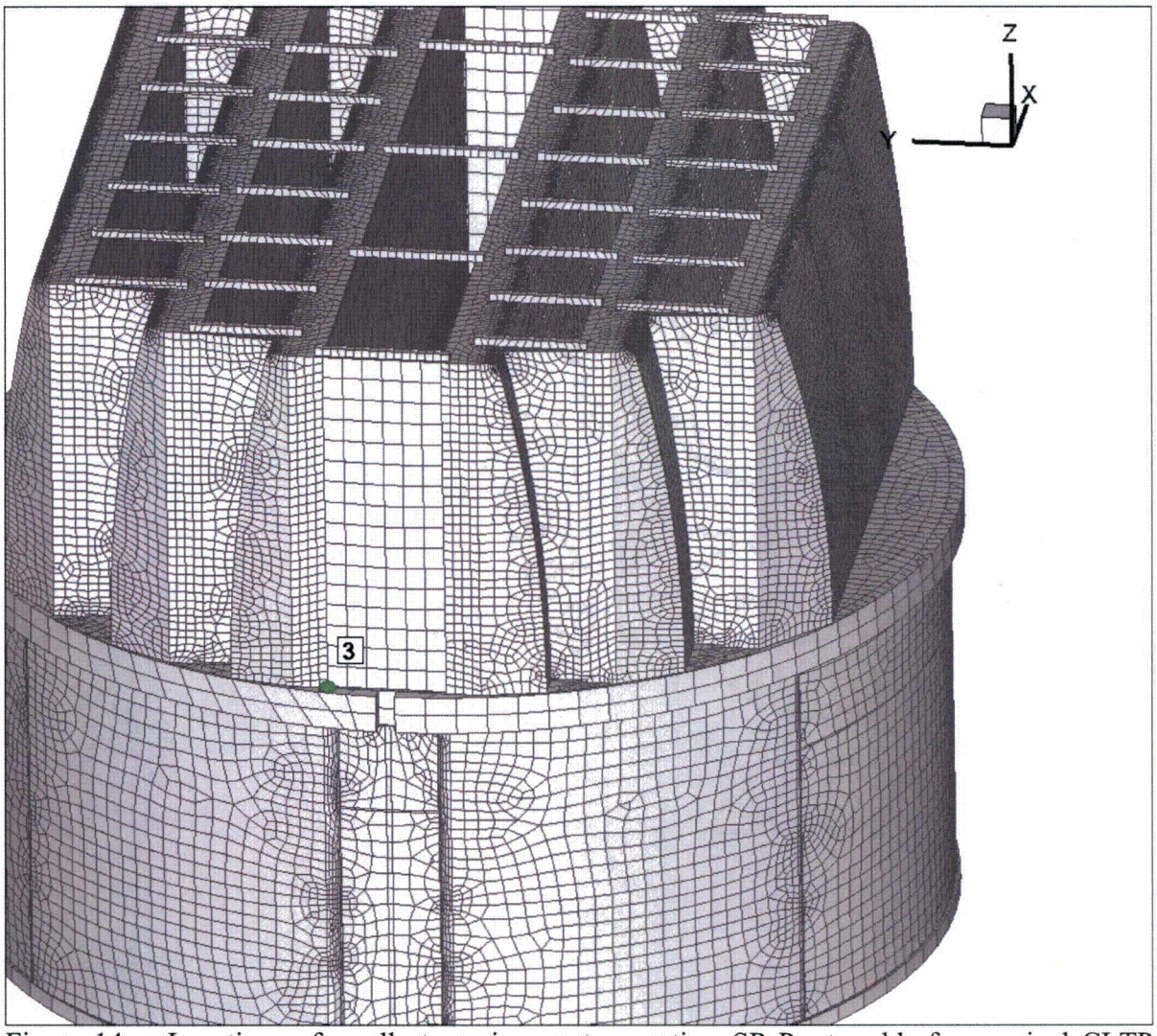

Figure 14c. Locations of smallest maximum stress ratios, SR-P, at welds for nominal CLTP operation. Numbers refer to the enumerated locations for SR-P values at welds in Table 7a. Second view showing location 3.

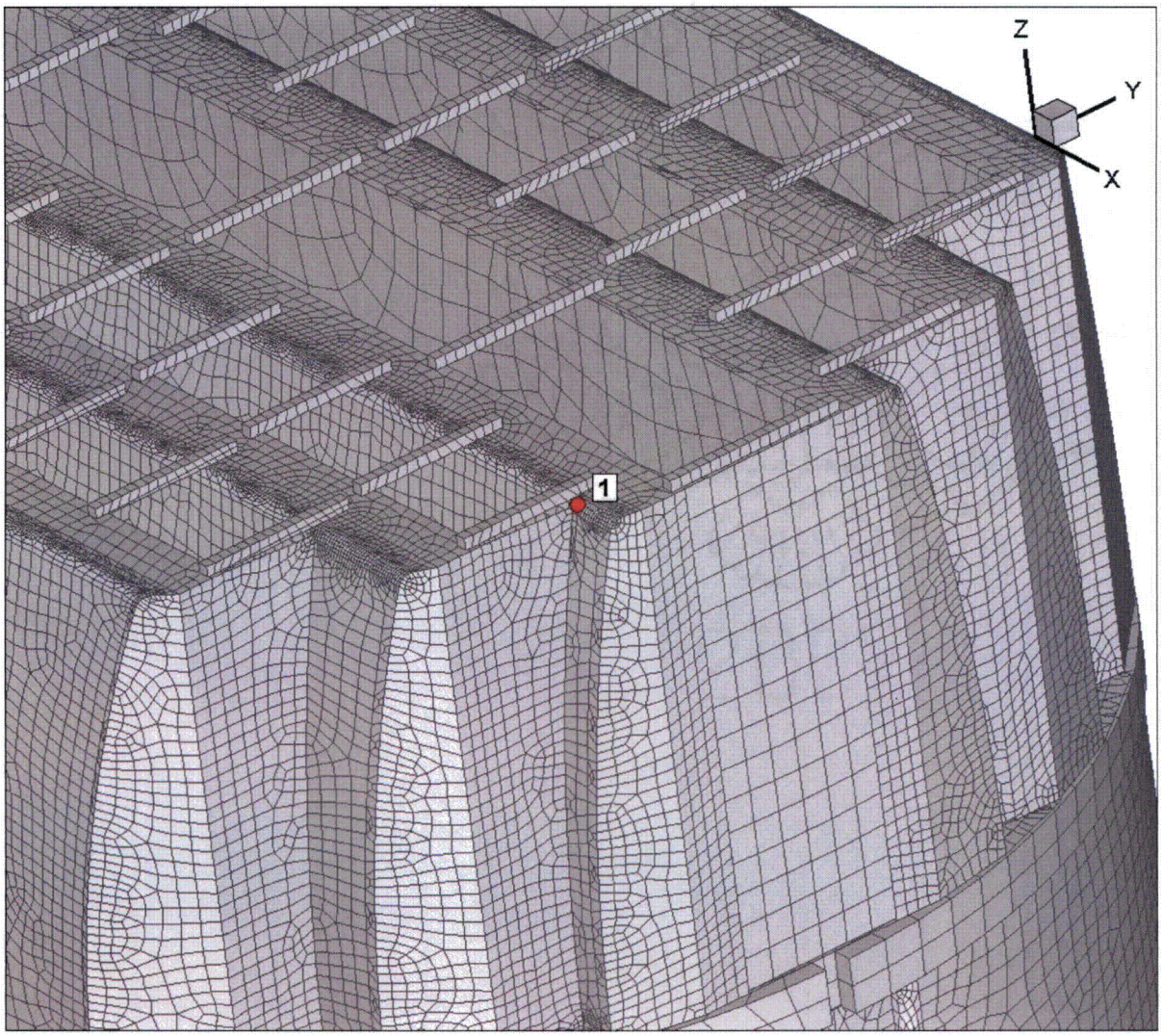

Figure 15a. Location of minimum stress ratio, SR-P, associated with maximum stress intensities at non-welds for CLTP operation with frequency shifts. The recorded stress ratio is the minimum value taken over all frequency shifts. The number refers to the enumerated location for SR-P values at non-welds in Table 7b.

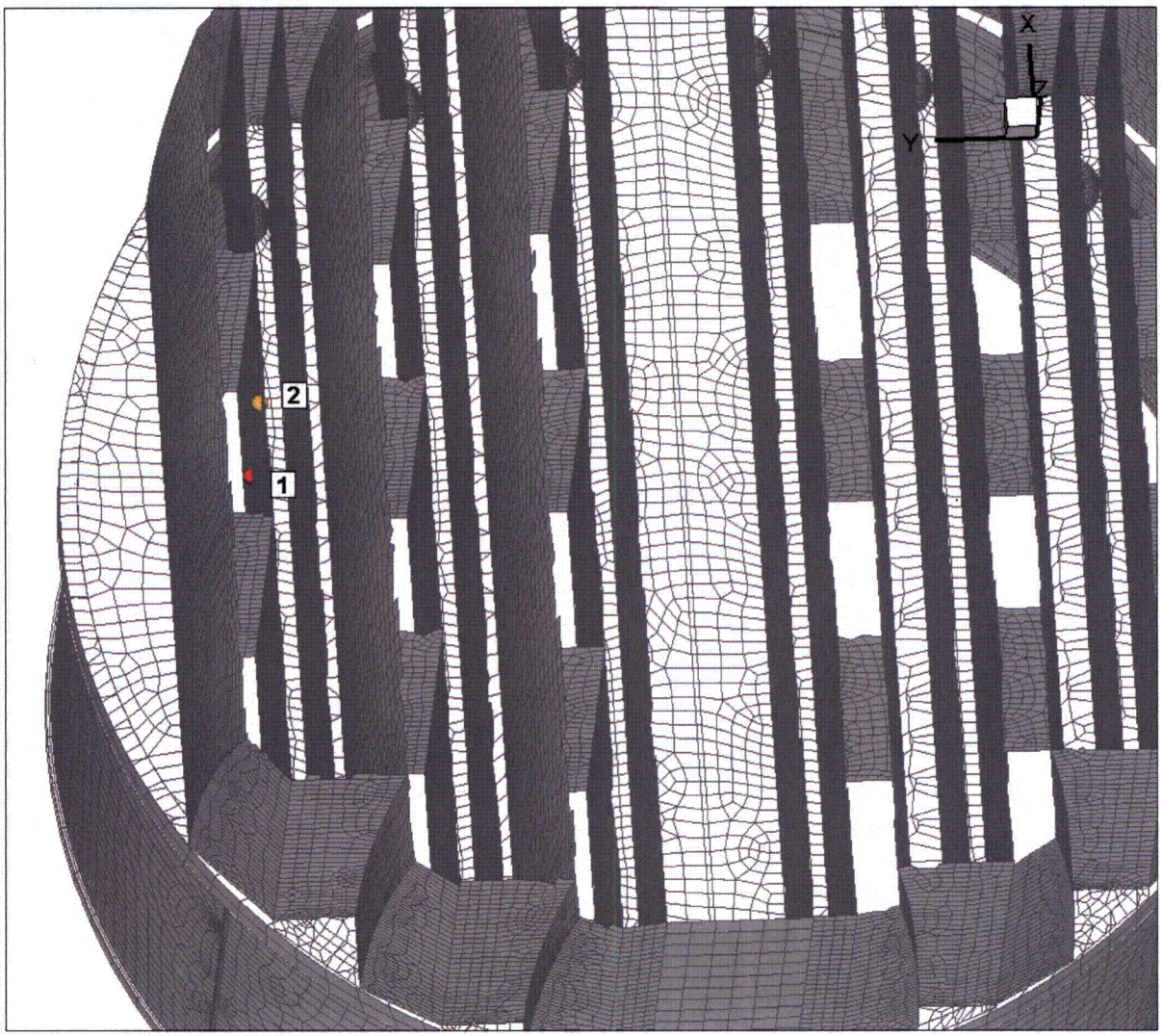

Figure 15b. Locations of minimum alternating stress ratios, SR-a, at non-welds for CLTP operation with frequency shifts. The recorded stress ratio at a node is the minimum value taken over all frequency shifts. Numbers refer to the enumerated locations for SR-a values at non-welds in Table 7b.

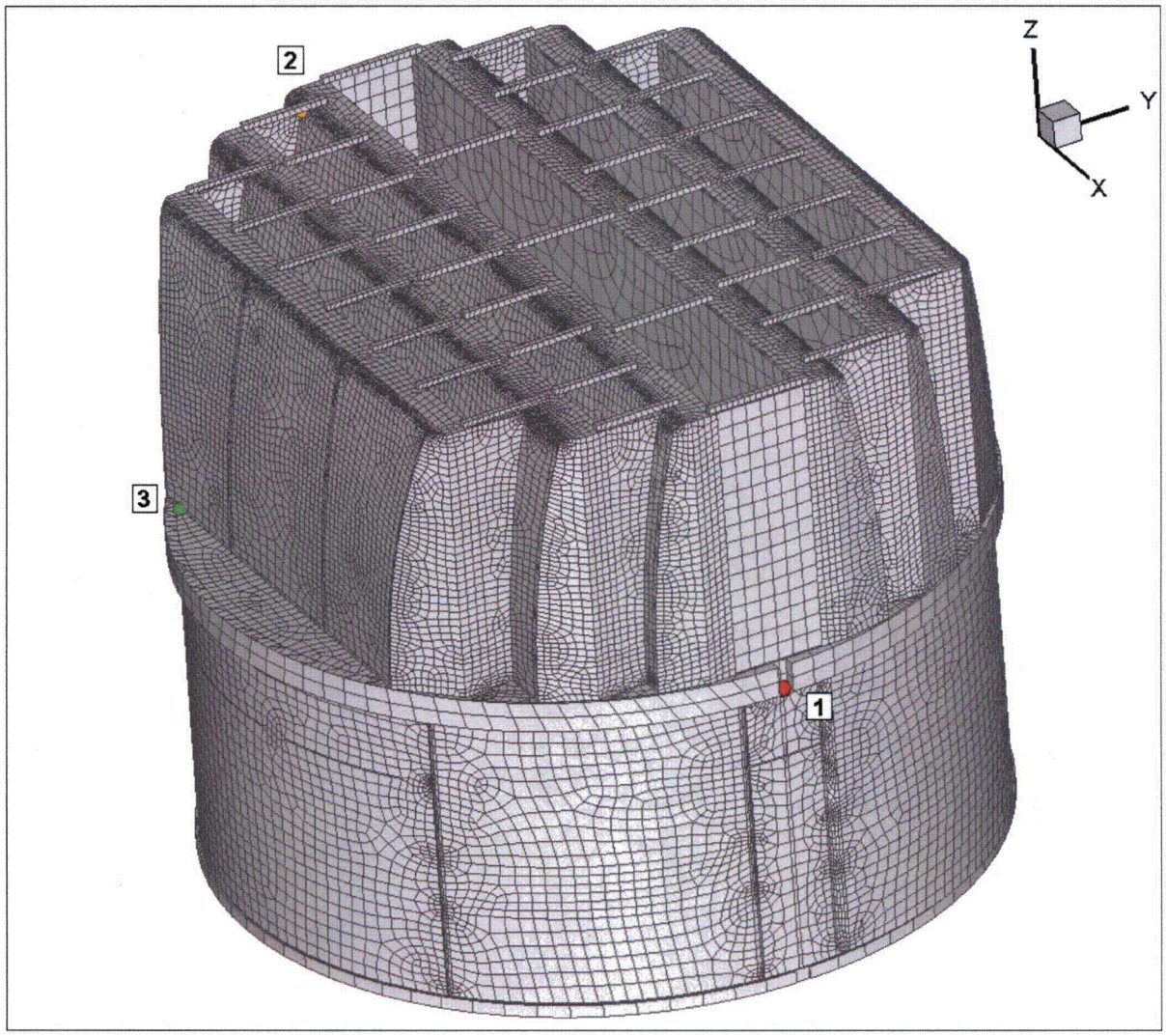

Figure 15c. Locations of minimum stress ratios, SR-P, associated with maximum stress intensities at welds for CLTP operation with frequency shifts. The recorded stress ratio at a node is the minimum value taken over all frequency shifts. Numbers refer to the enumerated locations for SR-P values at welds in Table 7b. This view shows locations 1-3.

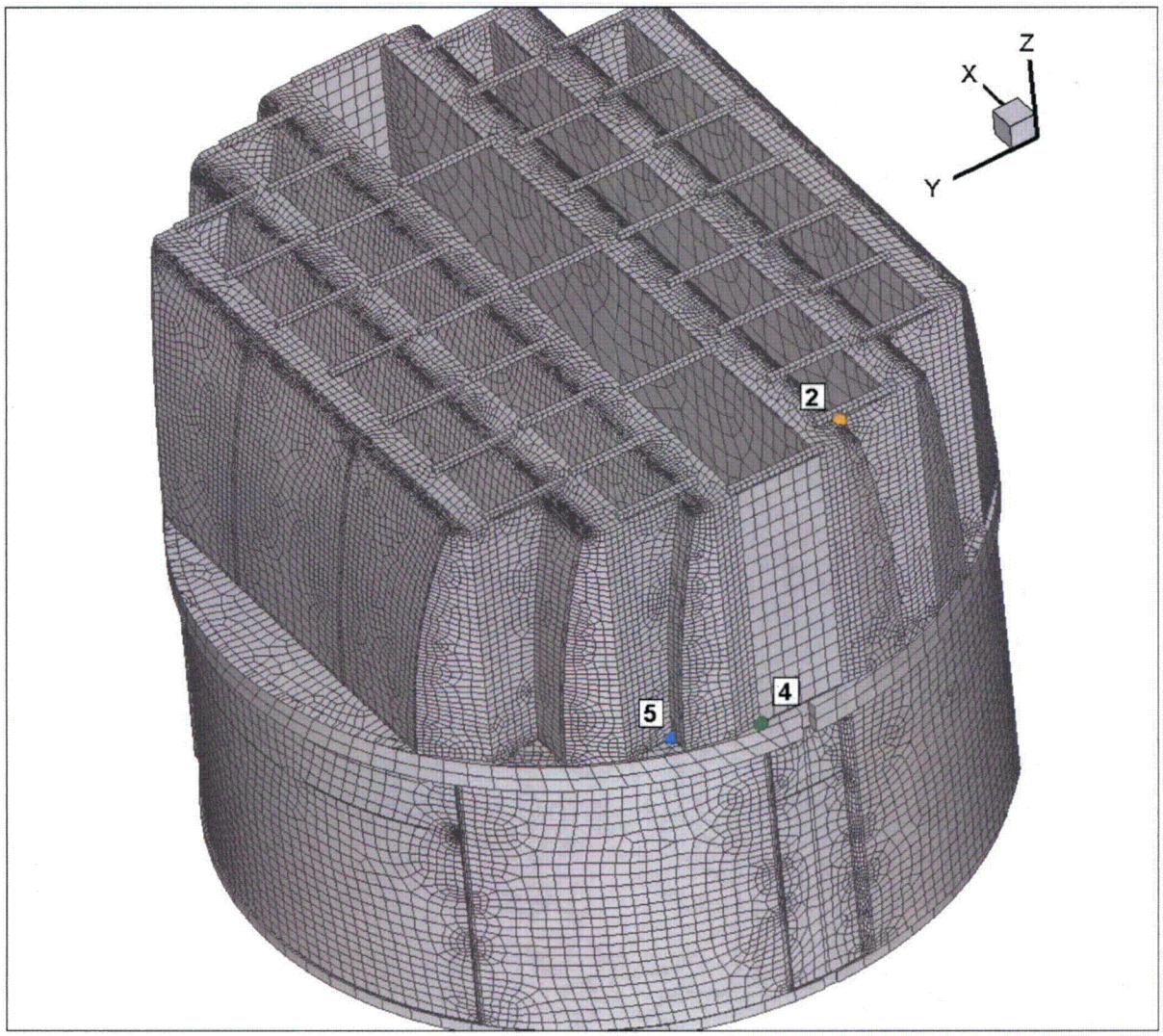

Figure 15d. Locations of minimum stress ratios, SR-P, associated with maximum stress intensities at welds for CLTP operation with frequency shifts. The recorded stress ratio at a node is the minimum value taken over all frequency shifts. Numbers refer to the enumerated locations for SR-P values at welds in Table 7b. This view shows locations 2, 4 and 5.

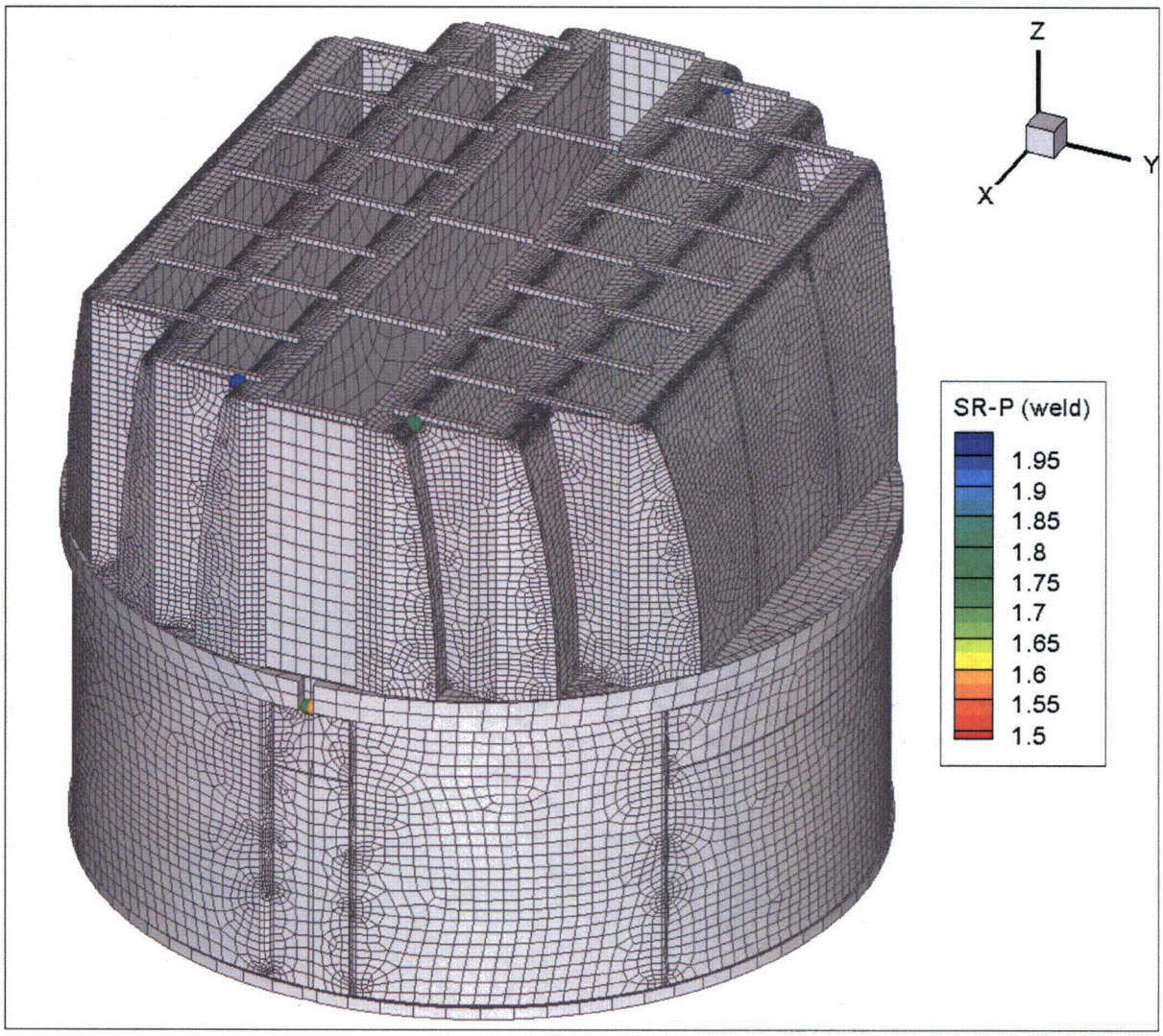

Figure 15e. Locations of minimum stress ratios, SR-P, associated with maximum stress intensities at welds for CLTP operation with frequency shifts. The recorded stress ratio at a node is the minimum value taken over all frequency shifts. This view displays *all* nodes with SR-P<2.0.

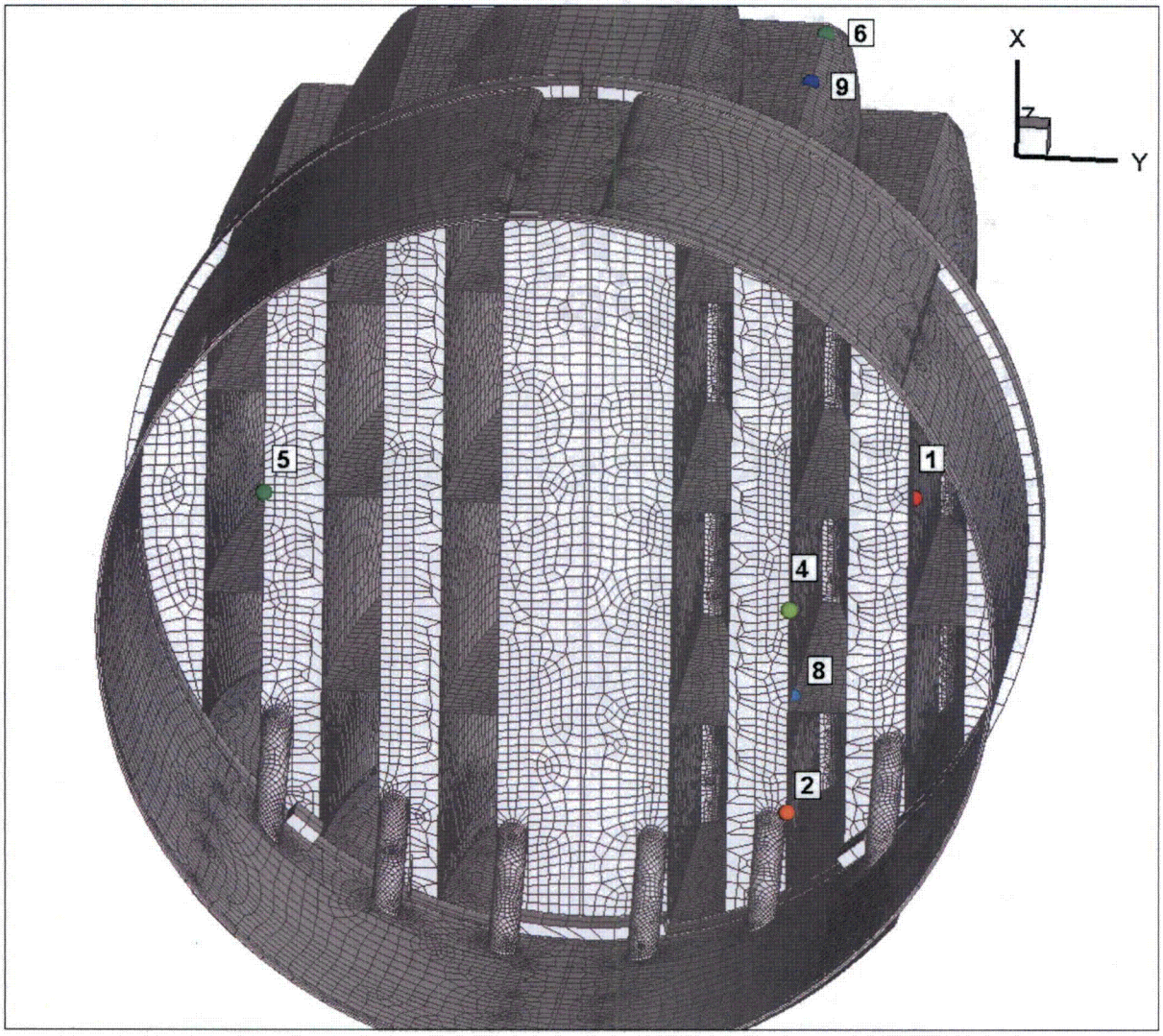

Figure 15f. Locations of minimum alternating stress ratios, SR-a, at welds for CLTP operation with frequency shifts. The recorded stress ratio at a node is the minimum value taken over all frequency shifts. Numbers refer to the enumerated locations for SR-a values at welds in Table 7b. First view showing enumerated locations 1, 2, 4-6, 8 and 9.

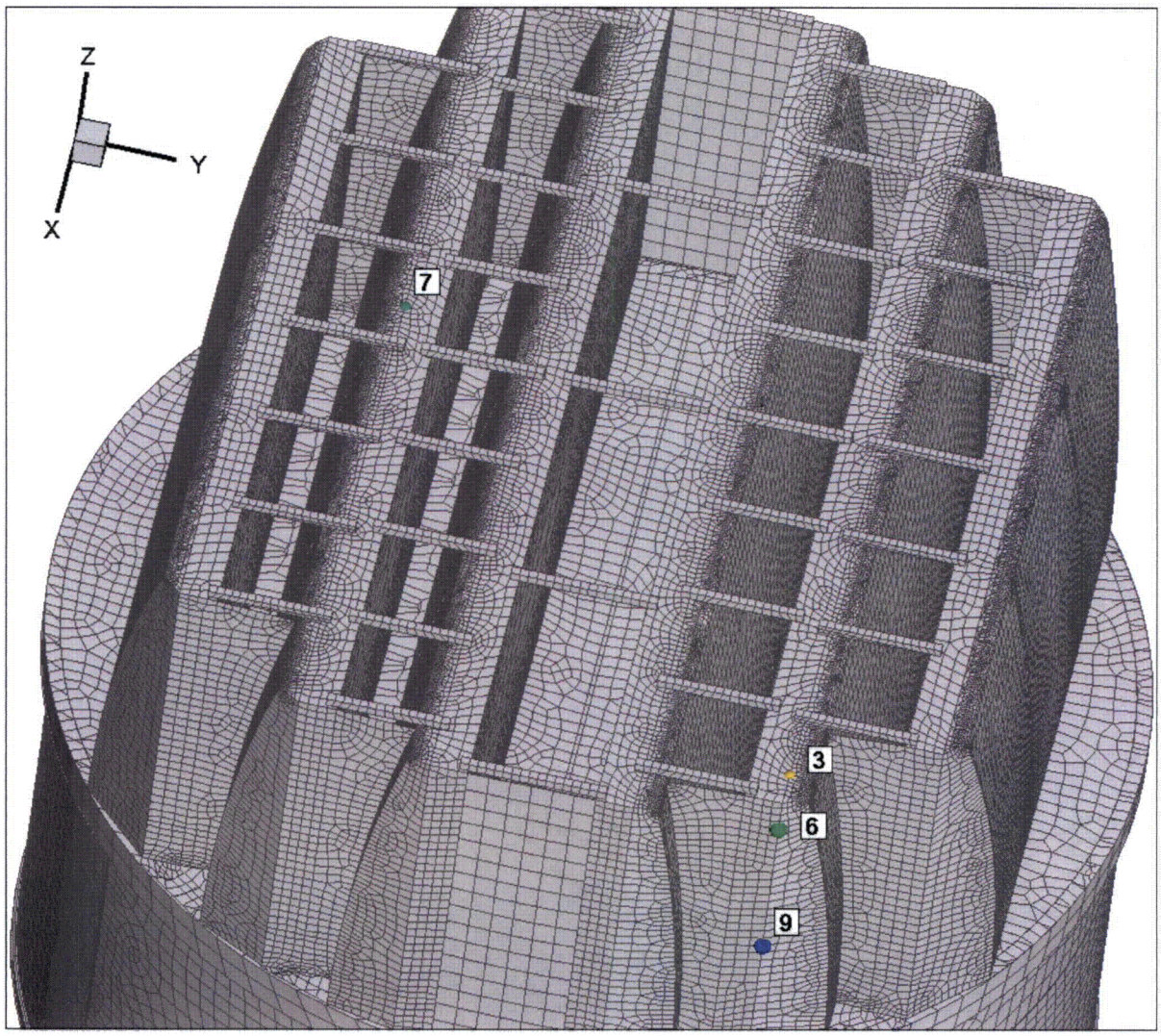

Figure 15g. Locations of minimum alternating stress ratios, SR-a, at welds for CLTP operation with frequency shifts. The recorded stress ratio at a node is the minimum value taken over all frequency shifts. Numbers refer to the enumerated locations for SR-a values at welds in Table 7b. Second view showing locations 3, 6, 7 and 9.

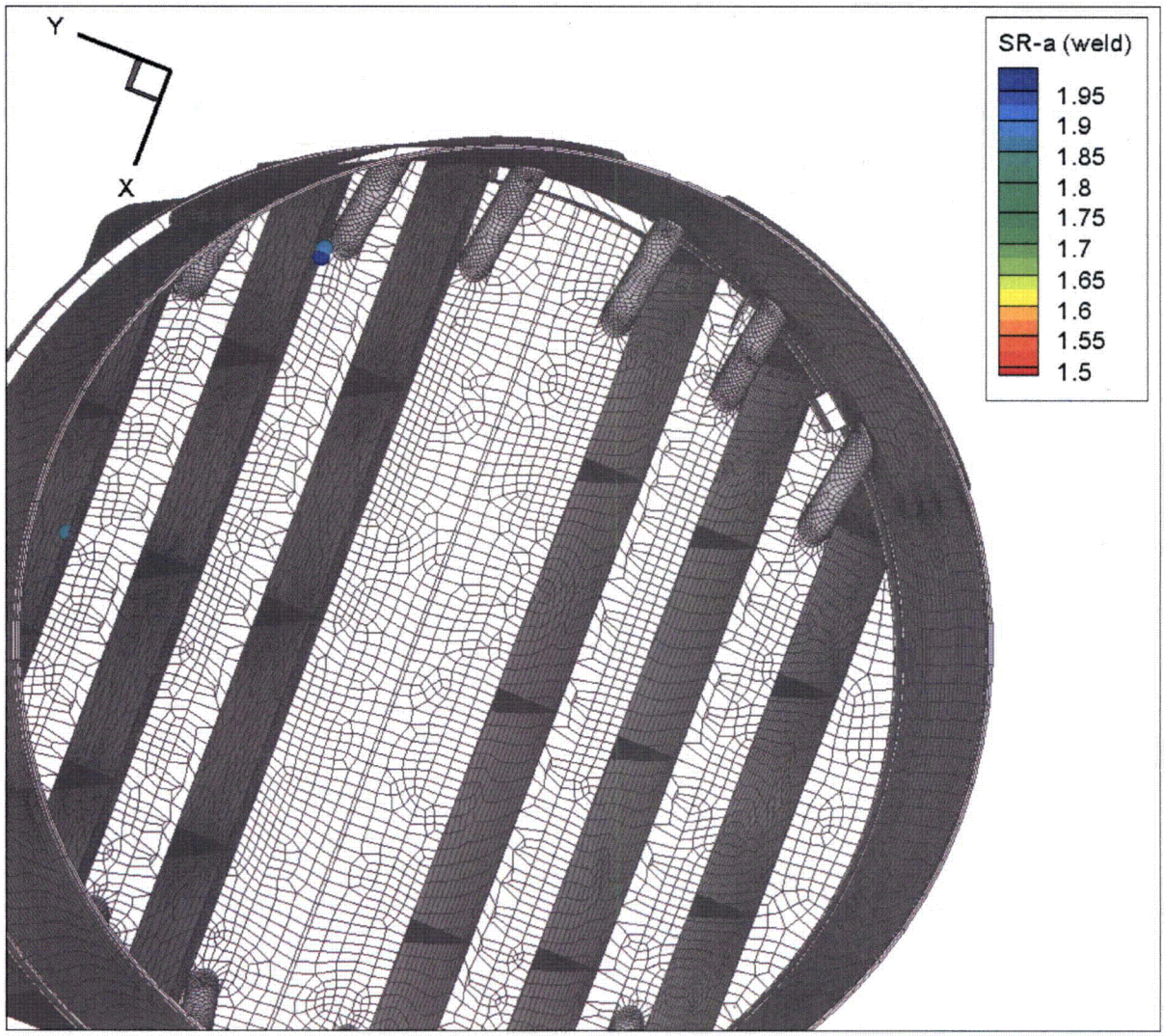

Figure 15h. Locations of minimum alternating stress ratios, SR-a, at welds for CLTP operation with frequency shifts. The recorded stress ratio at a node is the minimum value taken over all frequency shifts. This figure shows *all* nodes with SR-a<2.0.

5.3 Frequency Content and Sensitivity to Frequency Shift of the Stress Signals

As indicated previously, both the loads and stress signals contain a strong 80 Hz component and a second weaker, but significant 41 Hz component. This can be seen by examining the accumulative PSDs which are computed directly from the Fourier coefficients as

$$\Sigma(\omega_n) = \sqrt{\sum_{k=1}^{n} |\tilde{\sigma}(\omega_k)|^2}$$

where $\tilde{\sigma}(\omega_k)$ is the complex stress harmonic at frequency, ω_k. Accumulative PSD plots are useful for determining the frequency components and frequency ranges that make the largest contributions to the fluctuating stress. Unlike PSD plots, no "binning" or smoothing of frequency components is needed to obtain smooth curves. Steep step-like rises in $\Sigma(\omega)$ indicate the presence of a strong component at a discrete frequency whereas gradual increases in the curve imply significant content over a broader frequency range. From Parsival's theorem, equality between $\Sigma(\omega_N)$ (where N is the total number of frequency components) and the RMS of the stress signal in the time domain is established.

The accumulative PSD at nominal frequency shift for the σ_{zz} stress response at node 80204 is shown in Figure 16. This node is selected because it exhibits a strong alternating stress response at the 0% frequency shift and clearly reveals the two main contributors to the stress response. From the plot, the largest contribution occurs over the 80.0 Hz to 80.2 Hz frequency range and the second largest contribution is made over the 40.5 Hz to 42 Hz range. Examination of the other nodes reveal similar qualitative observations, through the relative jumps may differ and their significance compared to the initial static contribution can also vary. Similarly, when the load is shifted in the frequency space, a similar response results with the 80 Hz and [40.5 – 42] Hz rises suitably shifted. This is indicated in Figure 17 where the accumulative PSD for node 82290 at -7.5% and 0% frequency shifts are compared. This node exhibits a very weak response in the zero shift case. However, at -7.5% frequency shift, the node participates in a strong response. This behavior is consistent with a mode being excited by the 74 Hz signal (80 Hz shifted by -7.5%)

Further insight into the modal response can be obtained by examining how the maximum and alternating stress intensities of selected nodes vary with frequency shift. This evaluation is made in Figure 18 for the following nodes:

Nodes 88325 and 88252: - these nodes have the lowest stress ratios associated with a maximum stress intensity at any frequency shift.
Node 80204 – this node has a high alternating stress at zero frequency shift (see Table 6a).
Nodes 82290 and 86424 – these nodes have the lowest alternating stress ratios over all frequency shifts (see Table 7b).

To generate these plots the frequency shifts are made in 0.5% increments thus achieving a finer resolution than for the 2.5% increments used to evaluate all the nodes. This is a useful

advantage of the harmonic approach since, once the unit solution stresses are computed, the stress response at any shifted frequency can be easily and quickly evaluated thus allowing this higher resolution (in frequency shift) plot to be obtained in a few minutes. In a time-domain approach each frequency shift entails a complete finite element time simulation requiring days to weeks of computation time. For node 88325 the highest stress intensity of 9,610 psi occurs at the -0.5% frequency shift which is only 35 psi (or 0.4%) higher than the 9,575 psi value at zero shift. The maximum and alternating stress intensities vary by approximately 600 psi when frequencies are shifted in the ±10% range. For node 88252, the stress variation is slightly higher, but clearly shows no strong unresolved interior peaks.

Node 80204 shows two interior peaks, at -5.5% and 0% frequency shifts. These could be due to the excitation of one of many skirt modes present in the structure. Unlike the previous two nodes, the maximum and alternating stress intensities are now very close in magnitude due to the small static stress component. Both alternating and maximum stress intensities are relatively small as evident from the associated alternating stress ratio of SR-a>4. A much stronger frequency shift dependence is seen in the last two plots for nodes 82290 and 86424 (Figure 18d and e). Both plots show the peak (now resolved to 0.5%) at -7.5%. Further, in each case the behavior about the peak is accurately described by the frequency response of a single degree-of-freedom damped oscillator. For example, the half power points for node 82290 are ±0.78% about the -7.5% shift; the half power points for node 86424 occur at ±1.14% about the peak frequency shift. Both are close to the ±1% values expected for 1% damping. Differences are attributable to the presence of multiple modes in the stress response.

Since acoustic loads scale roughly with the square of the steam flow, it is reasonable to anticipate that under EPU conditions (where steam flow increases by 15%) the stresses would increase to by approximately $(115\%)^2=1.32$. Under this assumption the minimum alternating stress ratio would reduce from 1.86 to 1.86/1.32=1.41, which given that the applied loads already account for all end-to-end biases and uncertainties, still contains sufficient margin for sustained EPU operation. The stress ratios associated with maximum stress do not scale this way due to the large static component in these stresses. However, on the basis of Figure 18a-b (nodes having the highest maximum stress intensities, 88325 and 88252), one sees that other than the vertical displacement the alternating stress intensity and peak stress intensity curves have very similar forms. It is then reasonable to expect that adding the increase in alternating stress intensity, or $(1.32-1)=0.32$ times the alternating stress intensity, to the maximum stress intensity yields a rough estimate of the peak stress intensity at EPU operation. The peaks then become 9973 psi (for node 88325) and 8882 psi (node 88252) with corresponding stress ratios, SR-P=1.52 and SR-P=1.68 respectively, which are both still well within allowables. These simple scaling arguments, indicate that at EPU the minimizing stress ratio would be due to an alternating stress (SR-a=1.41) rather than a maximum stress.

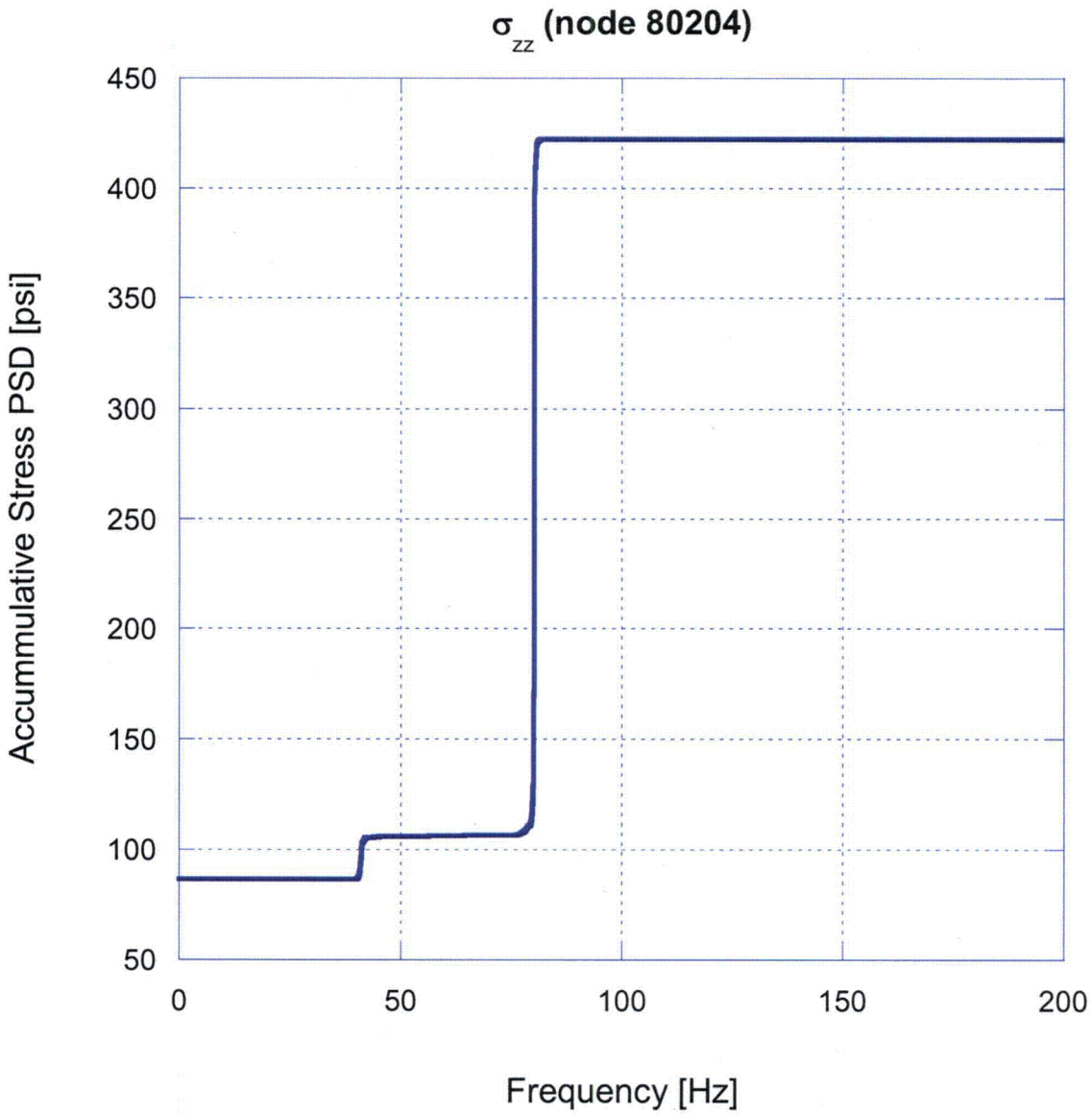

Figure 16. Accumulative PSD of the σ_{zz} stress response at node 80204 for nominal CLTP operation with zero frequency shift.

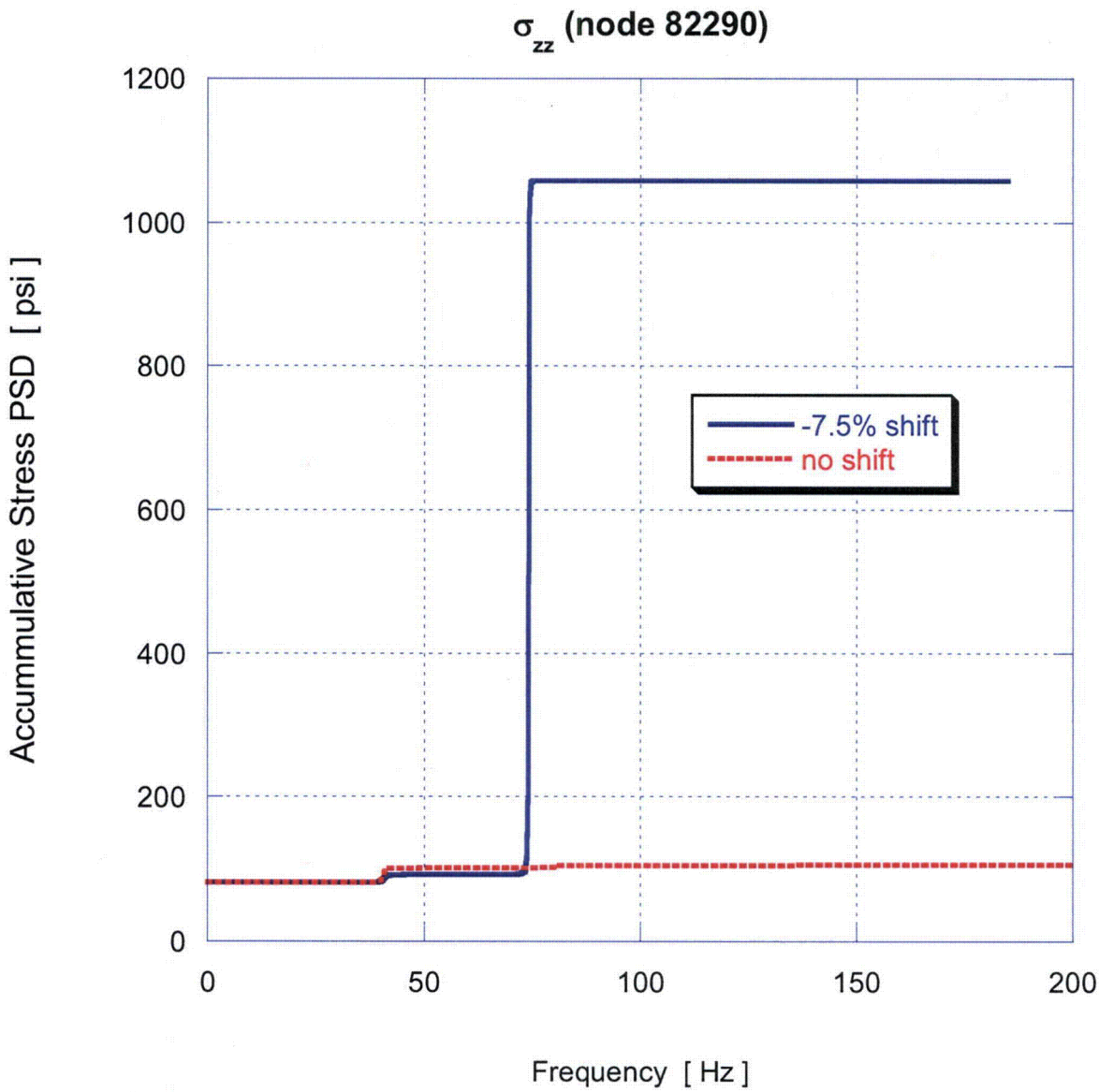

Figure 17. Accumulative PSD of the σ_{zz} stress response at node 82290 at -7.5% and zero frequency shifts

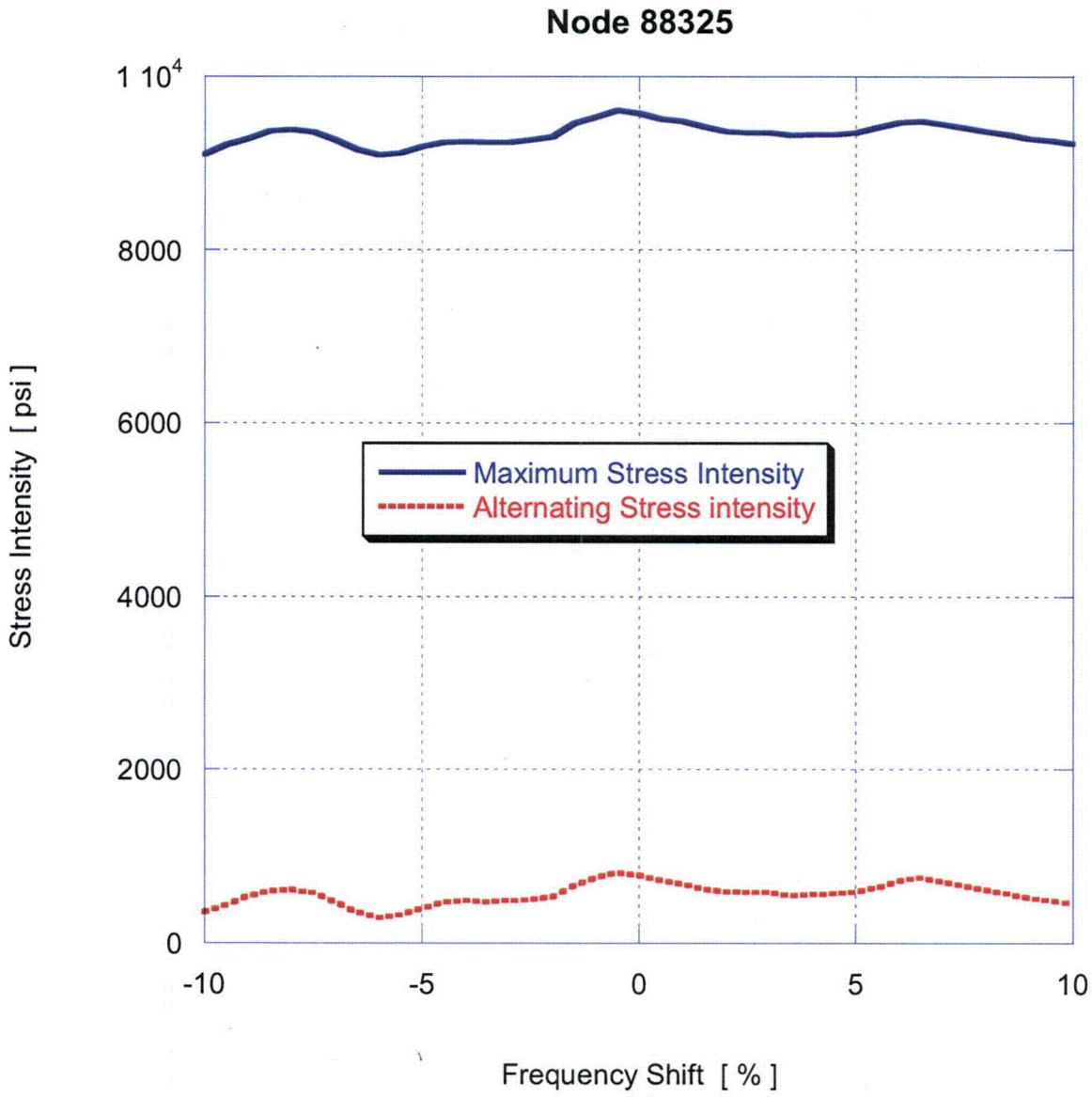

Figure 18a. Variation of maximum and alternating stress intensities with frequency shift for node 88325.

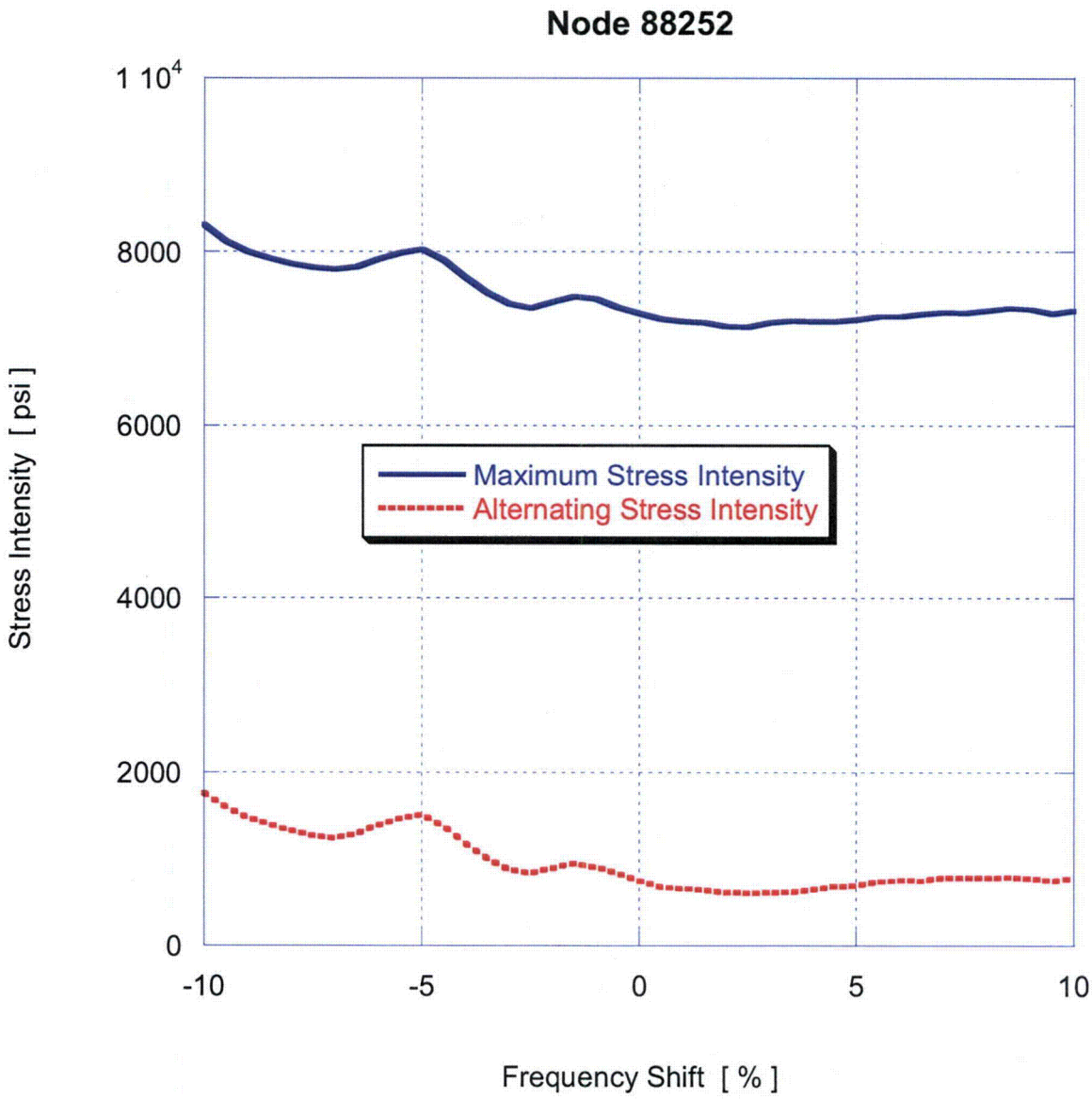

Figure 18b. Variation of maximum and alternating stress intensities with frequency shift for node 88252.

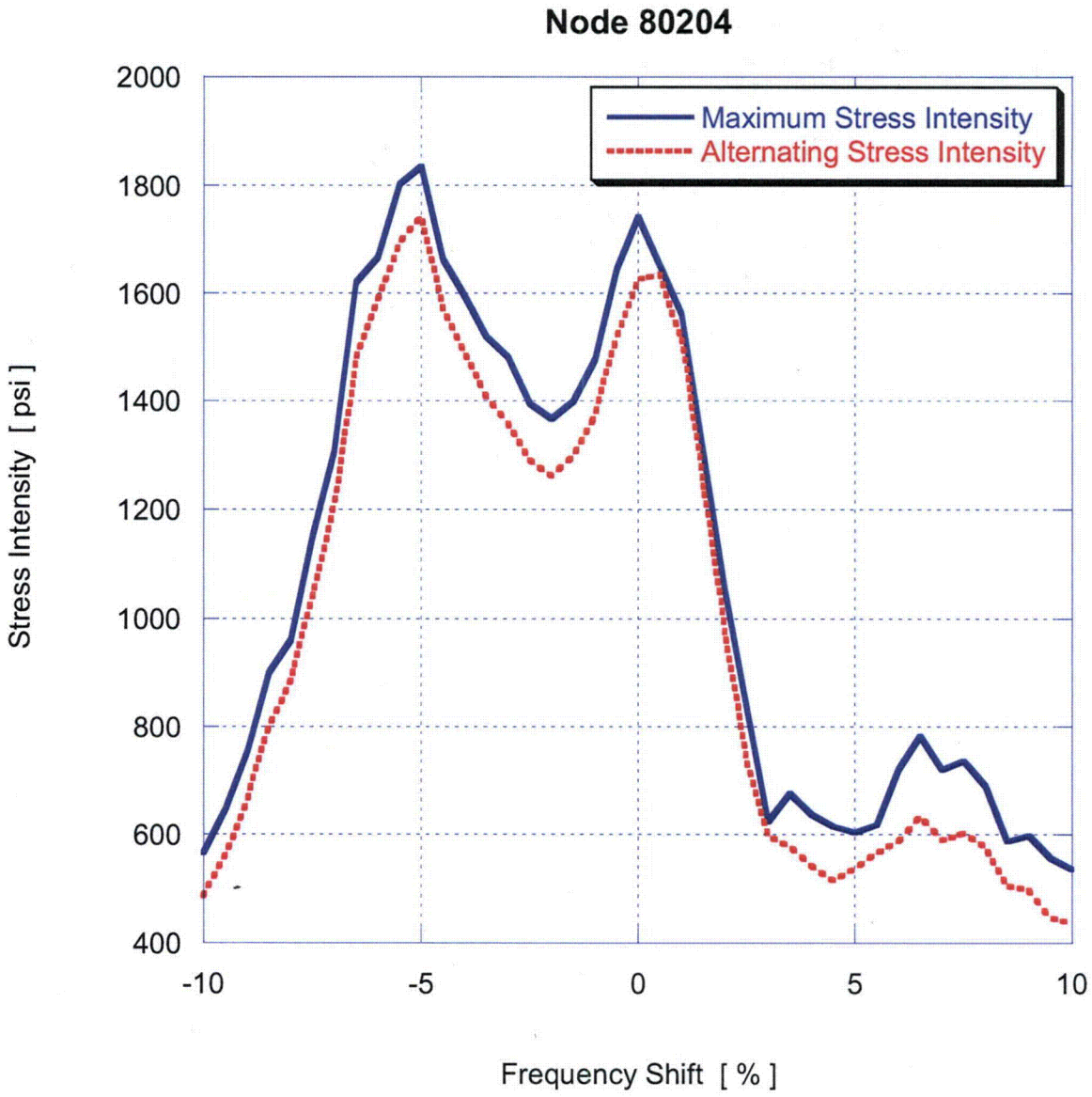

Figure 18c. Variation of maximum and alternating stress intensities with frequency shift for node 80204.

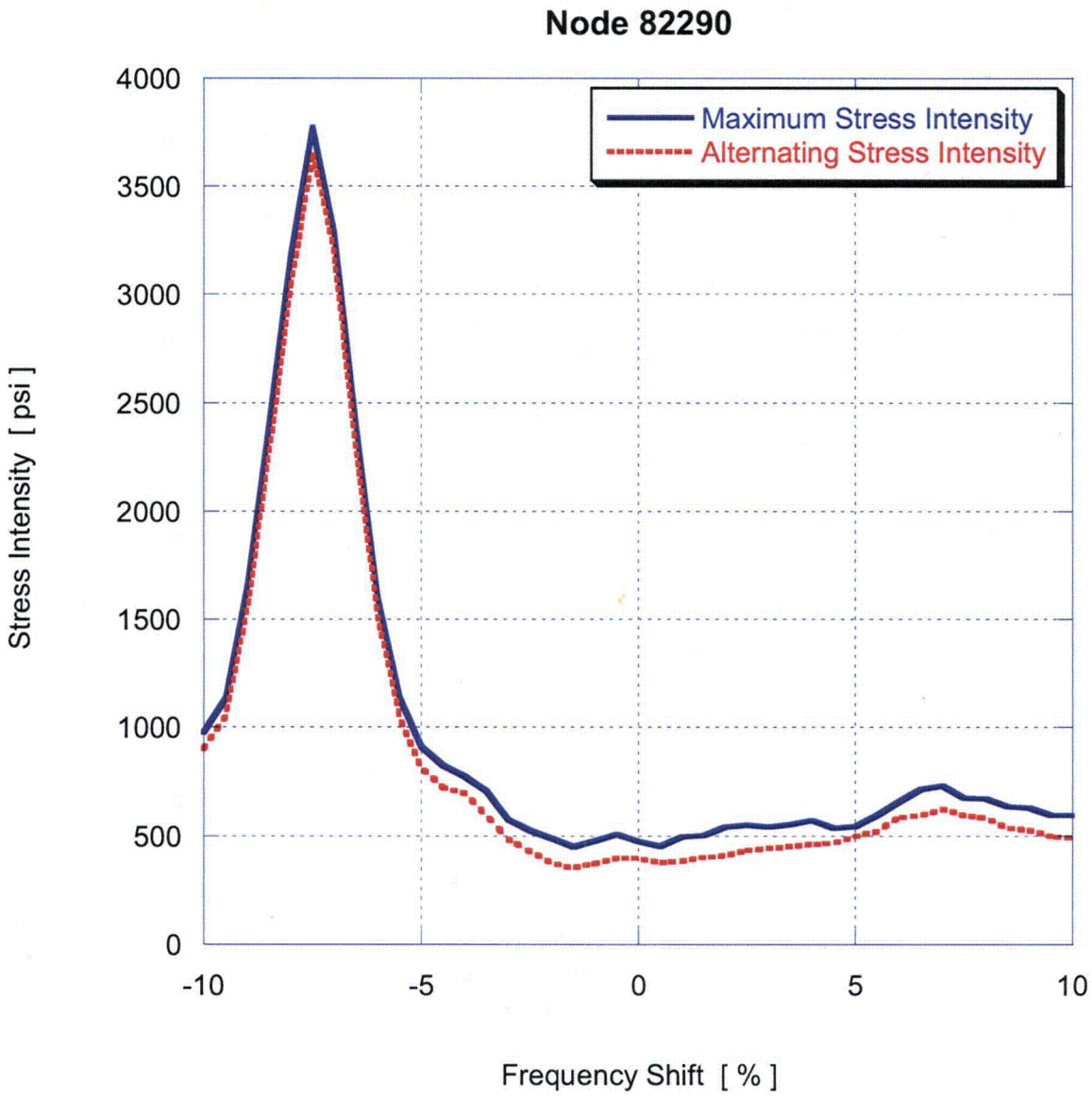

Figure 18d. Variation of maximum and alternating stress intensities with frequency shift for node 82290.

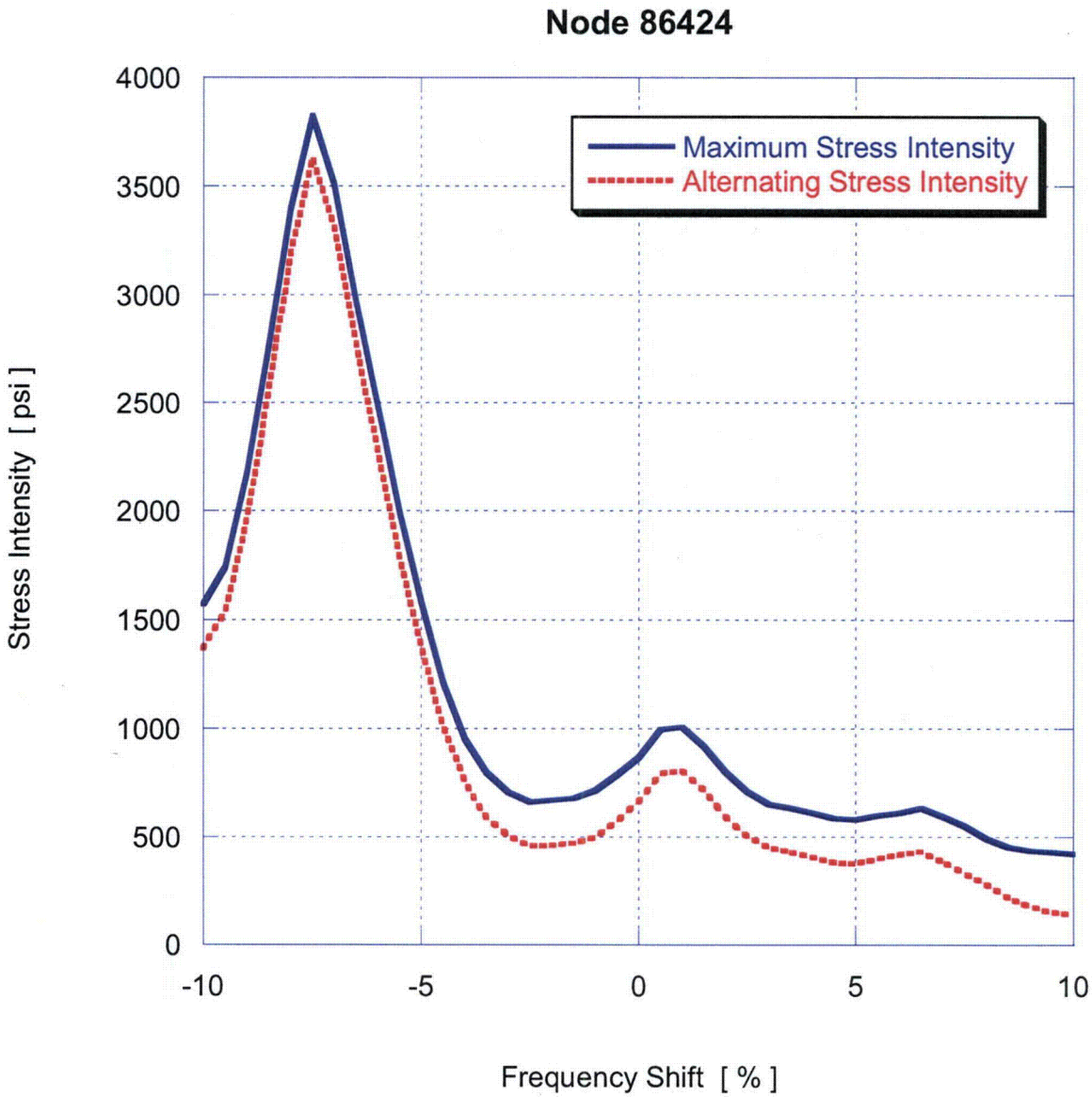

Figure 18e. Variation of maximum and alternating stress intensities with frequency shift for node 86424.

5.4 90% Removal of 80Hz MSL Signal

The origin of the 80 Hz component is largely due to the amplification of sensor noise and MSL turbulence in the ACM. It can be identified with a 'sloshing' mode where the acoustic pressure varies from negative minimum at one pair of MSL exits to a maximum value at the opposite pair with a zero value near the top of the steam dome. This mode experiences comparatively little damping because it does not produce significant motion at the steam/water interface. Since neither sensor noise nor the non-coherent turbulence constitute acoustic sources, they should not be included in the ACM and associated acoustic loads. The ACM analysis however, does not distinguish between the acoustic and non-acoustic fluctuations in the MSL signals that could lead to sizeable, but fictitious 80 Hz acoustic loads on the dryer that dominate the stress response. Removing these fictitious loads in a conservative manner is a non-trivial task however, since not only is it difficult to quantify how much of the 80 Hz signal is spurious, but the remaining part that does represent an acoustic load is subject to amplification because of its proximity (in frequency) to the aforementioned lightly damped 80 Hz sloshing acoustic mode.

Despite the absence of detailed information regarding sensor noise and turbulence, one can nevertheless obtain estimates of the steam dryer stress ratios on the basis of reasonable engineering estimates regarding the acoustic content in the 80 Hz signal. In particular, if one retains 10% of the 80 Hz signal, then the PSDs of the MSL pressures at the steam dryer entries still display a pronounced peak at 80 Hz, whereas pressure transducer measurements taken off the steam dome top do not indicate such a peak. This suggests that retaining 10% of the 80 Hz signal is conservative since to eliminate the associated peak even less of the signal must be retained.

Proceeding with this assumption, the pressure signals in each MSL were filtered by a simple narrow-band Gaussian notch filter centered at 80 Hz according to:

[[$^{(3)}$]]

where f is the frequency, and the stress intensities and stress ratios re-evaluated. This filter reduces the pressure to 10% of its unfiltered value at 80 Hz, but leaves the signal effectively unchanged outside the 78-82 Hz range.

The resulting stress ratios are tabulated in Table 8 for: (i) nominal CLTP operation; and (ii) as the minimum (worst case) stress ratios taken over all frequency shifts. It is clear that the elimination of this signal results in a significant reduction in alternating stresses and corresponding increase in alternating stress ratios. Comparing the minimum stress ratio over all frequency shifts before (SR-a=1.86 in Table 7b) and after filtering (SR-a=3.58 in Table 8b) of the 80 Hz signal shows that the worst case alternating stresses are reduced by a factor of 1.92. The worst case maximum stress ratios on the other hand remain virtually unchanged at SR-P=1.66 which is somewhat higher than the value of SR-P=1.58 obtained without filtering. This reflects the dominance of the static component to the maximum stress Table 8 at the support locations. The lowest alternating stress ratios now occur at different locations, namely the junctions between the hood supports and at a different frequency shift.

Table 8a. Locations with minimum stress ratios for CLTP conditions with no frequency shift using loads with 80 Hz component filtered. Stress ratios are grouped according to stress type (maximum – SR-P; or alternating – SR-a) and location (away from a weld or at a weld). Bold text indicates minimum stress ratio of any type on the structure.

Stress Ratio	Weld	Location	Location (in.)				Stress Intensity (psi)			Stress Ratio	
			x	y	z	node	Pm	Pm+Pb	S_{alt}	SR-P	SR-a
SR-P	No	1. outer portion of inner hood (top near closure plate)	109.0	-27.6	95.3	44886	5962	8480	<1500	3.07	>4
SR-a	No	NONE (All SR-a > 4)									
SR-P	**Yes**	**1. skirt/upper support ring**	**118.8**	**0.6**	**-2.0**	**88325**	**2233**	**9026**	**<1500**	**1.67**	**>4**
"	"	2. closure plate/hood	108.4	-27.9	94.9	88275	4355	7214	<1500	2.09	>4
"	"	3. central base plate/inner vane bank/side panel	-118.8	14.4	7.5	85994	4057	5583	<1500	2.48	>4
"	"	4. closure plate/middle side panel/top cover plate/ top perforated plate	-108.4	45.9	95.9	85891	3637	4354	<1500	2.77	>4
"	"	5. drain pipe/skirt	88.2	79.6	-20.5	91083	1889	5331	<1500	2.83	>4
"	"	6. inner hood backing bar/closure plate	-108.4	38.4	8.1	87035	3327	3528	<1500	3.02	>4
SR-a	Yes	NONE (All SR-a > 4)									

See Table 6a for coordinates description.

Table 8b. Locations with minimum stress ratios for CLTP conditions with frequency shifts using loads with 80 Hz component filtered. Stress ratios at every node are recorded as the lowest stress ratio identified during the frequency shifts. Stress ratios are grouped according to stress type (maximum – SR-P; or alternating – SR-a) and location (away from a weld or at a weld). Bold text indicates minimum stress ratio of any type on the structure.

Stress Ratio	Weld	Location	% Freq. Shift	Location (in.)				Stress Intensity (psi)			Stress Ratio	
				x	y	z	node	Pm	Pm+Pb	S_{alt}	SR-P	SR-a
SR-P	No	1. outer portion of inner hood (top near closure plate)	+10	109.0	-27.6	95.3	44886	6065	8638	<1500	3.02	>4
SR-a	No	NONE (All SR-a > 4)										
SR-P	**Yes**	**1. skirt/upper support ring**	**+10**	**118.8**	**0.6**	**-2.0**	**88325**	**2235**	**9096**	**<1500**	**1.66**	**>4**
"	"	2. closure plate/inner hood	+10	108.4	27.9	94.9	85409	4950	7255	<1500	2.03	>4
	"	3. central base plate/inner vane bank/side panel	+10	-118.8	14.4	7.5	85994	4067	5591	<1500	2.47	>4
	"	4. closure plate/middle side panel/top cover plate/ top perforated plate	+10	108.4	-45.9	95.9	91627	3685	4294	<1500	2.73	>4
	"	5. drain pipe/skirt	+10	88.2	79.6	-20.5	91083	1944	5491	<1500	2.75	>4
	"	6. inner hood backing bar/closure plate	+10	-108.4	38.4	8.1	87035	3361	3553	<1500	2.99	>4
	"											
SR-a	Yes	inner hood/hood support	+7.5	0.0	36.5	45.9	88023	856	1970	1919	7.66	3.58
"	"	inner hood/hood support	+7.5	0.0	35.2	57.1	88020	877	1909	1888	7.91	3.64
"	"	inner hood/hood support	+7.5	0.0	37.5	34.7	88026	725	1793	1720	8.42	3.99

See Table 6 for coordinates description.

6. Conclusions

A harmonic steam dryer stress analysis has been used to calculate high stress locations and calculated / allowable stress ratios for the HC1 steam dryer at CLTP load conditions using plant measurement data. A detailed description of the harmonic methodology and the finite element model for the HC1 steam dryer is presented. The CLTP loads obtained in a separate acoustic circuit model [2], including end-to-end bias and uncertainty [3], were applied to a finite element model of the steam dryer consisting mainly of the ANSYS Shell 63 elements and brick continuum elements. The resulting stress histories were analyzed to obtain maximum and alternating stresses at all nodes for comparison against allowable levels. These results are tabulated in Table 7 of this report. The minimum stress ratio at nominal operation is 1.58 and the minimum stress ratio taken over all frequency shifts is also 1.58. In both cases the minimum stress ratio corresponds to a maximum stress.

On the basis of these CLTP plant loads, the dynamic analysis of the steam dryer shows that the combined acoustic, hydrodynamic, and gravity loads produce the following minimum stress ratios:

Frequency Shift	Minimum Stress Ratio	
	Max. Stress, SR-P	Alternating Stress, SR-a
0% (nominal)	1.58	>4
-10%	1.66	3.03
-7.5%	1.61	1.86
-5%	1.64	2.61
-2.5%	1.63	3.56
+2.5%	1.61	3.58
+5%	1.61	3.12
+7.5%	1.60	3.46
+10%	1.64	3.76
All shifts	1.58 – 1.66	1.86 - 4

Assuming alternating stresses scale approximately with the square of the steam flow speed, then at 115% CLTP the minimum stress ratios are estimated as SR-a=1.41 (alternating stress intensity) and SR-P=1.52 (maximum stress intensity).

Examination of the spectral content in the stresses reflects a strong 80 Hz signal, part of which is not physical. Scaling the 80 Hz signal to 10% of its value results in minimum stress ratios (taken over all frequency shifts) of SR-P=1.66 (maximum stress intensity) and SR-a=3.58 (alternating stress intensity).

7. References

1 Continuum Dynamics, Inc. (2005). "Methodology to Determine Unsteady Pressure Loading on Components in Reactor Steam Domes (Rev. 6)." C.D.I. Report No. 04-09 (Proprietary).

2. Continuum Dynamics, Inc. (2007). "Acoustic and Low Frequency Hydrodynamic Loads at CLTP Power Level on Hope Creek Unit 1 Steam Dryer to 200 Hz" C.D.I. Report No. 07-18P (Proprietary)

3. Continuum Dynamics, Inc. (2007). "Methodology to Predict Full Scale Steam Dryer Loads from In-Plant Measurements, with the Inclusion of a Low Frequency Hydrodynamic Contribution (Rev. 0)" C.D.I. Report No. 07-09P (Proprietary).

4. Structural Integrity Associates (2007). "Hope Creek Main Steam Line Strain Gage Data: MSL Channel Combinations."

5. ANSYS Release 10.0. URL http://www.ansys.com. Documentation: ANSYS 10.0 Complete User's Manual Set

6. Press, W. H., S. A. Teukolsky, et al. (1992). *Numerical Recipes*, Cambridge University Press.

7. Continuum Dynamics, Inc. (2007). "Stress Analysis of the Hope Creek Unit 1 Steam Dryer at EPU Conditions Using 1/8th Scale Model Pressure Measurement Data (Rev. 2) " C.D.I. Report No. 06-27 (Proprietary).

8. O'Donnell W.J. (1973). "Effective Elastic Constants For the Bending of Thin Perforated Plates With Triangular and Square Penetration Patterns," ASME Journal of Engineering for Industry, Vol. 95, pp. 121-128.

9. U.S. Nuclear Regulatory Commission, (2007). Regulatory Guide 1.20 "Comprehensive Vibration Assessment Program for Reactor Internals During Preoperational and Initial Startup Testing," March 2007.

10. WRC Bulletin 432 (1998). "Fatigue Strength Reduction and Stress Concentration Factors For Welds In Pressure Vessels and Piping," WRC, NY, p.32

11. Pilkey W.D. (1997). *Peterson's Stress Concentration Factors*, 2nd ed., John Wiley, NY, p.139.

12. Lawrence F.V., Ho N.-J., Mazumdar P.K. (1981). "Predicting the Fatigue Resistance of Welds," Ann. Rev. Mater. Sci., vol. 11, pp. 401-425.

13. General Electric (GE) Nuclear Energy (2003). Supplement 1 to Service Information Letter (SIL) 644, "BWR/3 Steam Dryer Failure," September 5, 2003.

14. Tecplot 10 (2004). URL: http://www.tecplot.com. Documentation: *Tecplot* User's Manual Version 10 Tecplot, Inc. Bellevue, Washington October.

15. Flugge, W. (ed.) (1962). *Handbook of Engineering Mechanics*, McGraw-Hill, p.61-62.

16. Blevins R. (1979). "Formulas for Natural Frequency and Mode Shape," van Nostrand-Reinhold Co., p. 261

17. ASME (2004). ASME Boiler and Pressure Vessel Code, Section III, Article A-8000, Stresses in Perforated Flat Plates.

Appendix A. Comparison of ANSYS Frequency Predictions Against Analytical Formulas for Flat Plates

The computed modal masses affect the response amplitude, and while these masses can be computed using the ANSYS finite element (FE) software, there are no modal mass measurements or analytical solutions they can be compared against. One recourse for assessing bias errors and uncertainties is to consider a geometrically simple structure (e.g., a flat plate) for which analytical solutions for the modal amplitudes, masses, and responses are available. Predictions of these properties using an ANSYS FE model having the same elements and connections present in the steam dryer model can then be compared against these analytical results thus allowing one to estimate the errors in frequency as a function of response frequency.

Modal analysis was performed for: (i) a rectangular plate simply supported on all sides and with dimensions comparable to the vane bank side panel; and (ii) a rectangular plate clamped on all sides and with dimensions comparable to the section of the middle hood that experienced the lowest alternating stress ratios at SMT EPU conditions with +10% frequency shift. In all cases, the mesh has spatial resolution similar to that used in the steam dryer model and the same element type SHELL63 is employed. For the simply supported plate, simple analytical solutions are available for any aspect ratio. For the clamped plate case, tabulated frequency predictions are available only at selected aspect ratios. Thus, for this case dimensions were chosen to correlate most closely with the steam dryer dimensions while adhering to one of the tabulated aspect ratios.

The material properties used in the finite element model were: Young's modulus, E=25.55 10^6 psi; density, ρ=0.284 lbm/in^3 and Poisson's ratio, ν=0.3. Modal frequencies are readily obtained in ANSYS. Modal masses are more difficult to extract due to underlying assumptions regarding the normalization of modes and the absence of analytical modal mass information. However, since any error in the modal mass will be reflected in the computed frequencies (the modal frequencies depend on the generalized stiffness for the mode and the associated modal mass), the errors in modal frequencies are a good estimate of the errors in modal masses. The comparisons between ANSYS and analytical modal frequency predictions follow below.

Simply Supported Plate

Analytical eigenfrequencies for a plate that is simply supported on all sides is given by [15]:

$$f_{mn} = \frac{\pi}{2}\sqrt{\frac{D}{\rho h}}\left(\frac{m^2}{a^2}+\frac{n^2}{b^2}\right)$$

where $D = \frac{Eh^3}{12(1-\nu^2)}$, E is the Young's modulus, ρ is the density, h is the plate thickness, a and b denote the plate dimensions, and m and n are modal numbers. For the model of the vane bank side panel, h = 0.375", a = 8.5" and b = 88.4375". Then: D = 13940.6 Nm, and the lowest frequencies and relative errors are (note: m and n are mode numbers):

Table A1. Comparison of analytical and ANSYS predictions of natural frequencies for simply-supported plate.

m	n	Analytical frequency, Hz	ANSYS frequency, Hz	Rel. Error (%)
1	1	464.1	462.4	-0.37
1	2	476.8	474.8	-0.42
1	3	498.1	495.5	-0.52
1	4	527.8	524.4	-0.64

Thus the errors in computed frequencies are less than 1% and are due to mesh resolution.

Clamped Plate

The middle hood is modeled with a plate, clamped on all sides and of thickness h=0.125" and side lengths, a=17.92" and b = 44.8". This corresponds to the section of plate immediately adjacent to the location of high stress in the SMT calculation at EPU with +10% frequency shift. At this aspect ratio, b/a=2.5, the analytical eigenfrequencies are given by [16]:

$$f_{ij} = \frac{\lambda_{ij}^2}{2\pi b^2}\sqrt{\frac{D}{\rho h}}$$

where D = 516.32 Nm and the coefficients λ_{ij}^2, the lowest frequencies and relative errors are shown in the table below.

Table A2. Comparison of analytical and ANSYS predictions of natural frequencies for clamped plate.

i	j	λ_{ij}^2	Analytical frequency, Hz	ANSYS frequency, Hz	Rel. Error (%)
1	1	147.8	82.69	82.98	0.35
1	2	173.9	97.29	96.01	-1.32
1	3	221.5	123.92	121.14	-2.03
1	4	291.9	163.3	158.73	-2.8

The mesh used to calculate plate eigenfrequencies and the mesh on the steam dryer model are shown below.

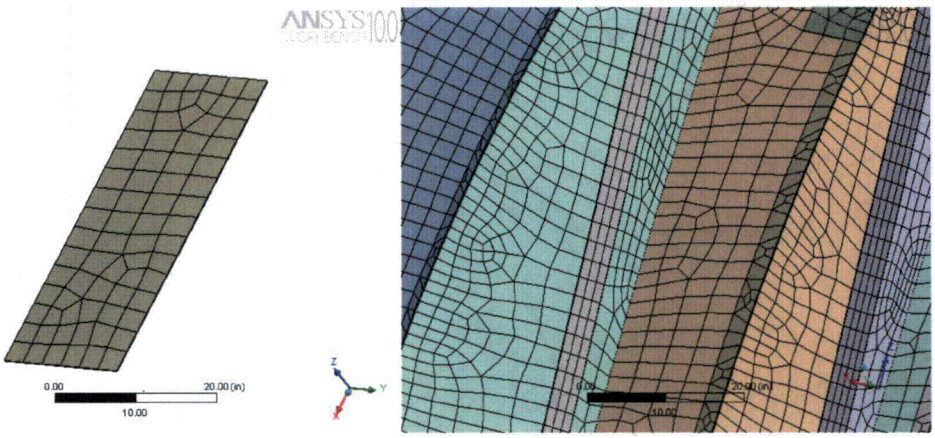

Left – mesh on the flat plate model for eigenvalue comparison calculations; right – mesh on the actual steam dryer FE model. The size of elements in both models is kept similar.

Appendix B. Comparison of Transient and Harmonic Simulations for the Browns Ferry Unit 1 Dryer

[[

[3]]]

[[

[3]]]

[[

[3]]]

[[

[3]]]

Figure 19a. [[

[3]]]

[[

[3)]]

Figure 19b. [[

[(3)]]

[[

[3]]]

Figure 20a. [[

[3]]]

[[

[3]]]

Figure 20b. [[

[3]]]

[[

[3]]

Figure 20c.

[3]]

[[

[3]]

Figure 20d. [[

[3]]

Appendix C. Structural Modeling of Perforated Plates

Modeling the perforated plates in the steam dryer assembly explicitly is computationally prohibitive and an alternative approach is adopted where the plates are characterized by modified material properties adjusted to match the key static and dynamic behavior. This Appendix summarizes the modeling method employed and its verification against measurements.

The perforated plates used in the steam dryer assembly are very thin, i.e. the ratio of thickness and pitch of perforation is less than unity so that the effective properties provided in ASME B&PVC, [17], for thick perforated plates cannot be used. Therefore, to model the steam dryer we have adopted the effective material properties reported by O'Donnell in [8] which directly apply to the bending of thin plates. In his work the effective properties are calculated by equating an average stress field over the periodicity cell in a perforated plate. Thus, for a given static loading the solid plate with the effective or modified material properties will yield a similar stress field as the perforated plate with original material properties. Comparisons are made against the values provided in ASME Code [17], as well as to experimental data where good agreement is obtained.

In order to apply these results to the steam dryer analysis the staggered 45° perforation was approximated with an equilateral staggered 60° perforation. The difference was judged insignificant for modeling purposes. The effective properties were therefore inferred from Fig. 8 (Young's modulus) and Fig. 9 (Poisson ratio) of [8].

Verification

[[

$^{(3)}$]]

[[

[3]]]

Figure 21. [[

[3]]]

[[

[3]]]

Figure 22. [[

[3]]]